University of Minnesota
ST. ANTHONY FALLS HYDRAULIC LABORATORY

Project Report No. 161

THE FLOW AND STABILITY CHARACTERISTICS OF ALLUVIAL RIVER CHANNELS

by

Alvin G. Anderson,
Gary Parker,
and
Addison Wood

Prepared for

AGRICULTURAL RESEARCH SERVICE
United States Department of Agriculture

September 1975
Minneapolis, Minnesota

TABLE OF CONTENTS

TABLE OF CONTENTS
(Continued)

ACKNOWLEDGMENTS

This report is on the work conducted under Agricultural Research Service Agreement No. 12-14-3001-102 for the conduct of research by Dr. Alvin G. Anderson, Director of the St. Anthony Falls Hydraulic Laboratory and Professor of Civil Engineering. Dr. Gary Parker gave major assistance to Dr. Anderson in the research program, with Mr. Addison Wood directing the experimental work by Mr. S. Dhamotharan. Mr. Jeffrey Ferguson worked with Mr. Wood on the development of instrumentation and computer programs.

Before the completion of the report on this research, a heart attack resulted in Dr. Anderson's untimely death. The report, therefore, is in large part the work of Dr. Gary Parker. Dr. C. S. Song, Warren Dahlin, and Mary H. Marsh also assisted in its completion. The report was typed by Marilyn Jarosz.

The authors express their gratitude to these and the other members of the staff of the St. Anthony Falls Hydraulic Laboratory who contributed to this program.

INTRODUCTION AND SUMMARY

Alluvial rivers, insofar as they transport the material of which their channels are composed, possess the freedom to alter their geometry through the phenomena of erosion and deposition. River channels can be loosely divided into bed and bank regions, and geometry alteration phenomena can likewise be divided into bed processes and bank processes.

An analysis of bank processes is dependent on a general knowledge of bed processes. Bed processes associated with wide, equilibrium rivers, in which bank processes are negligible, are examined in Chapter I of this report. An attempt is made to find the most general possible forms for sediment transport and bed resistance relationships. The forms are general enough so that existing equations can be expressed within their framework. Bank processes, and in particular bank erosion, are the subject of the remainder of the report.

Bank erosion is one of the important mechanisms by which a stream determines its own channel. In this sense nature is her own engineer; artificial alteration of channel width or alignment often have only temporary success, since natural forces that work to restore the unaltered state are present.

In broad terms, two modes of bank erosion can be identified. "Primary" bank erosion refers to the global process by which the scale of river width over an entire reach is determined. In the case of natural rivers, primary bank erosion (or its opposite, bank building) leading to a distinct change in geomorphologic state is often an extremely slow process occurring in response to geologic or meteorologic changes such as discharge decrease due to glacial recession or tectonic lifting. However, channel widening due to a succession of extreme floods (Schumm and Lichty)[1], and channel narrowing due to a reduction of flood peak through reservoir construction and subsequent vegetation growth (Northrup)[2] have been observed to occur in periods of a few years.

---

[1] S.A. Schumm and R.W. Lichty, Channel Widening and Flood-Plain Construction Along Cimarron River in Southwestern Kansas, Geological Survey Professional Paper 352-D, U.S. Government Printing Office, Washington, 1963.

[2] W.L. Northrup, Republican River Channel Deterioration, Proceedings of the Federal Inter-Agency Sedimentation Conference 1963, Agricultural Research Service, U.S. Department of Agriculture Miscellaneous Publication No. 970, pp. 409-424, Washington, D.C., June 1963.

The problem of primary bank erosion is of practical importance in the proper design of canals and river training projects, when the engineer is required to choose a width that nature will maintain as stable.

"Secondary" bank erosion refers to local processes by which the stream, without essentially altering its width, changes its alignment from place to place with accompanying bank erosion or building. Typical examples of secondary bank erosion are meandering and braiding.

In Chapter 2, meandering and braiding and resulting secondary bank erosion are examined both analytically and experimentally from the point of view of stability. A combination of theory and experiment leads to a general exposition of bar-forming tendencies in straight rivers. A diagram based on the analysis is presented which divides fluvial morphology into straight, meandering, and braided regimes based on the two parameters: $\frac{D}{B}$ (the depth-width ratio) and $\frac{S}{F}$ (slope divided by Froude number). It is shown that for field conditions, if sediment transport exists, then either meandering or braiding tendencies also always exist. These tendencies cannot be damped without complete bank stabilization, for example, with riprap. The results cast doubt on the permanence of the straight alignment of channelized streams. Predictive relations for meander length are presented and compared with data. Furthermore, the applicability of laboratory studies to field meandering and braiding is examined qualitatively.

At the end of Chapter 1 and in Chapter 3 the conditions are considered which are necessary for the establishment of stable channels in which primary bank erosion does not occur. Only the case in which both river bed and banks are composed of non-cohesive material is examined. It is shown that lateral bank curvature leads to a redistribution of bed stress such that stable, non-eroding banks can coexist with a bed in active transport. The analysis suggests that regime equations for channel geometry and flow characteristics can be analytically derived, and although this is not done herein an outline of the problem is presented.

LIST OF SYMBOLS

A	coefficient in the Einstein-Brown bedload equation in Chapter 1
A	channel cross-sectional area in Chapter 3
A	coefficient in equation 3-10
A_{11}	coefficient in equation AII.11a
A_{12}	coefficient in equation AII.11a
A_{21}	coefficient in equation AII.11a
A_{22}	coefficient in equation AII.11a
A_3	coefficient in equation AII.11a
A_4	coefficient in equation AII.11a
A_{51}	coefficient in equation AII.11a
A_{52}	coefficient in equation AII.11a
A_{53}	coefficient in equation AII.11a
A_{61}	coefficient in equation AII.11a
A_{62}	coefficient in equation AII.11a
A_7	coefficient in equation AII.11a
a	coefficient in equation 3-10
B	channel water surface width
B	coefficient in equation 3-10
B_f	flume width
B_I	initial width
B_s	width of bank region, Chapter 3
B_w	wandering belt width, Chapter 2
b	coefficient in equation 3-10
C	friction factor (resistance coefficient)
C	coefficient in equation 3-10
C	bar migration rate, Appendix II

C_B bank full friction factor, Chapter 1

C_E effective friction factor, Appendix IV

C_I initial friction factor

C_o unperturbed friction factor

C_s concentration by weight of sediment in transport

C_{sB} bank full sediment concentration

C_T total friction factor, Appendix IV

C_w wall friction factor, Appendix IV

C_1 coefficient in the solution to equation 3-11a

C_2 coefficient in the solution to equation 3-11a

$\bar{C}$ coefficient in equation 3-5

$\bar{C}_o$ coefficient in the asymptotic expansion for $\bar{C}$ in Chapter 3

$\bar{C}_1$ coefficient in the asymptotic expansion for $\bar{C}$ in Chapter 3

$\bar{C}_2$ coefficient in the asymptotic expansion for $\bar{C}$ in Chapter 3

$\tilde{C}_1$ coefficient in the solution to equation 3-11b

$\tilde{C}_2$ coefficient in the solution to equation 3-11b

D channel depth

D dimensionless perturbed depth in Appendix II

D_{fI} initial screed depth of flume channel, Chapter 1

D_I initial depth

D_o unperturbed channel depth, Chapter 2

D_o maximum channel depth, Chapter 3

D_s typical sediment diameter

D_{50} sediment diameter such that 50% is finer

$\bar{D}$ cross-sectionally averaged depth, Chapter 3

D' perturbed depth in Appendix II

$\hat{D}$ depth coefficient in equations AII.9

e	bed porosity
F	froude number
F_I	initial froude number
f	Darcy-Weisbach friction factor in Chapter 2
f	functional notation in Chapter 3
f_B	functional notation in equation 1-3
f_Q	functional notation in equation 1-4
f_1	functional notation in equation 1-11
f_1	functional notation in equation 1-15
f_2	functional notation in equation 1-12
f_2	functional notation in equation 1-16
f_3	functional notation in equation 1-17
$\tilde{f}_1$	functional notation in equation 1-9
$\tilde{f}_2$	functional notation in equation 1-10
g	gravitational acceleration
H	water surface height above datum in Appendix II
H	dimensionless water surface height perturbation in Appendix II
H_o	reference water surface height in equations AII.6
H'	perturbed water surface height in Appendix II
$\hat{H}$	water surface height coefficient in equation AII.9
J	a constant equal to 30 in Chapter 3
j	lateral channel curvature in Chapter 3
K	dimensionless meander or braid wave number in Chapter 2
K	bed roughness in Chapter 3
K_B	dimensionless width wave number in Chapter 2
K_1	coefficient in Peterson's relations, Chapter 1
K_1	dimensionless dynamic width wave number in Chapter 2
K_2	coefficient in Peterson's relations, Chapter 1

L_f	flume length
M	mass of sediment in flume in Appendix I
M_I	initial mass of flume sediment in Appendix I
M_1	coefficient in equations AII.8
M_2	coefficient in equations AII.8
m	number of braids in a river
m_1	coefficient in Peterson's relations in Chapter 1
m_2	coefficient in Peterson's relations in Chapter 1
N_1	coefficient in equations AII.8
N_2	coefficient in equations AII.8
n_1	coefficient in Peterson's relations in Chapter 1
n_2	coefficient in Peterson's relations in Chapter 1
P	a parameter in the Einstein-Brown equation in Chapter 1
P	welted perimeter in Chapter 3
P_i	various dimensionless sediment factors in Chapter 1
Q	water discharge
Q_s	sediment discharge
Q^*	dimensionless sediment discharge
Q^*_B	dimensionless bank full sediment discharge
$\tilde{Q}$	dimensionless water discharge
$\tilde{Q}_B$	dimensionless bank full water discharge
q	water discharge per unit width in Chapter 1
q_s	sediment discharge per unit width in Chapter 1
q_s	unperturbed sediment discharge per unit width in Chapter 1
q^*	Einstein sediment discharge
$\tilde{q}$	dimensionless water discharge per unit width
q_l	longitudinal component of vector of sediment discharge per unit width

q_2	lateral component of vector of sediment discharge per unit width
q_i'	perturbed vector of sediment discharge per unit width
R	relative roughness in Chapter 1
R	hydraulic radius in Chapter 3
R_B	bank full relative roughness in Chapter 1
R_P	a type of particle Reynolds number in Chapter 1
r	sediment buoyancy parameter
S	river channel water surface or energy slope at equilibrium
S_I	initial slope
s	ratio of depth to maximum depth in a cross-section
t	time
U	vertically averaged velocity of flow in Chapter 1
U	unperturbed vertically averaged flow velocity in Chapter 2
U(Z)	velocity distribution along a normal to the bed in Chapter 3
U_*	shear velocity
U^*	dimensionless flow velocity
u	magnitude of velocity vector
u_1	longitudinal component of vertically averaged velocity in Appendix II; also denotes dimensionless form of same
u_2	lateral component of vertically averaged velocity in Appendix II; also denotes dimensionless form of same
u_i'	perturbed velocity vector
$\hat{u}_1$	velocity coefficient in equations AII.9
$\hat{u}_2$	velocity coefficient in equations AII.9
x_1	longitudinal distance
x_2	lateral distance
y	lateral distance, Chapter 3
Z	distance normal to bed

Z_o	height of flume exit weir above datum
α	coefficient in equation 3-5
α_1	coefficient in equation 1-18
α_2	coefficient in equation 1-18
β	dimensionless sediment transport rate in Appendix II
γ	coefficient in equation 3-10
δ	stress depth
δ_{ij}	Kronecker delta
ϵ_1	ratio of width of bank region to total width in Chapter 3
ϵ_2	an estimate of lateral channel bed curvature in Chapter 3
ϵ^*	parameter defined in equation 2-1
η	dimensionless lateral distance in Chapter 3
η	dimensionless bed height perturbation in Appendix II
η	coefficient in Appendix III
η_o	dimensionless amplitude of bed height perturbation
η_E	effective value of η in Appendix IV
η_w	wall value of η in Appendix IV
θ	parameter defined in Chapter 3
λ	longitudinal meander or braid wave length
λ_A	Anderson meander wave length scale
λ_{A1}	First form of modified Anderson wave length scale
λ_{A2}	Second form of modified Anderson wave length scale
λ_H	Hansen meander wave length scale
λ_T	a meander wave length scale
λ_W	Werner meander wave length scale
μ	coefficient of static Coulomb friction for submerged sediment
ν	kinematic viscosity of water
ξ	coefficient in equation 3-3

ξ	coefficient in Appendix III
ξ_E	effective value of ξ in Appendix IV
ξ_w	wall value of ξ in Appendix IV
π	3.14159...
ρ	fluid density
ρ	dimensionless lateral distance
ρ_s	sediment density
Σ	magnitude of the vector Σ_i
Σ_i	generalized slope vector in Appendix II
σ	standard deviation of sediment size distribution in Chapter 2
σ	dimensionless stress depth in Chapter 3
σ	coefficient in Appendix IV
σ_c	critical dimensionless bed stress depth
σ_{cB}	critical dimensionless bank stress depth
σ_o	coefficient in the asymptotic expansion 3-9
σ_1	coefficient in the asymptotic expansion 3-9
σ_2	coefficient in the asymptotic expansion 3-9
$\tilde{\sigma}_o$	coefficient in the asymptotic expansion 3-7
$\tilde{\sigma}_1$	coefficient in the asymptotic expansion 3-7
$\tilde{\sigma}_2$	coefficient in the asymptotic expansion 3-7
τ	bed stress
τ^*	Shields stress
τ_G^*	Shields grain stress
τ_c^*	critical Shields stress
τ_B^*	bank full Shields stress
τ_o	unperturbed bed stress
τ_1	longitudinal component of bed stress
τ_2	lateral component of bed stress

τ_i'	perturbed bed stress vector
Φ_w	functional notation in equation 1-13
Φ_o	functional notation in equation 2-2
Φ_1	functional notation in equation 2-3
ϕ	complex wave celerity in Appendix II
ϕ_i	imaginary part of ϕ, also called coefficient of instability
ϕ_r	real part of ϕ
φ^*	coefficient defined in Chapter 2
ϕ_1	functional notation in equation 1-7
ϕ_2	functional notation in equation 1-8
$\tilde{\phi}_1$	functional notation in equation 1-5
$\tilde{\phi}_2$	functional notation in equation 1-6
ψ	ratio of grain stress to total stress in Engelund's relations
ψ	function in Chapter 3
$\bar{\psi}$	coefficient in Appendix III
Ω	depth-width ratio
Ω_B	bank full depth-width ratio

CHAPTER 1

FLOW IN STRAIGHT ALLUVIAL CHANNELS

1.1 Introduction

Fluvial bank erosion is closely related to the sediment transport and channel resistance aspects of river hydraulics. Consequently, the processes which lead to the establishment of stable, non-eroding banks are presumably explainable in the context of sediment hydraulics.

Most of the past research in sediment hydraulics has been concerned with the determination of sediment load and resistance in channels with non-erodible banks, such as in the laboratory flumes of Vanoni and Brooks (1957).* Thus "bed" processes are perhaps better understood than "bank" processes. An explanation of "bank" processes must be predicated on an understanding of "bed" phenomena.

The field of fluvial hydraulics is fraught with conflicting theories that have existed side-by-side for decades in the absence of conclusive evidence. On the other hand researchers who have offered different explanations of certain bed phenomena have failed to realize the underlying equivalence of the various theories. Further progress depends upon the development of general principles that will unify river hydraulics as a whole.

In this chapter an attempt is made to develop a more complete framework for the specification of alluvial river flow within which existing and future sediment transport and resistance relations can be expressed. Initially a formulation for bed processes, which ignores banks altogether, is developed. This is then extended to the case of erodible banks. The treatment for bed processes is a generalization of (and owes much to) previous treatments by, for example, Yalin (1964), Alam, Cheyer, and Kennedy (1966), Willis and Coleman (1969), Ashida and Michiue (1972), Vanoni (1974), and Peterson (1975).

1.2 The Formal Alluvial River

The interaction of water and sediment has traditionally been investigated in terms of an abstraction, consisting of two-dimensional (longitudinal and vertical) uniform, steady flow over a bed consisting of statistically uniform, non-cohesive erodible material (Fig. 1-1). For such a flow, channel width is infinite and need not be considered; thus bed processes are isolated from bank processes. Rivers fulfilling the above restrictions do not exist in

*For Chapter 1 references see pages 14-15.

nature, so they are termed "formal alluvial rivers" herein.

The formal alluvial river is approximately realized in laboratory flumes with solid walls, and in straight reaches of rivers and canals which have complete bank protection, with the restriction that the depth-width ratio be small enough to render bank effects negligible. When bank effects are not negligible, a correction for bank influences can be made using, for example, Johnson's (1942) method, which has experimental support (Williams, 1970).

1.3 Parameters

The pertinent variables of formal river hydraulics are water discharge per unit width q, vertically averaged flow velocity U, flow depth D, water surface slope S, bed stress τ, sediment discharge per unit width q_s, typical sediment diameter D_s, sediment and water density ρ_s and ρ, water kinematic viscosity ν, acceleration of gravity g, and various dimensionless sediment shape, size distribution, and porosity factors P_i, $i = 1,2,3,\ldots$ The first five quantities represent averages over irregularities due to bed forms. Note that channel width B, being infinite, need not be included.

There are twelve parameters in the above list (P_i is counted once as a vector parameter). Either more or fewer parameters could be included, requiring the application of more or fewer constraints henceforth. The above list is considered to be both brief and basic.

1.4 Non-Dimensional Groupings

Dimensional analysis is used to reduce the parameter list. The method, of course, provides no new physical information, but rather determines the minimum list that need be considered without loss of generality. From the twelve dimensional parameters, exactly nine independent dimensionless groupings can be formed; within these bounds the specific parameters are arbitrary. The following list is chosen herein.

$$\tilde{q} = \frac{q}{\sqrt{rg D_s}\, D_s}$$ dimensionless discharge per unit width

$$r = \left(\frac{\rho_s}{\rho} - 1\right)$$ sediment buoyancy parameter

$$\tau^* = \frac{\tau}{\rho r g D_s}$$ Shields stress

$$R = \frac{D}{D_s}$$ relative roughness

$S =$	slope
$q^* = \frac{q_s}{\sqrt{rgD_s}\,D_s}$	Einstein sediment discharge
$C = \frac{\tau}{\rho U^2}$	friction factor (resistance coefficient)
$R_P = \frac{\sqrt{rgD_s}\,D_s}{\nu}$	particle Reynolds number
$P_i =$	sediment factors (e.g. standard deviation)

All of these parameters, in addition to a host of others that can be formed from them (e.g. Froude number), have been used previously by various investigators. Note that the Shields stress, the friction factor, and the relative roughness have not been divided into grain and bed form components; also sediment discharge has not been divided into bed and suspended load. Such differentiations are not necessary for the treatment herein, although they can be included consistently if desired.

1.5 General Constraints: Load and Resistance Relationships

The specification of constraints on the dimensionless variables allows for further reduction. Constraints are of two types: universal and specific. Two universal constraints are those imposed by mass and momentum conservation of the water; $q = UD$ and $\tau = \rho gDS$, or in dimensionless form

$$\tilde{q} = \sqrt{(\tau^*/C)}\,R \qquad (1\text{-}1)$$

$$\tau^* = RS/r \qquad (1\text{-}2)$$

Thus two parameters can be eliminated from the non-dimensional list; they are arbitrarily chosen to be R and $\tilde{q}$.

Two additional universal constraints express the behavior of the water and sediment interaction. They are commonly termed bed resistance and sediment transport rate relationships, and from the standpoint of continuum mechanics are the appropriate constitutive relationships of water-sediment flow. The most general forms for these constraints are

$$f_B\,(C,\ q^*,\ \tau^*,\ S;\ R_P,\ r,\ P_i) = 0 \qquad (1\text{-}3)$$

$$f_Q\,(C,\ q^*,\ \tau^*,\ S;\ R_P,\ r,\ P_i) = 0 \qquad (1\text{-}4)$$

Eliminating C and q^* in the above relationships reduces them to

$$C = \tilde{\Phi}_1\,(\tau^*,\ S;\ R_P,\ r,\ P_i) \qquad (1\text{-}5)$$

$$q^* = \tilde{\Phi}_2\,(\tau^*,\ S;\ R_P,\ r,\ P_i) \qquad (1\text{-}6)$$

The semicolons have been inserted to indicate that the three parameters to the right of them are completely determined by the type of sediment used and temperature. (Note that non-cohesive sediment only is considered).

The fact that rivers are observed to behave in a systematic fashion indicates that relationships (1-5) and (1-6) must exist. It is not, however, necessary that the relationships be single-valued, and indeed in the transition regime (Froude number $F = \frac{U}{\sqrt{gD}} \sim 1$) there is reason to suspect double-valued behavior.

Although the above relationships are of the most general form, other parameters could have been used. The Shields stress has been used simply to facilitate comparison with previous relationships. However many investigators (e.g. Maddock, 1969) have claimed that bed resistance or sediment transport correlates better with velocity than with bed stress. Both modes of expression are consistent in the context of the present analysis. If a dimensionless average velocity $U^* = \frac{U}{\sqrt{rgD_s}}$ is defined, equations (1-5) and (1-6) can be transformed, using equations (1-1) and (1-2), into

$$C = \Phi_1\,(U^*,\ S;\ R_P,\ r,\ P_i) \qquad (1\text{-}7)$$

$$q^* = \Phi_2\,(U^*,\ S;\ R_P,\ r,\ P_i) \qquad (1\text{-}8)$$

The parameters τ^* and S could also have been replaced by q and F, for example, in a completely consistent fashion. It is this flexibility of the constitutive equations that can bring unity to the variety of relationships available in the literature.

The generality of the above relationships is however in marked contrast to most of the relationships that exist in the literature, which try to relate q^* and C to a single parameter, usually the Shields stress. For example, consider the Einstein-Brown (Brown, 1950) bed load relationship. It has the form

$$q^* = 40A^3$$

where $A = P\tau^*_G$, G refers to grain stress, and P is a function of R_p. This relationship gives q^* as a function of two parameters where five are required in general, and furthermore it assumes some kind of similarity to reduce them to a single variable. Such fortuitous circumstances are indeed conceivable, but the relatively poor predictive quality of this relationship and other similar relationships suggests otherwise.

The fact that the relationship for bed resistance and sediment transport occur as a pair should be noted. A consistent treatment must include the two together.

1.6 Formal River Flow Relationships

The parameters τ^* and C can be eliminated from equations (1-5) and (1-6) using equations (1-1) and (1-2). The resulting relationships can be expressed in the form

$$S = \tilde{f}_1 (\tilde{q}, R; R_p, r, P_i) \qquad (1\text{-}9)$$

$$C_s = \tilde{f}_2 (\tilde{q}, R; R_p, r, P_i) \qquad (1\text{-}10)$$

where $C_s = (1 - C_s) \dfrac{(r+1)^{q^*}}{\tilde{q}} = \dfrac{(r+1)^{q^*}}{\tilde{q}}$

is the concentration by weight of sediment material in transport. (The approximation is valid for most cases of practical interest.) A format similar to the above was first suggested by Peterson (1975).

If equations (1-9) and (1-10) are known, for example in graphical form, and if bed material and temperature are specified, then specification of any two of the parameters $\tilde{q}$, C_s, R, and S is enough to allow for calculation of the other two.

Most existing load and resistance equations are cumbersome, and in cases of practical interest an iterative procedure must be employed. However, any pair of load and resistance relationships can be reduced to the form of equations (1-9) and (1-10). A comparison with laboratory flume data or the prediction of flume and river behavior is then a direct calculation.

1.7 Specific Constraints

Four general constraints on the nine original variables have been delineated. A complete specification of the flow requires five more constraints.

Specification of the type of sediment on the bed and the water temperature provides a determination of r, R_p, and P_i. These constraints are specific in that they vary from flume to flume and from river to river. Two more specific constraints are required to make the problem determinate.

In the case of the laboratory sediment-feed flume (as an approximation to the formal river) appropriate values of $\tilde{q}$ and q^* (and thus $\tilde{q}$ and C_s) are selected by the operator. From equations (1-9) and (1-10) the as yet unknown equilibrium slope S and relative roughness R can be calculated

In a recirculating flume with an outlet weir of constant elevation, conservation of sediment material can be used to show that, in addition to $\tilde{q}$, S is also predetermined, allowing for a calculation of the unknowns R and C_s. In another type of recirculating flume, $\tilde{q}$ and R are predetermined, and the unknowns C_s and S can be calculated from equations (1-9) and (1-10).

In the case of the wide natural river of assumed constant width, the constraints take a more complex form. In principle the value of $\tilde{q}$ at a section of a river is determined by that fraction of the precipitation occurring in the watershed above the section which appears as runoff. Furthermore q^* is determined by the rate of watershed denudation caused by runoff. However, discharge $\tilde{q}$ and slope S are two fluvial parameters that can be determined with relative ease. The time scales associated with watershed denudation or tectonic lifting are so large that for many purposes, including the analysis of meandering and braiding, it is sufficient to consider the discharge $\tilde{q}$ and the river channel slope S as specific constraints.

Thus for natural rivers equations (1-9) and (1-10) take a most interesting and useful form. For a given river it is known that the energy slope varies little from S even during floods, and can be assumed to be known. Equation (1-9) provides a discharge-depth relationship and equation (1-10) a discharge-load relationship from which flood stage and other characteristics can be obtained directly from information concerning discharge.

1.8 Simplification and Evaluation

Equations (1-9) and (1-10) can be evaluated explicitly and accurately using laboratory and field data. Once evaluated, both a practical tool and a

basis for comparison of the results of theoretical and semi-theoretical derivations is available. Both equations contain six variables, but some simplification seems warranted. The alluvial material in most laboratory flumes and in nearly all rivers has a specific gravity of 2.65; thus r can be taken to be a constant equal to 1.65. Another reasonable assumption is that the parameters P_i have a negligible effect on other flow characteristics. This approximation is supported in the case of the standard deviation of the sediment size distribution by Vanoni and Brooks (1957), but is probably not completely accurate. Indeed, in the cases of aggradation and degradation, not considered herein, the assumption would be untenable. However, for equilibrium flows with sediment which has at least a roughly Gaussian size distribution, the deviations in flow pattern due to two different distributions with the same average diameter is apparently small.

Equations (1-9) and (1-10) then reduce to

$$S = f_1 (\tilde{q}, R; R_p) \qquad (1\text{-}11)$$

$$C_s = f_2 (\tilde{q}, R; R_p) \qquad (1\text{-}12)$$

In this form they can be expressed graphically by the use of observed data. This has not been done to date due to the lack of sufficient data, and in particular the lack of sediment transport data from natural rivers. However, it can be expected that the necessary information will be available in the near future. (See the compendium of over 6,000 sets of data from rivers, canals, and laboratory flumes of Peterson and Howells, 1973).

1.9 Examples of Formal River Flow Graphs

Any pair of load and resistance equations can be cast in the form of equations (1-11) and (1-12). As an example, Peterson's (1975) diagrams are presented in Figs. 1-2a through 1-2j in which C_s and S are given as contour functions of $\tilde{q}$ and R for a specific range of values of R_p. As a practical matter $R_p = \frac{\sqrt{rgD_s}D_s}{\nu}$ has been replaced by particle diameter D_s, because much of the data lacks the temperature information necessary to calculate ν. The graphs were determined by fitting equations of the form

$$\tilde{q} = K_1 R^{m1} S^{n1}$$

$$\tilde{q} = K_2 R^{m2} C_s^{n2}$$

to the data of Peterson and Howells (1973). The constraints K_1, K_2, m_1, m_2, n_1, and n_2 are found to be functions of D_s, as given in Fig. 1-3.

The enormous amount of data used to determine the Peterson graphs insures that they are at least roughly accurate over most of the range of river parameters and in this respect are superior to relationships which have been evaluated by use of flume data and extrapolated to field conditions. However, it appears that the form of the assumed equations is too simple to account for some observed river phenomena that have been well-documented in the laboratory, such as transition effects and a general tendency for the lines of constant C_s to crowd as R decreases. This will be discussed in greater detail later.

Engelund's (1967) similarity theory of sediment transport is one of the more advanced semi-theoretical approaches in that both resistance and load relationships are derived together. His analytical relationships apply to lower-regime flow with dune (rather than ripple) resistance. They may be expressed in the form

$$\psi_r^* = .06 + .4\, r^{*2}$$

where ψ_r^* is grain stress, ψ is defined by

$$(C\psi)^{-1/2} = 6 + 2.5\, \ell n\, (\psi R/2.5)$$

and

$$Cq^* = 0.05\, r^{*5/2}$$

When plotted as formal river flow relationships in Fig. 1-4, only a single page is required because of the absence of the particle Reynolds number R_p. This is partly because the equations do not apply to the two transitional regimes from smooth to rough flow and from lower to upper regime. However, a comparison with Peterson's equations shows that even in the hydraulically rough regime where dune resistance is to be expected, the parameter R_p plays an important role and thus cannot be ignored in its entirity. On the other hand, the laboratory-verified tendency for lines of constant concentration to crowd together at low values of R or $\tilde{q}$ shows clearly on the Engelund plot but is absent from the Peterson plots. The latter also fails to delineate critical conditions for sediment movement.

A third example was constructed by combining the graphical resistance relationships of Alam, Cheyer, and Kennedy (1966) with the Meyer-Peter and Muller (1948) load relationship, which was arbitrarily modified to account for variation in the critical Shields stress with particle Reynolds number. The load relationship

is $$q^* = 8\,(\psi\tau^* - \tau_c^*)^{3/2}$$

where τ_c^* is given as a function of R_P in Fig. 1-5. This figure is essentially equivalent to the modified Shields diagram given by Gessler (1971). Alam et al. divide the friction factor C into a component due to grain stress, ψC, and a component due to bedform stress, $(1 - \psi)C$. They use the relationship

$$(8\psi C)^{-1/2} = -2 \log_{10} \left(\frac{1}{14.8R} + \frac{2.51}{\sqrt{8\psi C}\, 4\tilde{q} R_P}\right)$$

for grain stress and provide a graphical plot of $(1 - \psi)C$ as a function of R and U^*. It can be shown that for sufficiently large values of R_P the dependence of C on R_P becomes negligible, and behavior rather similar to the Engelund graph results. The Alam et al. resistance relationship apply only to sand-bed rivers with values of D_s between .088 and .930 mm. For this reason a single graph was calculated, with $R_P = 29$, (D_s = .37 mm at 20°C) which appears as Figure 1-6. The character of the curves of constant S is a result of their being determined directly from actual data rather than through curve-fitting. The double-valued behavior of the curves at high slopes (for $S = 2 \times 10^{-3}$ and $\tilde{q} = 8 \times 10^3$, two values of R, 5.6×10^2 and 8×10^2, exist) appears to reflect transition from lower (dune) to upper (antidune) regime.

1.10 The Self-Formed Non-Cohesive River

The above results apply strictly to a river of infinite width. A similar analysis may be made for a real river with finite width and with banks and bed composed of non-cohesive material of a statistically homogeneous size distribution. The method is completely general, in an attempt to provide a framework for graphical solution of the flow in such channels.

Longitudinally uniform, steady-state flow in a straight river channel with the above characteristics is considered. Since the banks are erodible, they may be altered by the flow. For given hydraulic conditions it may be surmised that among all the cross-sections that will carry the required sediment load without eroding the banks, the cross-section with minimum width is somehow uniquely determined.

It is commonly assumed that discharges close to bank full are those most effective in determining channel geometry. Discharges smaller than the bank full range presumably have less erosive power. Discharges greater than bank full

encourage deposition as well as erosion. Thus bank full discharges appear to have the greatest erosive power with respect to the total channel geometry, and it can be expected that bank erosion or deposition will occur until a geometry that is stable at bank full flow eventually develops. Since no further bank erosion will then occur, the developed width can be expected to be close to the minimum necessary to provide long-term balance in the river. The problem, in terms of primary bank erosion, becomes that of finding the channel geometry which is just stable at bank full discharge.

1.11 The Width Relationship

The fact that the banks are composed of erodible material introduces an extra degree of freedom when compared with formal river hydraulics. Thus, the list of nine dimensionless parameters presented earlier, τ^*, q^*, $\tilde{q}$, R, S, C, r, R_P, and P_i, must be increased by one, the depth-width ratio, $\frac{D}{B} = \Omega$. Likewise, if the problem of specifying the width of the channel is to be determinate, an additional constraint must exist. The dimensionless variables can be reduced in a fashion that is analogous to formal channel flow, so that the most general form of the width relationship is

$$\Omega_B = \Phi_W \left(\tau_B^*, S; R_P, r, P_i \right) \qquad (1\text{-}13)$$

where the subscript B indicates that τ^* and Ω are to be evaluated at bank-full conditions.

Nearly all non-cohesive rivers are wide ($\Omega < 10^{-1}$) so that the banks have negligible effect on the bed and equation (1-13) can be used directly in conjunction with equations (1-5) and (1-6) evaluated at bank full conditions and with values of depth, discharge, and sediment load that have been cross-sectionally averaged.

1.12 Flow Relationships for Self-Formed, Non-Cohesive Channels

Since width is an unknown, total discharge of water and sediment Q and Q_s are more meaningful parameters than the values per unit width. Dimensionless total water and sediment discharges are defined to be

$$\tilde{Q} = \frac{Q}{\sqrt{r g D_s}\, D_s^2} \qquad \text{and} \qquad Q^* = \frac{Q_s}{\sqrt{r g D_s}\, D_s^2}$$

The dimensionless mass balance equation (1-1) is expressed in the form

$$\tilde{Q}_B = \frac{R_B^2 \tau_B^{*1/2}}{\Omega_B C_B^{1/2}} \tag{1-14}$$

where the subscript B indicates that R, C and C_s (equation 1-16) are to be evaluated at bank full conditions. Between equations (1-2), (1-5), (1-6), (1-13), and (1-14) it can be seen that resistance, load, and width relationships can be cast in the forms

$$S = f_1 (\tilde{Q}_B, R_B; R_P, r, P_i) \tag{1-15}$$

$$C_{sB} = f_2 (\tilde{Q}_B, R_B; R_P, r, P_i) \tag{1-16}$$

$$\Omega_B = f_3 (\tilde{Q}_B, R_B, R_P, r, P_i) \tag{1-17}$$

where again the relationship may be multi-valued. It is then possible to specify, at least in principle, the relationship between bank full geometry and discharge. Neither sufficient data nor plausible theory exists at present which would provide a general and useful determination of these relationships, the best attempt perhaps being regime theory. However, a tentative approach to the problem will be presented in Chapter 3.

1.13 Specific Constraints for Self-Formed, Non-Cohesive Rivers

Mass and momentum balance, and load, resistance, and width relationships provide five constraints on the ten variables. As before, if sediment characteristics and temperature are known in the case of specific rivers, then r, R_P, and P_i are known.

In the case of a laboratory sediment-feed flume with an erodible-bank channel, $\tilde{Q}_B$ and Q_B^* (or equivalently $\tilde{Q}_B$ and C_{sB}) are arbitrary and thus provide the two final constraints.

An erodible-bank recirculating flume presents a different problem. If it is assumed that the flume has a constant-elevation outflow weir, but is free to aggrade or degrade at the inflow point, the appropriate constraint can be derived by realizing that sediment is conserved in the system. The constraint (derived in Appendix 1) is

$$B = B_I / [1 + (S_I - S)\, a_1] \tag{1-18}$$

or in dimensionless form

$$\frac{R_B}{\Omega_B} = \alpha_2 / [1 + (S_I - S)\,\alpha_1] \qquad (1\text{-}19)$$

where $\alpha_1 = L_f / 2\,D_{fI}$ and $\alpha_2 = B_I / D_s$, L_f is flume length, D_{fI} is the initial depth of the channel molded in the sand (not depth of flow), and B_I and S_I are initial channel width and slope, respectively.

If experiments in channels with erodible banks are provided with initial cross-sections that are narrower than the one which ultimately develops, then according to equation (1-18) if the width increases to a value $B_I + \Delta B$, then

$$\Delta S \simeq \frac{1}{\alpha_2} \frac{\Delta B}{B_I}$$

where $S = S_I + \Delta S$. Thus the constraint indicates that increased width should be accompanied by increased slope.

Approximate constraints for the natural non-cohesive river may be established on the assumption that bank full discharge Q_B and slope S are known.

Thus if equations (1-15) through (1-17) are known, enough constraints exist to enable a determination of bank full geometry and flow characteristics in straight, non-cohesive rivers. The major practical drawback at present is the lack of a good width relationship.

1.14 A Comparison of Sediment Feed and Recirculating Systems

Both recirculating and sediment-feed flumes have been used to provide laboratory approximations of natural rivers. It is clear that neither provides the same constraints that exist in nature. Furthermore, neither type is intrinsically superior to the other. The equivalence of the two methods is indicated by the fact that both cases are covered by the same universal constraints and can be solved using the same sets of equations [equations (1-9) and (1-10) for formal flow, and equations (1-15) through (1-17) for self-formed non-cohesive flow.] Rather, the two methods simply view different parts of the same totality.

In sediment-feed flumes the final result obtained is independent of the slope (or cross-sectional geometry if the banks are erodible) of the initial channel. Any excess sediment is eventually washed out of the system, and any sediment deficiency is eventually supplied from upstream. Thus initial slope, depth, or cross-sectional geometry do not affect the final result. However

the results obtained in recirculating flumes are highly dependent upon the initial conditions of the channel. In the case of formal flow, once the depth or slope is set, depending on the specific flume type, this value must be maintained no matter what other changes take place. In the case of self-formed non-cohesive flow, equation (1-19) shows that initial channel geometry will always affect the final results. To see this, consider a particle of sand eroded from the banks of the initial channel. If the flume was of the sediment-feed type, it would be eventually physically removed from the system. In recirculating flumes, this particle of sand from the banks of the initial channel remains on the bed of the channel, moving from place to place but never leaving the system, and thus in a sense the system "remembers" its initial state.

An examination of Fig. 1-6 illustrates a point of interest concerning the constraints on formal flow. It can be seen that if $\tilde{q}$ and R (or $\tilde{q}$ and C_s) are specified, then a unique solution exists for S and C_s (or S and R). However specification of $\tilde{q}$ and S does not always lead to unique solutions for R and C_s; in fact in the transition region it can be seen that two values of R and C_s exist.

1.15 Conclusion

A general framework has been developed for the solution of formal river and self-formed non-cohesive river flow. General derivations for resistance, load, and width relationships have been established. These relationships can be evaluated with data, and all existing empirical or semi-theoretical relationships that are dimensionally homogeneous can be cast in the general form in a way that facilitates comparison. The format leads to a direct graphical solution for such parameters as depth and sediment discharge.

It has been shown that enough constraints exist to specify solution sets, but that these solution sets are not necessarily unique. The meaning of the various specific constraints associated with flume type has been clarified.

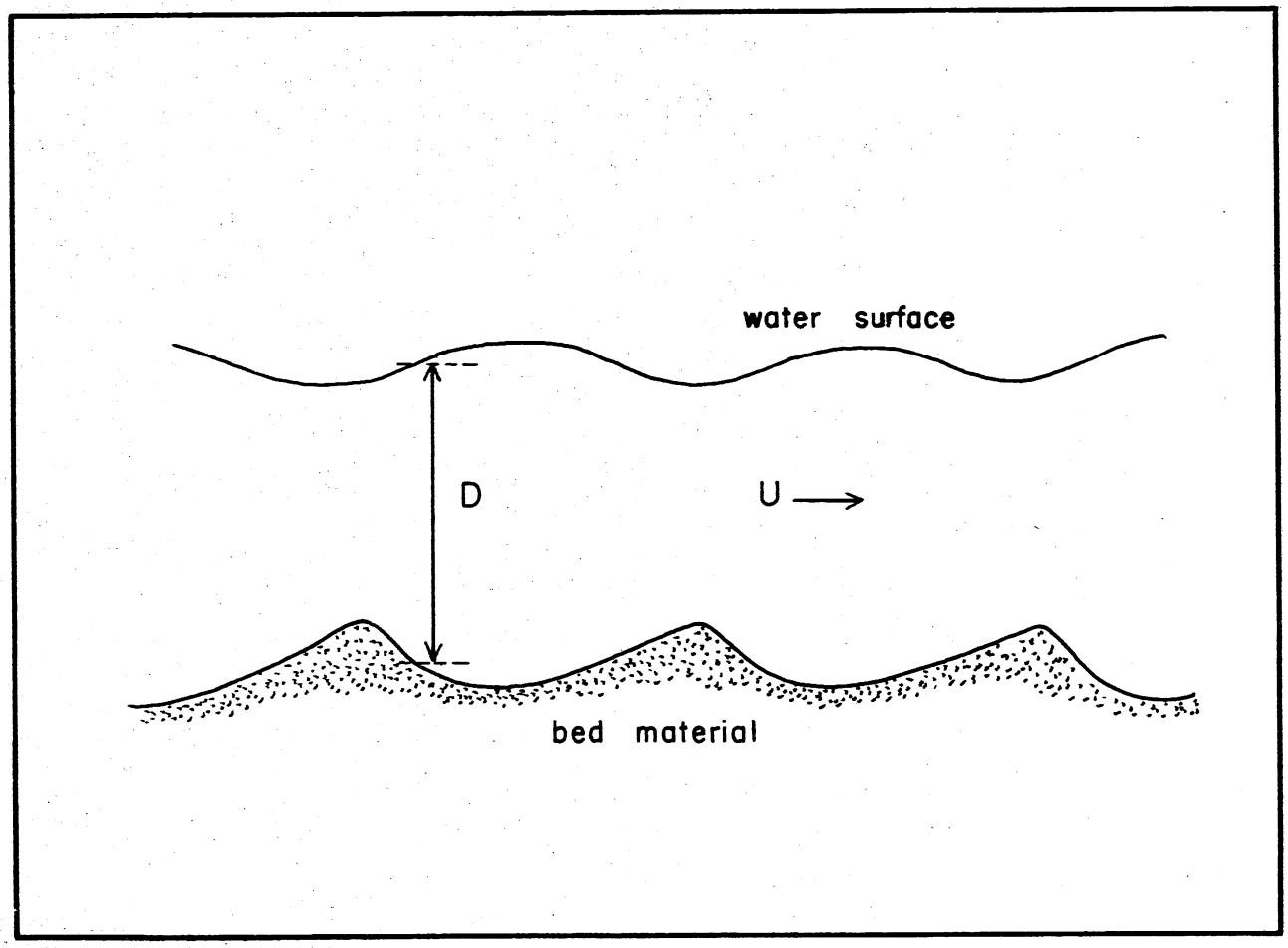

Fig. 1-1. A longitudinal cross-section of a formal alluvial river of infinite width. D is channel depth and U is vertically averaged flow velocity.

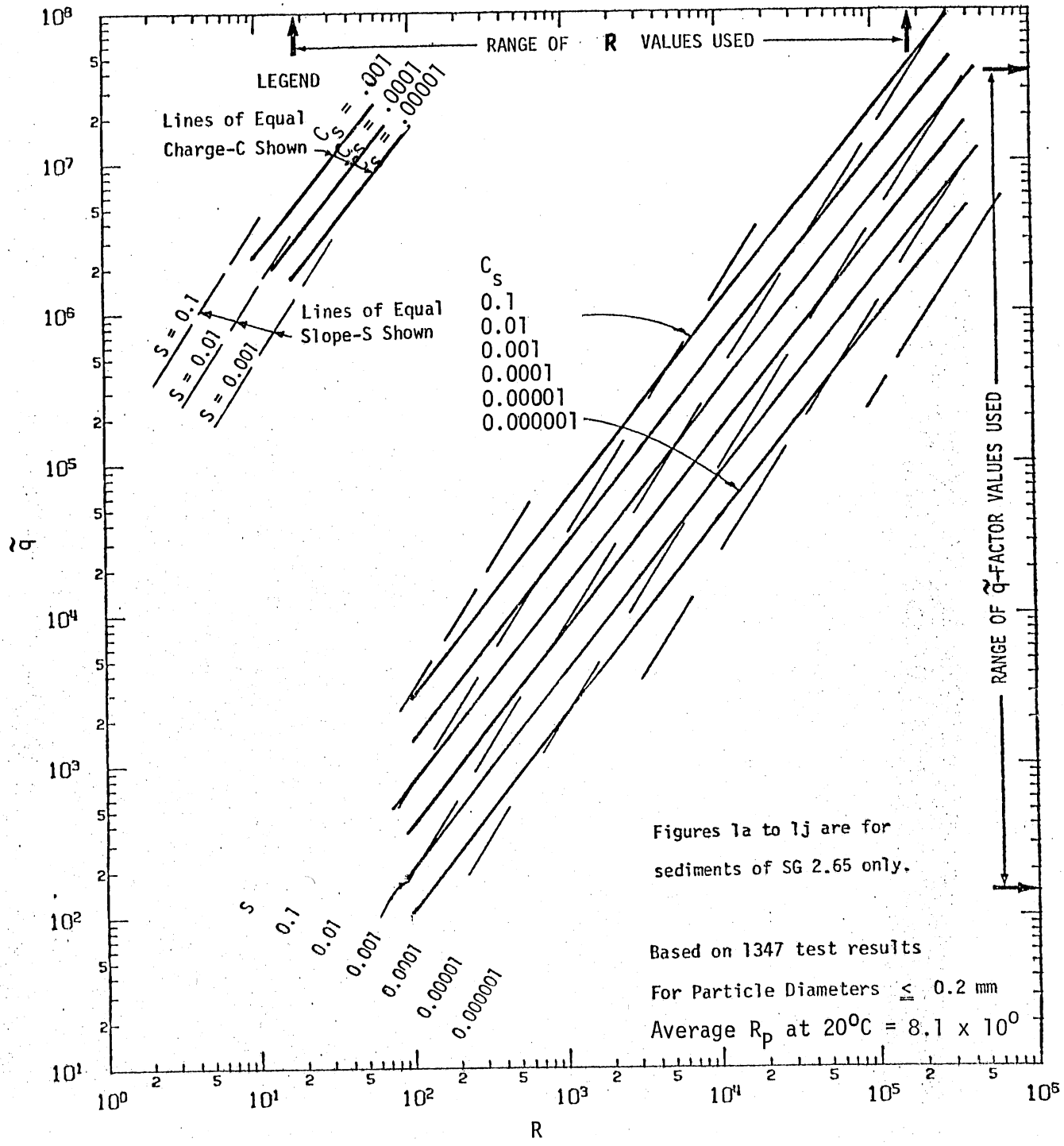

Fig. 1-2a. Peterson's (1975) preliminary $\tilde{q}$-R-S-C_s relationships.

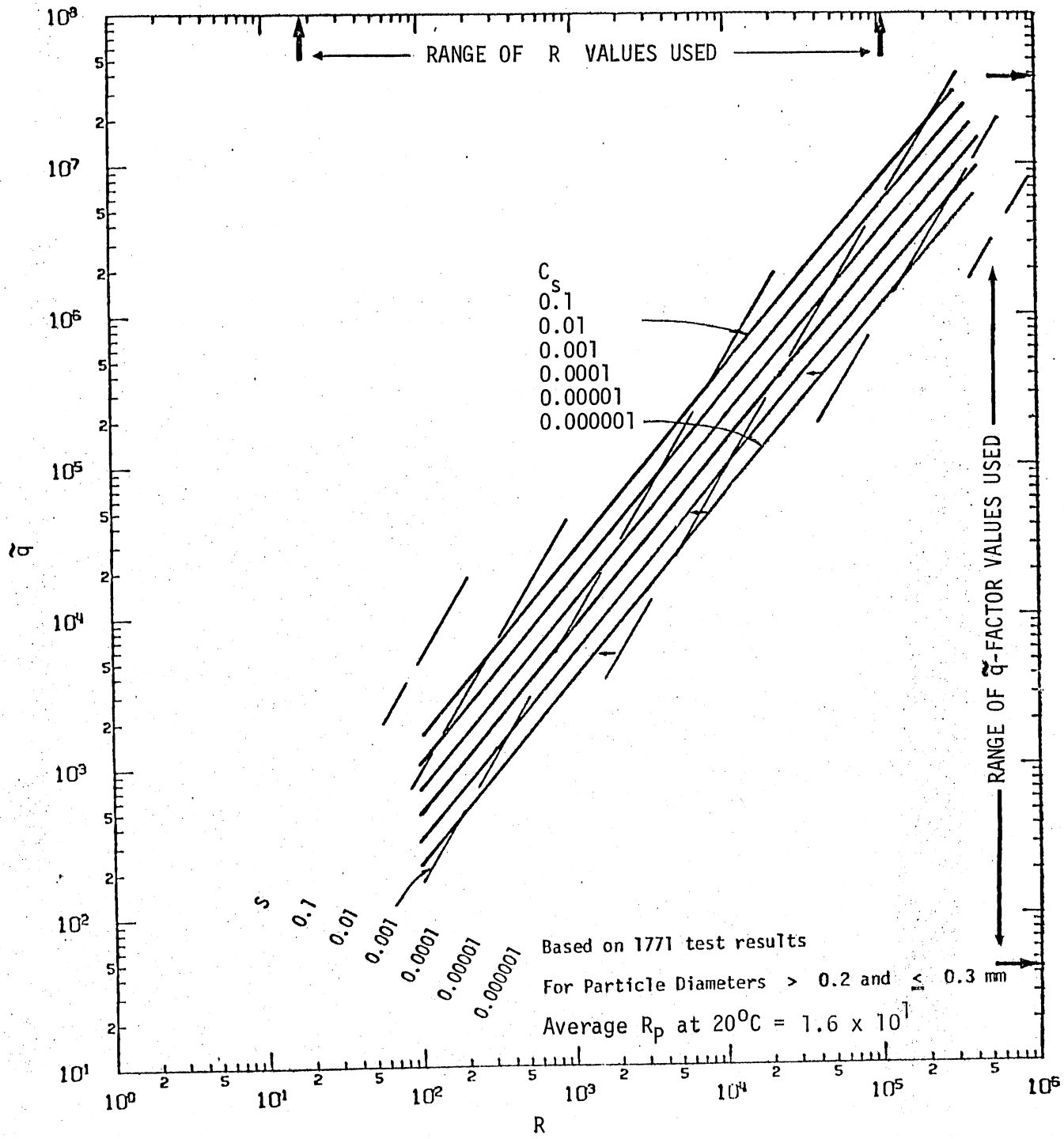

Fig. 1-2b. Peterson's (1975) preliminary $\tilde{q}$-R-S-C_s relationships.

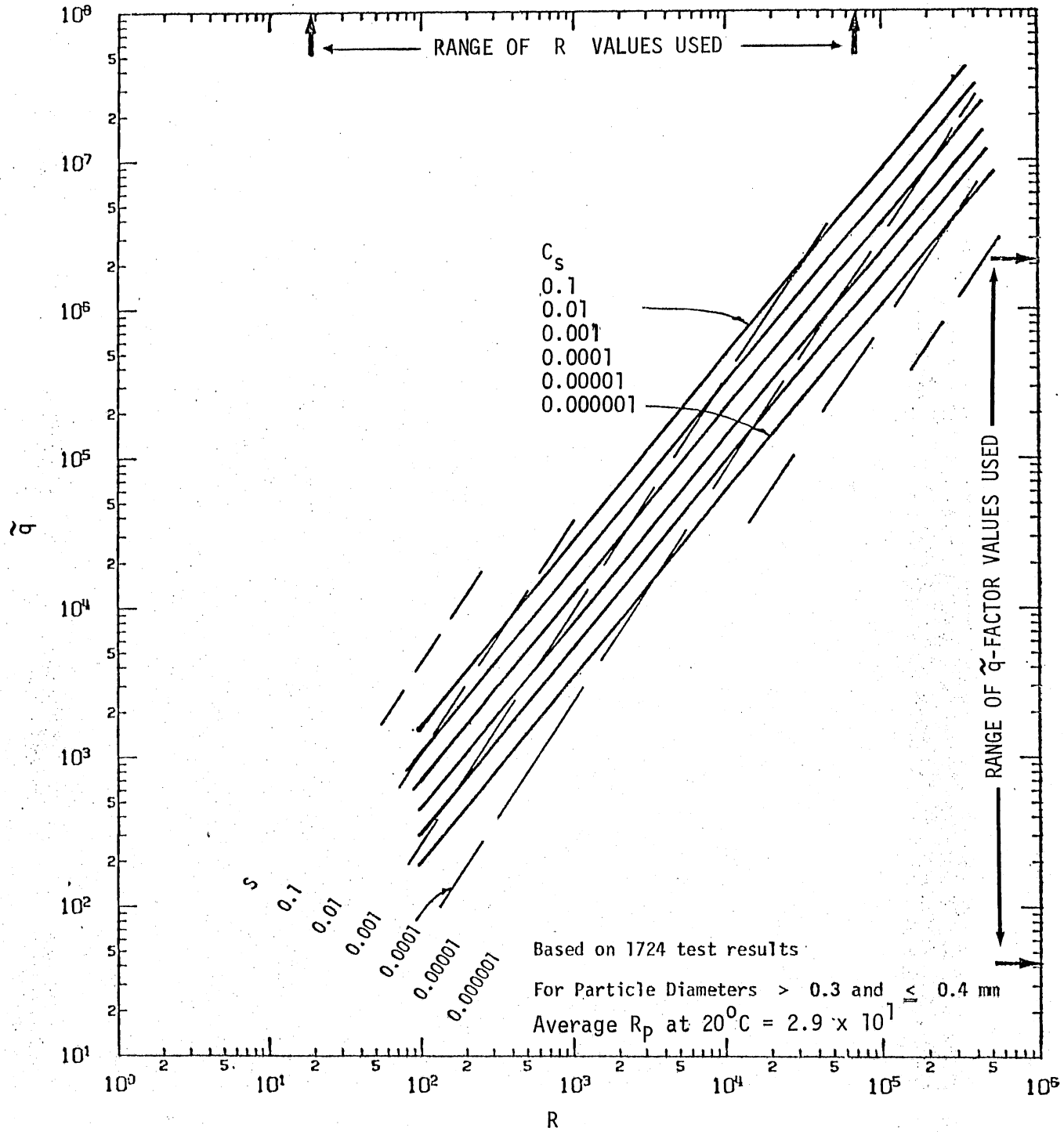

Fig. 1-2c. Peterson's (1975) preliminary $\tilde{q}$-R-S-C_s relationships.

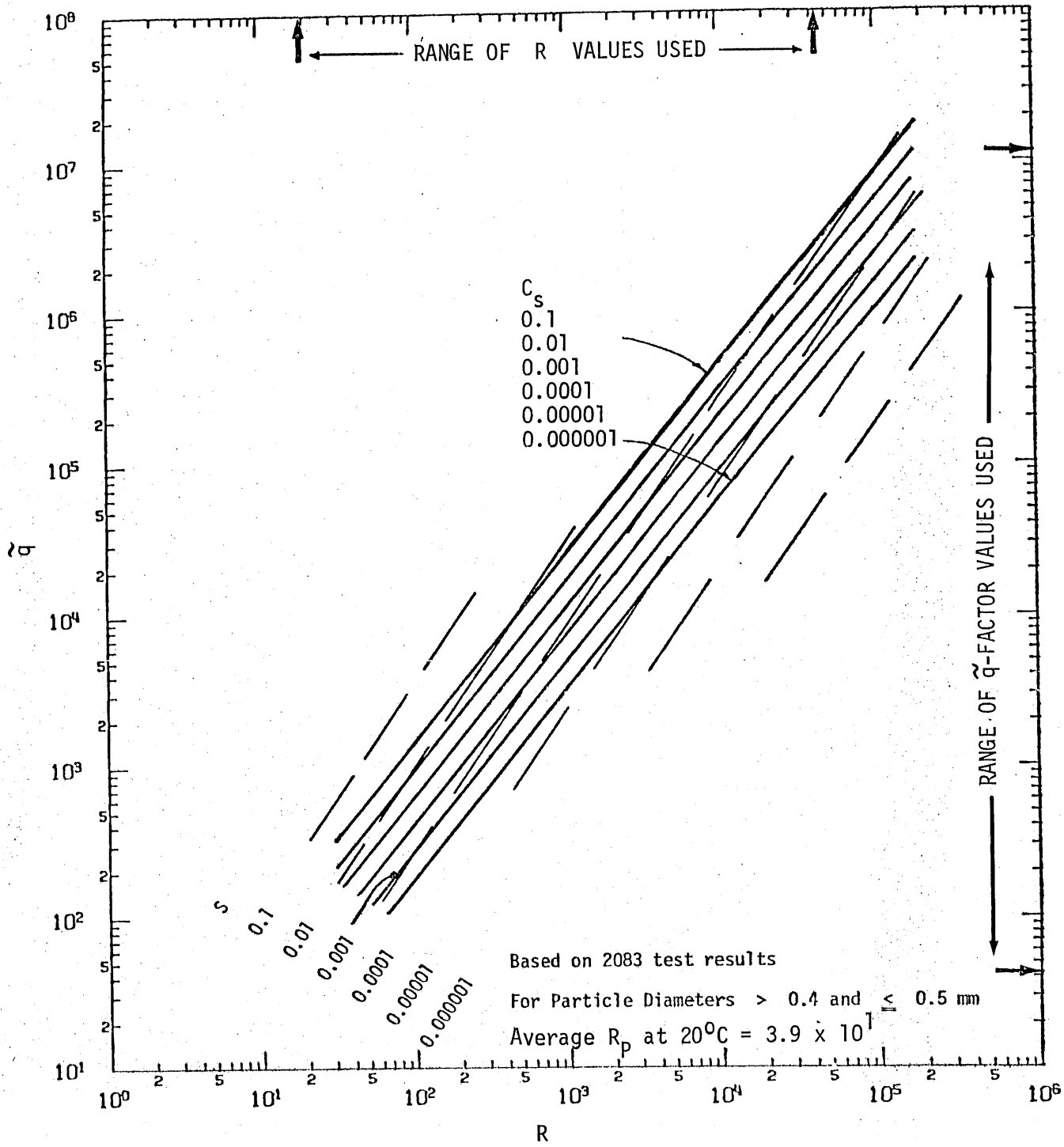

Fig. 1-2d. Peterson's (1975) preliminary $\tilde{q}$-R-S-C_s relationships.

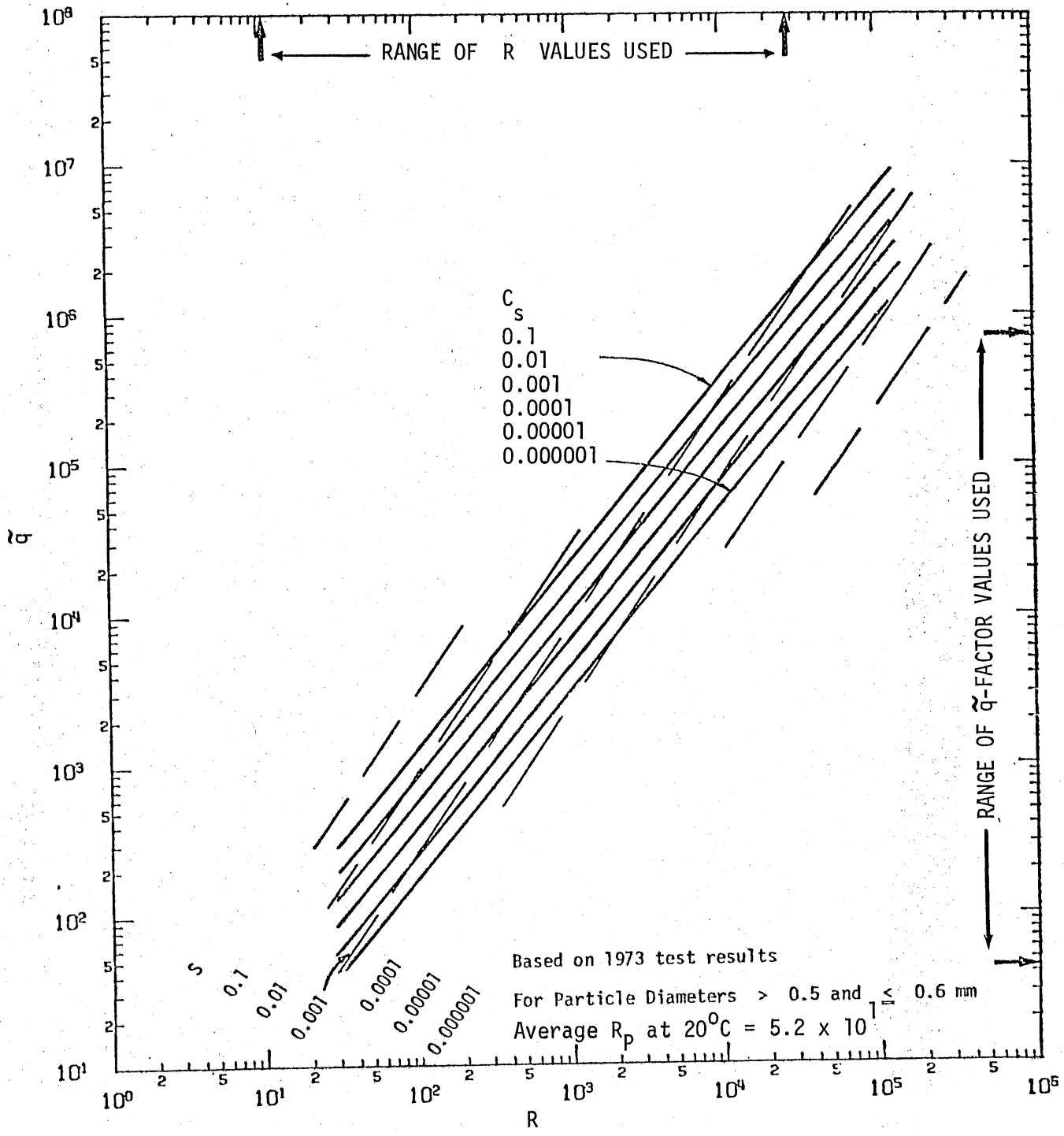

Fig. 1-2e. Peterson's (1975) preliminary $\tilde{q}$-R-S-C_s relationships.

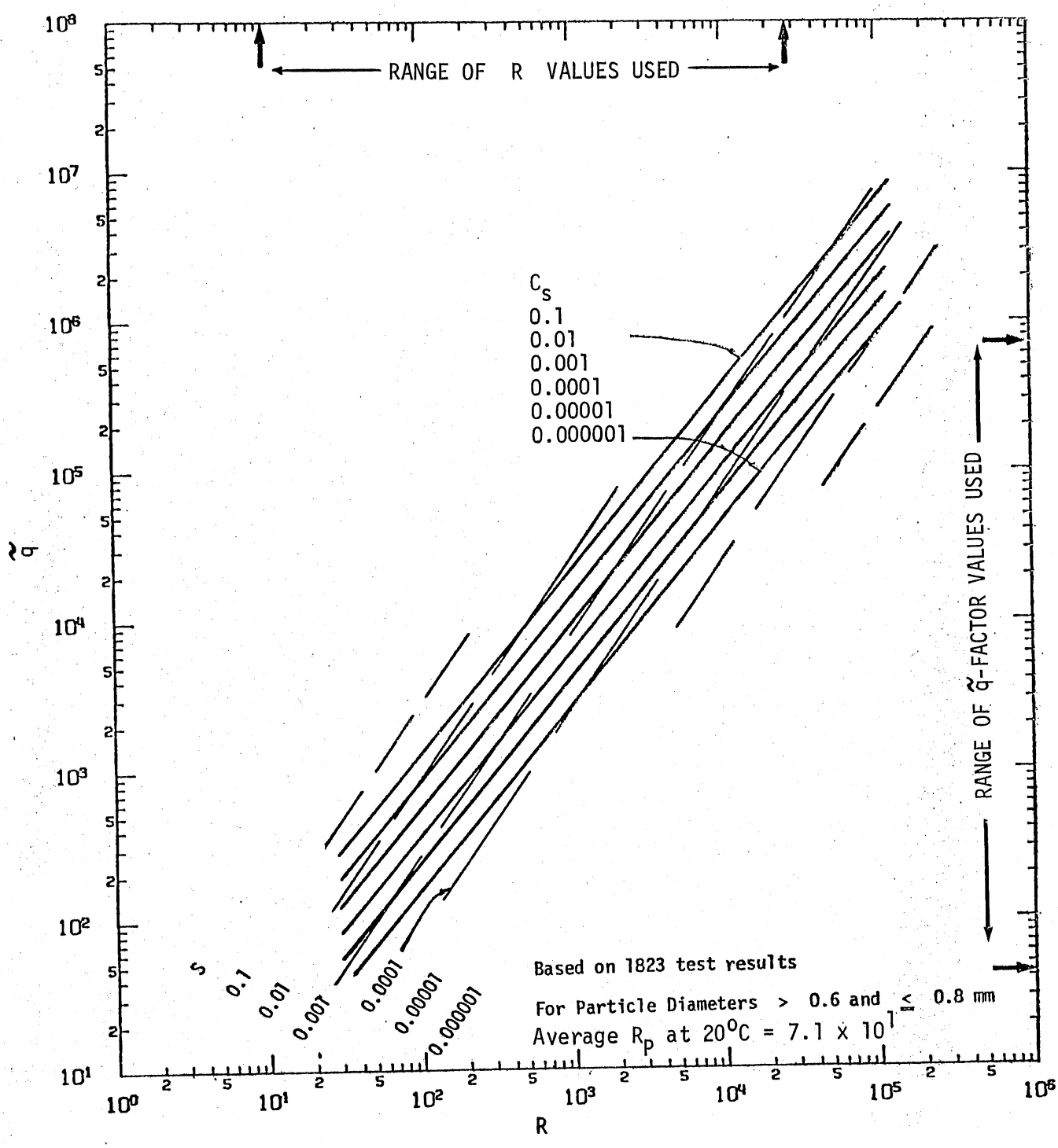

Fig. 1-2f. Peterson's (1975) preliminary $\tilde{q}$-R-S-C_s relationships.

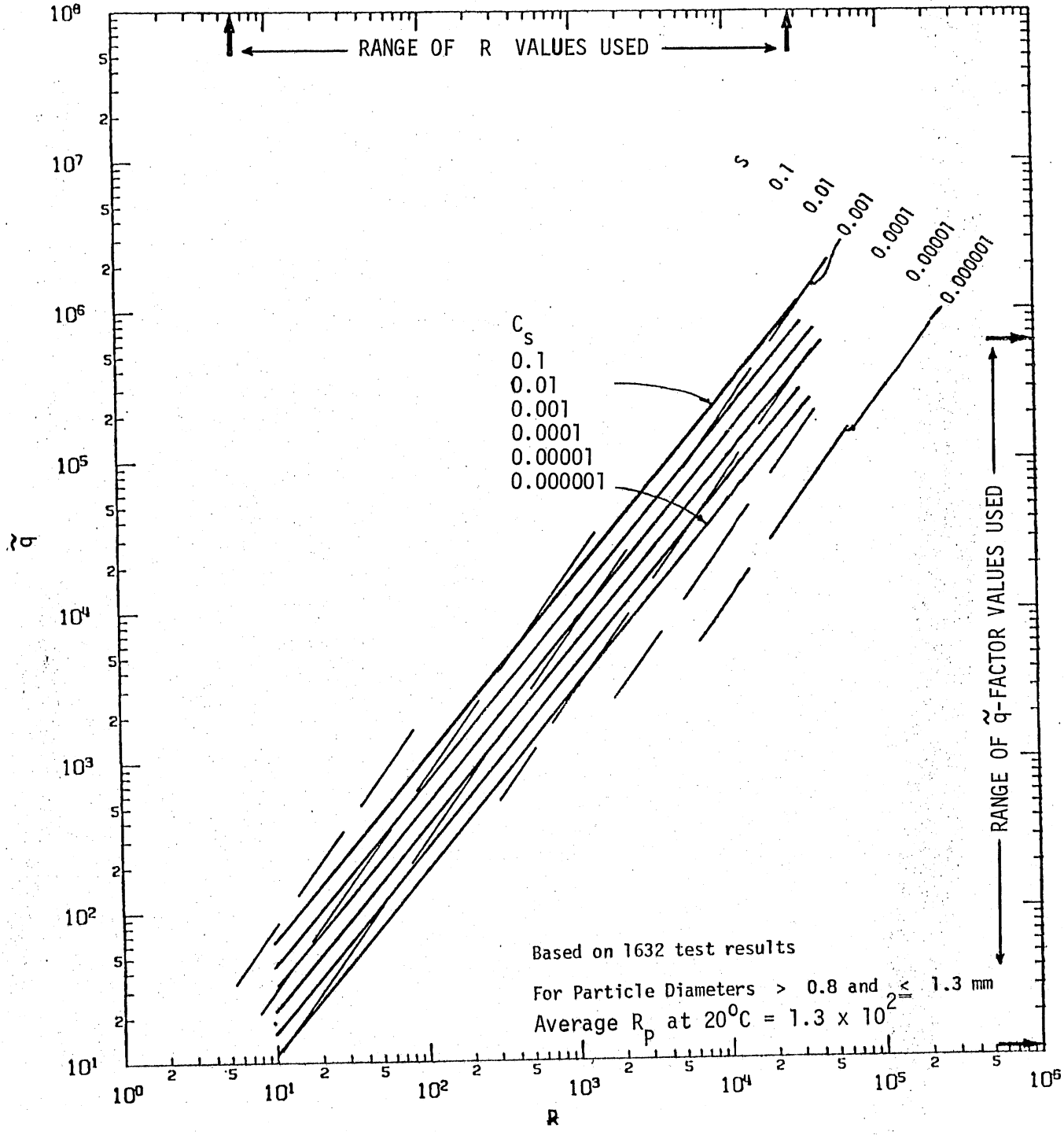

Fig. 1-2g. Peterson's (1975) preliminary $\tilde{q}$-R-S-C_s relationships.

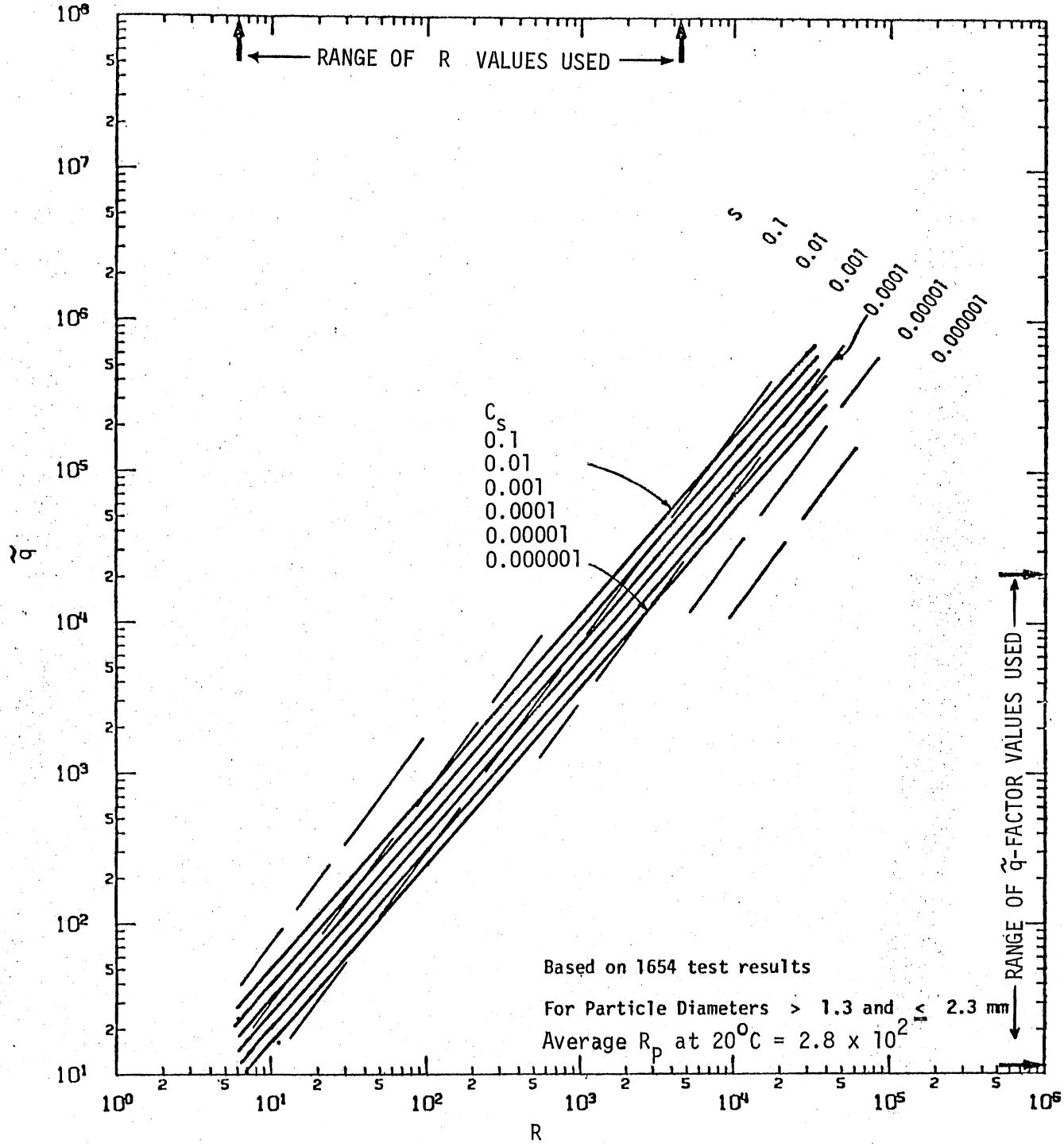

Fig. 1-2h. Peterson's (1975) preliminary $\tilde{q}$-R-S-C_s relationships.

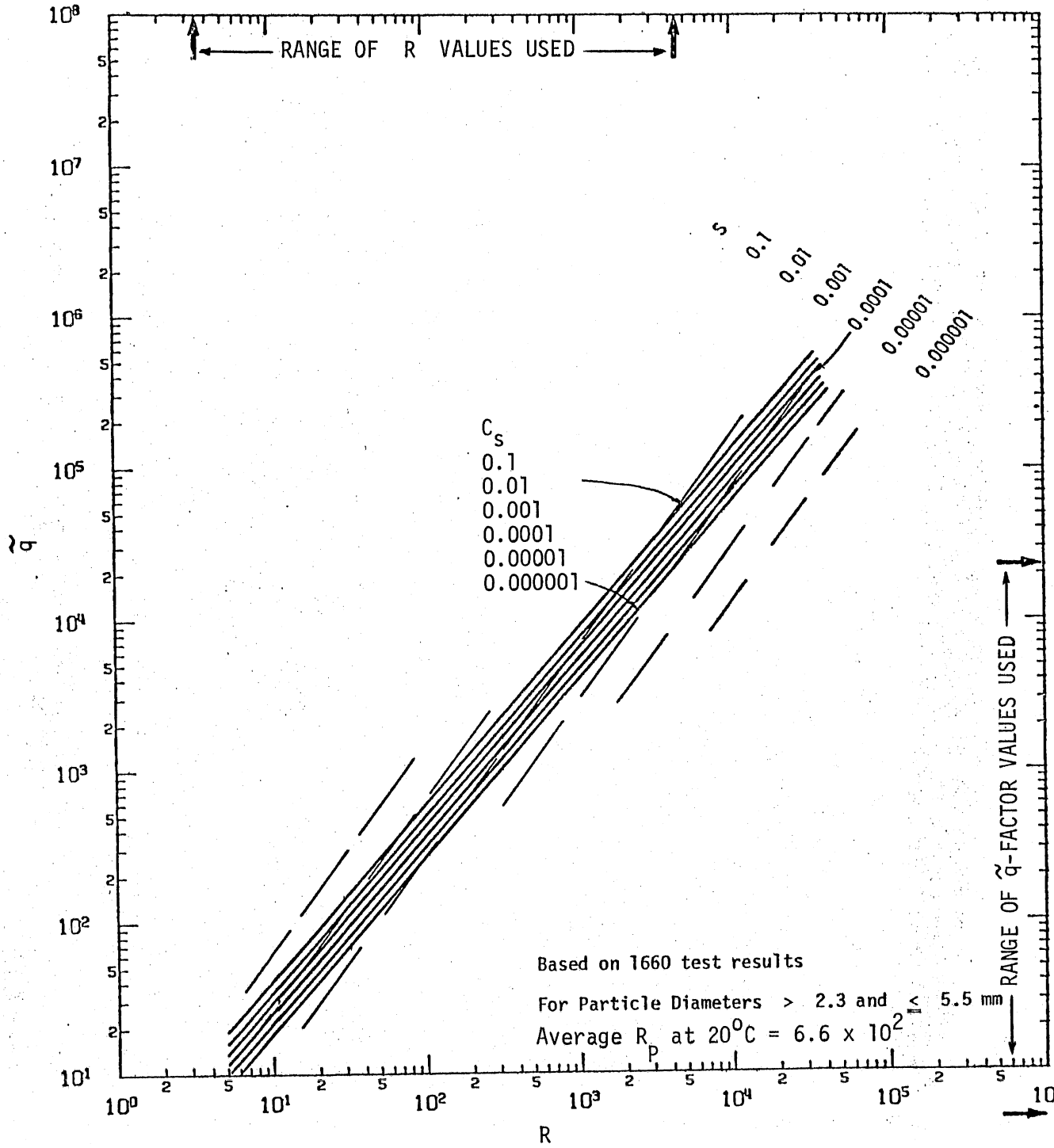

Fig. 1-2i. Peterson's (1975) preliminary $\tilde{q}$-R-S-C_s relationships.

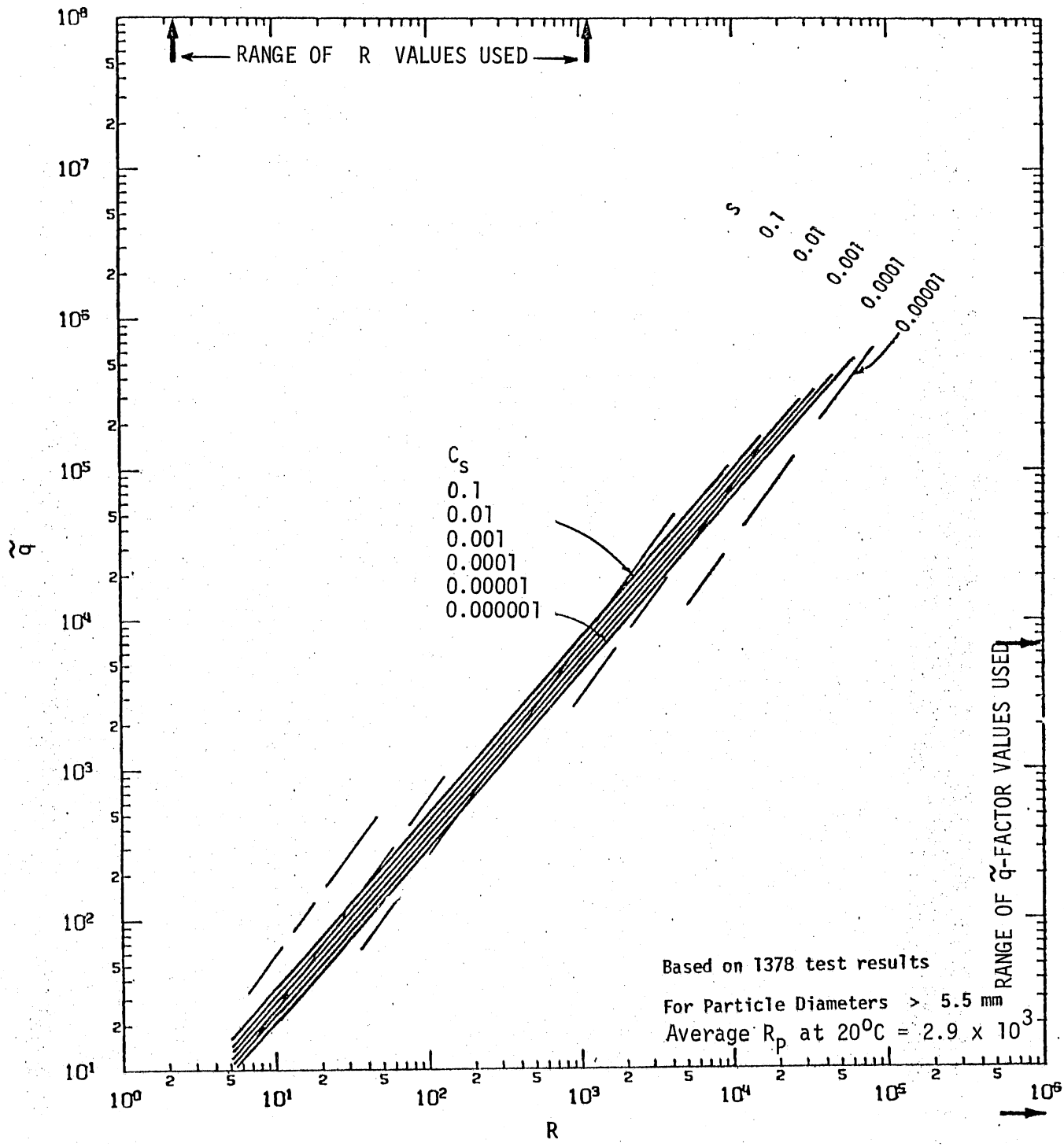

Fig. 1-2j. Peterson's (1975) preliminary $\tilde{q}$-R-S-C_s relationships.

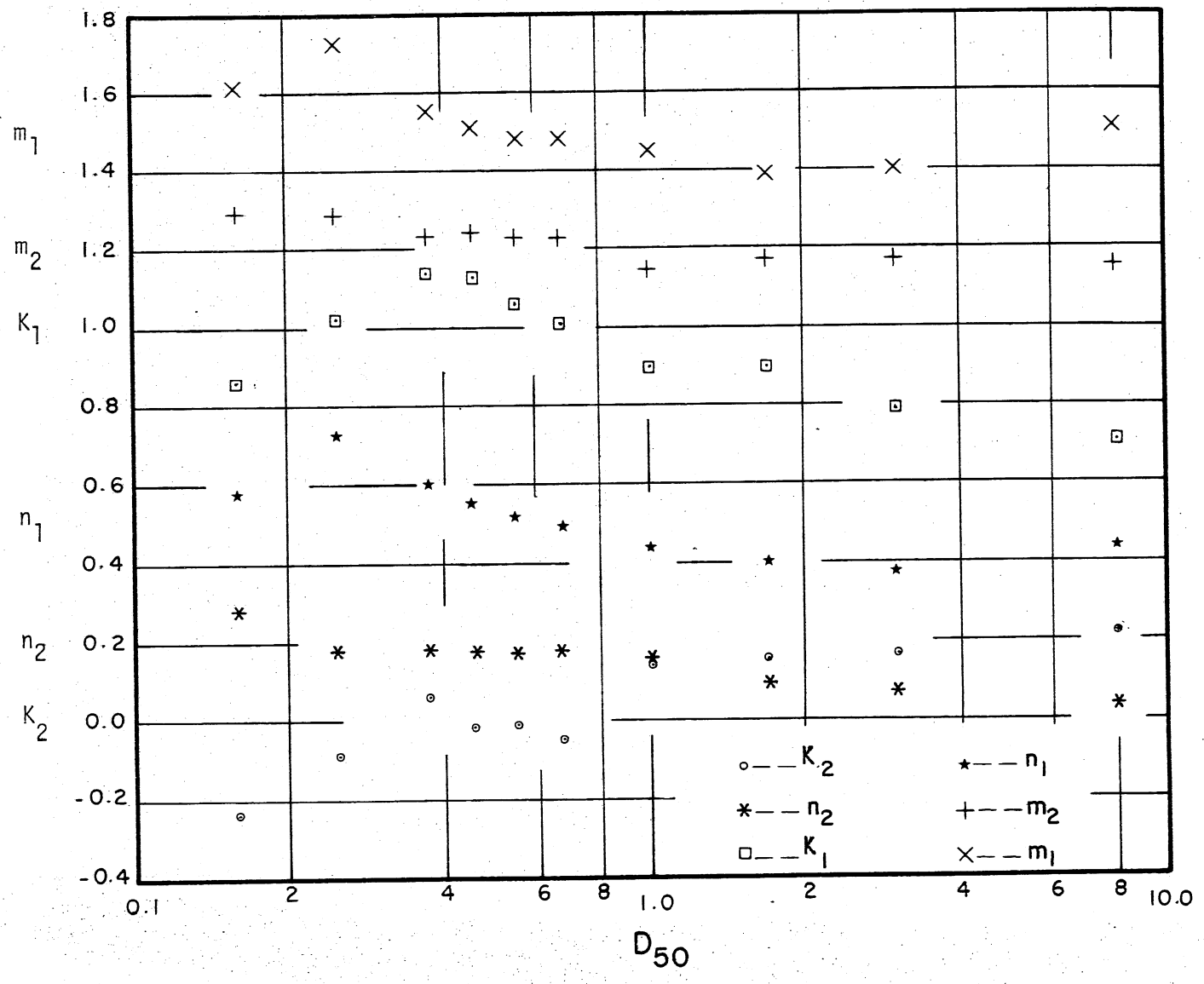

Fig. 1-3. The parameters K_1, K_2, m_1, m_2, n_1, and n_2 as functions of D_s, as computed from Peterson's (1975) relationships.

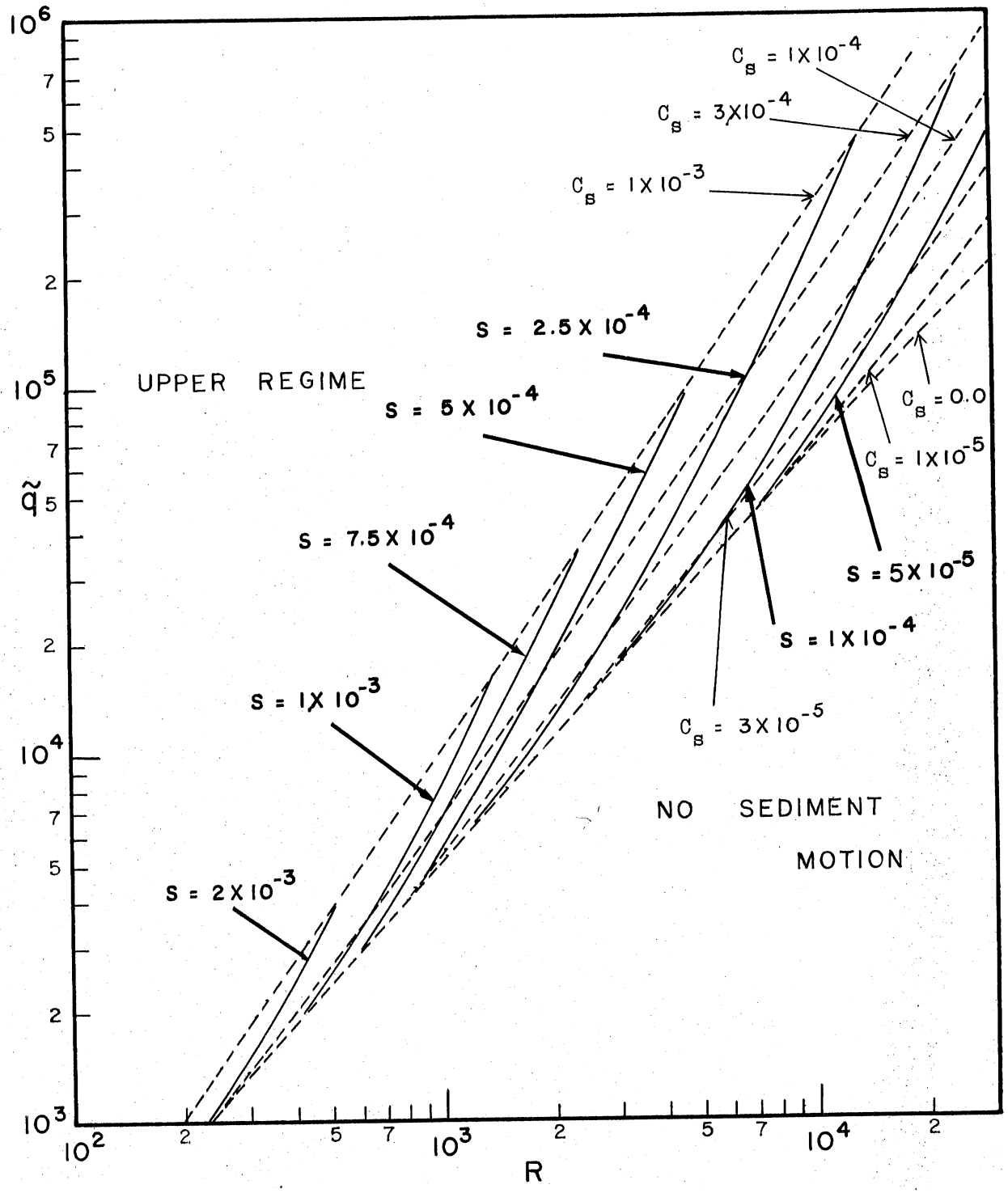

Fig. 1-4. Engelund's (1967) $\tilde{q}$-R-S-C_s relationship.

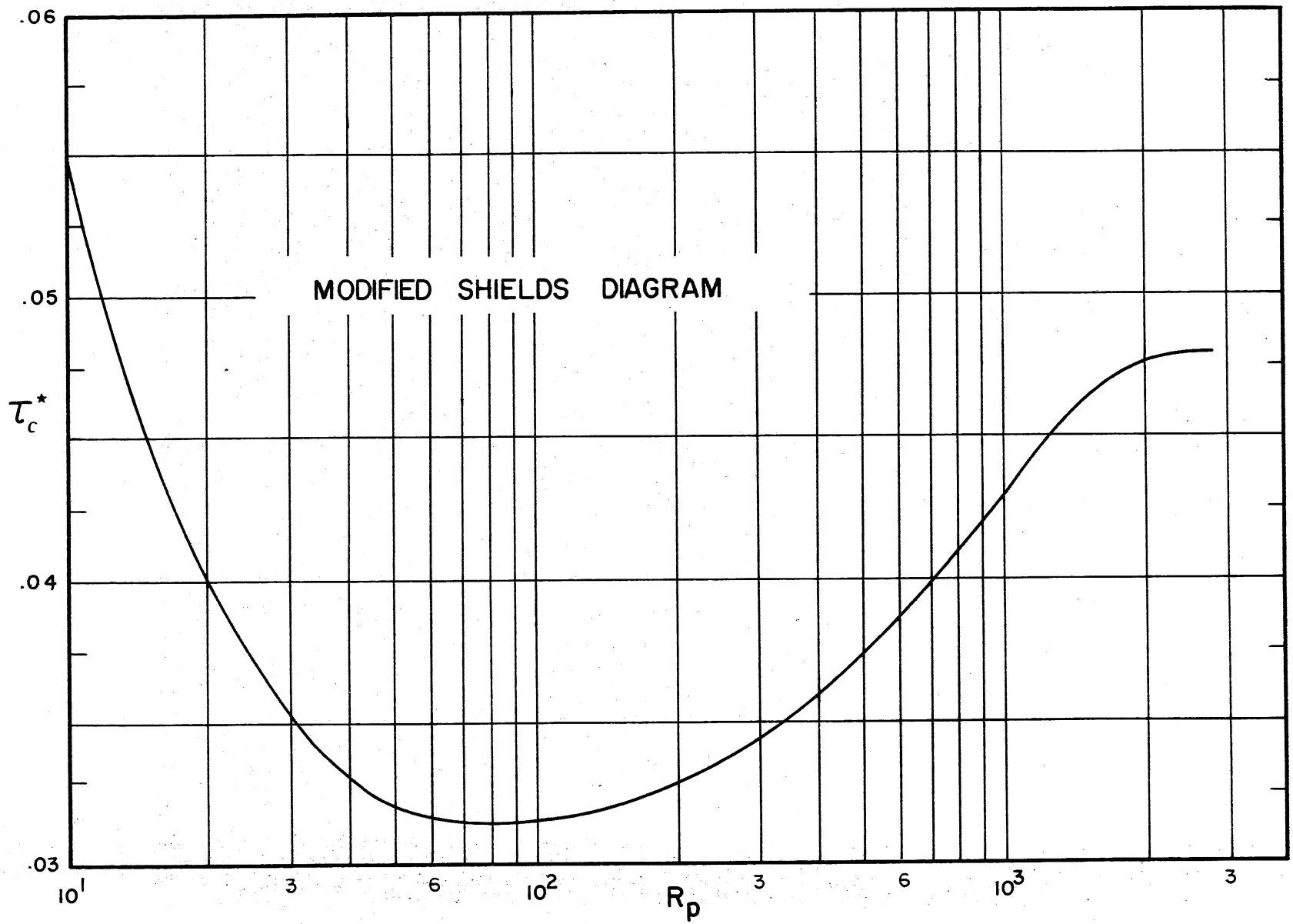

Fig. 1-5. Critical Shields stress τ_c^* as a function of particle Reynolds number R_p.

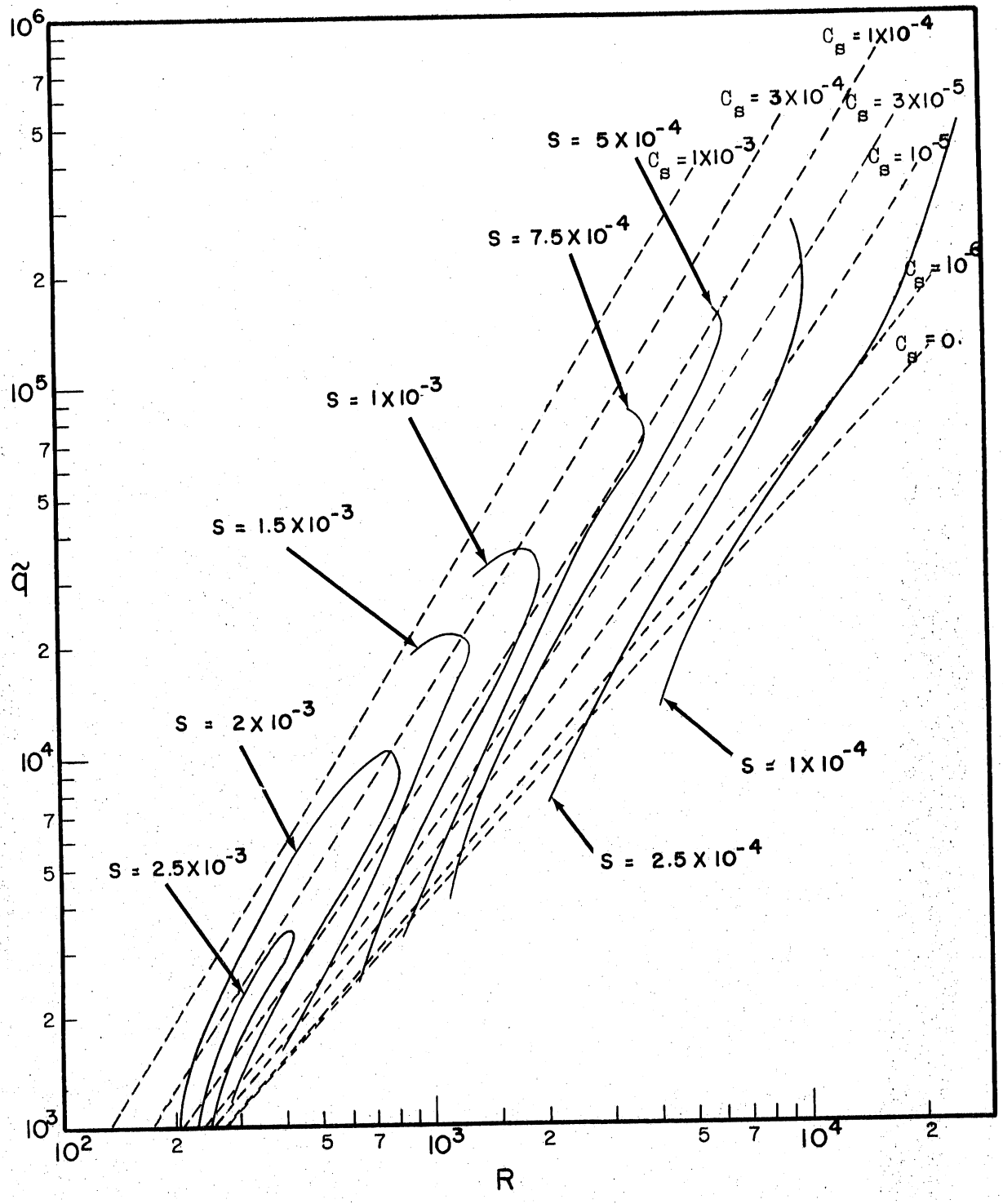

Fig. 1-6. Meyer-Peter et al. (1948) - Alam et al. (1966) $\tilde{q}$-R-S-C_s relationship for $R_p = 29$.

References for Chapter 1

Alam, A.M.Z., T.F. Cheyer, and J.F. Kennedy. Friction Factors for Flow in Sand Bed Rivers, Mass. Inst. of Tech. Hydrodynamics Laboratory Rpt. No. 78, 1966, 98 pp.

Ashida, K. and M. Michiue. "Study on Hydraulic Resistance and Bed-Load Transport Rate in Alluvial Streams," Trans. Japan Society of Civil Engineering, No. 206, October, 1972.

Brown, C.B. "Sediment Transportation," in Engineering Hydraulics, (H. Rouse, ed.), Wiley, New York, 1950, pp. 769-857.

Engelund, F. A Sediment Transport Theory Based on Similarity, Progress Rpt. No. 13, Coastal Engineering Laboratory, Technical University of Denmark, 1967.

Gessler, J. "Beginning and Ceasing of Sediment Motion," In Vol. I, River Mechanics, (H.W. Shen, ed.), Fort Collins, Colorado, 1971, Chapter 7, pp. 1-22.

Johnson, J.W. "The Importance of Considering Sidewall Friction in Bed-Load Investigations," Civil Engineering, Vol. 12, 1942, pp. 652-653.

Maddock, T., Jr. The Behavior of Straight Open Channels with Movable Beds, U.S. Geological Survey, Prof. Paper 662-A, 1969, 68 pp.

Meyer-Peter, E. and R. Muller. "Formula for Bed-Load Transport," Proc., 2nd Congress, Intl. Assoc. for Hydr. Res., Stockholm, 1948, pp. 39-64.

Peterson, A.W. Universal Flow Diagram for Mobile Boundary Channels. Personal communication from the Department of Civil Engineering, University of Alberta, Canada, 1975.

Peterson, A.W. and R.F. Howells. A Compendium of Solids Transport Data for Mobile Boundary Channels, Rpt. No. HY-1973-ST3, Department of Civil Engineering, University of Alberta, Canada, 1973.

Vanoni, V.A. "Factors Determining Bed Forms of Alluvial Streams," Jrnl. of the Hydr. Div., American Society of Civil Engineering, No. HY3, March, 1974, pp. 363-378.

Vanoni, V.A. and N.H. Brooks. Laboratory Studies of the Roughness and Suspended Load of Alluvial Streams, Rpt. No. E-68, Sedimentation Laboratory, California Institute of Technology, 1957, 121 pp.

Williams, G.P. Flume Width and Water Depth Effects in Sediment-Transport Experiments, U.S. Geological Survey, Prof. Paper 562-H, 1970, 37 pp.

References, Chapter 1 (Cont'd.)

Willis, J.C. and N.L. Coleman. "Unification of Data on Sediment Transport in Flumes by Similitude Principles," Water Resources Research, Vol. 5, No. 6, December, 1969, pp. 1330-1336.

Yalin, M.S. "On the Average Velocity of Flow over a Movable Bed," La Houille Blanche, No. 1, 1964, pp. 45-51.

CHAPTER 2

THE NATURE OF MEANDERING AND BRAIDING

2.1 Introduction

It is evident that rivers in nature are rarely straight. They most typically wind in and around bars and banks of their own creation. Two basic types of deviation from the straight are recognized in rivers, meandering and braiding. (Various other minor subclassifications exist, as Dury (1969),* has noted.)

Meandering rivers generally possess single channels that wind in a moderately regular fashion between alternating point bars (Figs. 2-1 and 2-2). These bars, combined with a primary pool and crossing pattern with the pools opposite the bar apex and the shallow crossing located between alternate pools, are characteristic of meandering streams. In addition, a secondary pattern of alternate pools and riffles, with a longitudinal wave length that is much shorter than the primary pattern, is often present in streams of considerable sinuosity (Keller, 1972), (Fig. 2-3). The entire pattern exhibits, to varying degrees, a tendency to migrate downstream.

Meandering and its associated bar pattern is observed to occur at any discharge, any slope, and in any type of bed material, and is much more common than braiding. At the same discharge, a stream with lower slopes and finer bed material will show a greater tendency to meander. As slopes become exceedingly flat and bed and bank material tends toward silt, meandering of spectacular sinuosity may be observed. Sinuosity may develop to the point that meander bends are cut off, leaving isolated oxbow lakes. The banks are cohesive and erosion-resistant due to the presence of clay and silt (Schumm, 1960), and thus the channel tends to be narrow and deep. Fine material carried in suspension may be deposited on the banks during floods, creating natural levees and back swamps. It is the interaction of water and sediment when flow takes place that creates the meander pattern. The prominent bars and the winding patterns which are apparent to the observer during the low flow regime are actually properties of the stream bed that were developed by flood discharges, at which time they are inundated. A stream viewed during the low water period represents a relatively inactive stream pattern that was created by successive flood occurrences.

*For Chapter 2 references, see pages 79-80.

Braided channels are similar to meandering channels in that they are characterized by bars which are formed at flood discharges. The bars appear as islands during low flow, during which the channel is divided into a number of channels that wind between the islands. Braided rivers often have low depth-width ratios and high slopes, and often have beds and banks composed of coarse sediment. These conditions are typically fulfilled in or at the base of mountainous regions. Rivers have a tendency to be braided in their upstream reaches but to have meanders in their downstream reaches. In some cases, however, the reverse may be true. For example, the Congo River has a low-slope with reaches that apparently braid due to their great width, and the Yellow River (Ning, 1961) has wide, steep-sloped reaches that braid in the alluvial silt. A tendency for the downstream shifting of the bar pattern is also observed in braided channels. The typical lack of cohesion of the channel material and the steep slopes often lead to more rapid changes in braided channels than those observed in meandering streams.

Both the meandering and the braided states are characterized by bar patterns. For reasons that are not well understood, this characteristic pattern is necessary for equilibrium. The equilibrium itself has a statistical nature so that, although particular bars migrate, are modified, or are cut off, the gross pattern remains the same with respect to time.

2.2 Initiation of Meandering and Braiding in Straight Channels

The fact that straight channels do not exist in nature suggests that straight channels do not represent a stable equilibrium. More positive evidence is found in connection with man-made channels. A classic example of this is the Skuna River above Grenada Reservoir in Mississippi (Yang and Stall, 1973) which was a typical meandering stream until channelized in a straight alignment (Fig. 2-4). The response of the stream was a tendency to reattain its former equilibrium. Shortly after straightening, an alternate bar pattern appeared within the new channel, giving the low flow a sinuous alignment.

The incipient meander pattern in the new channel closely resembles the old pattern. Examples from a drainage ditch, from Anderson (1967) (Fig. 2-5), and an artificially aligned and revetted reach of the Rio Grande River, from Fahnestock and Maddock (1964), illustrate the formation of alternate bars characteristic of incipient meandering or braiding in straight channels. At low flow, when the bars are exposed, the sinuosity of the flow can be clearly

seen. Such incipient meandering or braiding in straight channels rarely represents stability. This is vividly depicted in the laboratory results shown in Fig. 2-6 where the incipient pattern leads to local bank erosion, and, in time, to the establishment of fully-developed channel meandering. The photos were taken during a low flow in order to delineate the bed pattern. Keller (1972) and Kinoshita (1957) have documented the same process in the field (Fig. 2-7). Figure 2-8 shows channel meandering which has developed in an initially straight irrigation canal.

The fact that this process occurs rather slowly in nature gives the impression of permanence to channelized streams that have been given a straight alignment. It appears, however, that permanence can be affected only by bank revetment sufficiently resistant to prevent all bank erosion (in which case bar formation remains in the incipient stage) or by eliminating the sediment load, in which case the agent for bar formation no longer exists. The second option can be attained in the case of artificial canals by preventing the entrance of sediment into the system by appropriate head works and by design so that the critical conditions for sediment movement are never reached. However, this option is usually not available in the case of a channelized natural watercourse.

2.3 The Concept of Bar Instability

Field and laboratory observations have indicated that straight rivers have a natural tendency to form bars leading to either meandering or braiding. This tendency will be referred to as "bar instability."

The nature of the instability can be examined by using the methods of classical stability analysis. First, a solution for the straight flow is obtained, and then perturbations characteristic of meandering or braiding are imposed on the solution. If the perturbations tend to grow in time, the straight channel is unstable and a transition to a meandering or braided state will occur; otherwise, the channel will remain straight.

Stability analysis provides no information about the exact nature of the final equilibrium state after an instability has developed. However, it helps to answer the question as to which straight channels will remain straight, which will meander, and which will braid. Furthermore, an estimate of the instability wave length and braid number can be obtained. Such information

is invaluable for the analysis of problems involving local bank erosion.

The analysis of actual rivers presents insurmountable difficulties, so recourse is had to an idealized model that retains the essence of the problem. The proposed model alluvial river is assumed to have a hydraulically smooth bed consisting of erodible material, parallel, vertical, non-erodible banks, and an undisturbed rectangular cross-section on which the bar-like perturbations will be superimposed (Fig. 2-9). Channel alignment is assumed to be straight, with constant longitudinal slope S and constant discharge Q. Alternate bar patterns of the same type as those observed in the field have been produced in the laboratory, in flumes corresponding exactly to the proposed model river, by Kinoshita (1957) and Chang, Simons, and Woolhiser (1971). Sinusoidal, bar-like perturbations with arbitrary longitudinal wave length, λ, and number of braids, m, are to be introduced on the originally flat bed. In Fig. 2-10 the planform of the model river at low flow, when the bars are exposed, is given for various degrees of braiding. It can be seen that in terms of the proposed analysis, meandering becomes a special case of braiding that possesses one braid.

The stability analysis of the system under consideration should provide a unified treatment of meandering and braiding which, traditionally, have been assumed to be due to completely different processes--the former supposedly being caused by secondary helical flow induced by channel curvature and the latter supposedly due to channel aggradation.

2.4 Results of Wide-Channel Stability Analysis

An outline of an analysis of bar instability in the model alluvial channel is presented in Appendix II. The analysis is valid for channels that are so wide ($\frac{D}{B} << 1$) that bank effects are negligible. The following parameters are defined;

D_o	is unperturbed flow depth
B	is channel width
U	is unperturbed flow velocity
$F = \frac{U}{\sqrt{gD_o}}$	is unperturbed Froude number

$K = \frac{2\pi D_o}{\lambda}$ is meander or braid wave number (dimensionless)

$K_B = \frac{2\pi D_o}{B}$ is channel width wave number (dimensionless)

$C_o =$ is friction coefficient defined by $C_o = \frac{\tau_o}{\rho U^2}$ where τ_o is bed stress, and

$\beta = \frac{q_s}{(1-e)\, U D_o}$ is a dimensionless sediment transport rate where e is bed porosity

Meander-Braid Regime Criterion. Let ϵ^* be a parameter (See Appendix II) defined by

$$\epsilon^* = \frac{C_o}{\frac{1}{2} F^{-1} K_B} = \frac{1}{\pi} \frac{S}{F} \frac{B}{D_o} \qquad (2.1)$$

Then meandering occurs for $\epsilon^* << 1$, or $\frac{S}{F} << \frac{D_o}{B}$. Braiding occurs for $\epsilon^* >> 1$, or $\frac{S}{F} >> \frac{D_o}{B}$. Transition between meandering and braiding occurs for $\epsilon^* \approx O(1)$ or $\frac{S}{F} \approx \frac{D_o}{B}$. These relationships represent a theoretical illustration of the frequently observed fact that meandering channels have small slopes and are narrow and braiding channels have steep slopes and are wide. A meander-braid regime diagram constructed using these criteria is presented in Fig. 2-11.

Number of Braids. When m is greater than unity ($m > 1$), the number of braids m is always adjusted so that $m \sim \epsilon^*$. Therefore, processes such as aggradation, which lead to steeper slopes and wide channels, aggravate the tendency to braid. Since m can only take integral values equal to or greater than unity, $m = 1$ regardless of the value of ϵ^* in the case of meandering ($\epsilon^* << 1$). This may be related to the fact that narrow channels often develop greater sinuosity than wide channels.

Meander and Braid Wave Length. For the case of meandering an explicit relationship for K, and thus meander length λ, can be derived. It has the form $K \sim (K C_o)^{1/2}$, where $K_1 = 1/2\ mF^{-1} K_B$ and $m = 1$, giving

$$\frac{\lambda}{\sqrt{B_o D_o}} = 2\sqrt{\pi}\ \Phi_o C_o^{-1/2} F^{1/2} \qquad (2.2)$$

$$\text{or} \quad \frac{\lambda}{\sqrt{B D_o}} = 2\sqrt{\pi}\ \Phi_1 C_o^{-1/2} \tag{2.3}$$

where

$$\Phi_o = \left[\frac{(1 + N_2)(1 + M_2) + M_2(1 - N_1) + F^{-2}(1 - N_1)(M_1 - M_2 - 1)}{M_2 M_1^{\,2}(N_1 - 1)}\right]^{1/4}$$

$$\Phi_1 = F^{1/2}\,\Phi_o$$

where the M's and N's are coefficients defined in Appendix II. The difference between these equations is only in how the Froude number is absorbed into the parameters Φ_o and Φ_1. Equation (2.2) has the same form as Anderson's (1967) relationship. Thus, equations (2.2) and (2.3) are referred to as, respectively, the first and second forms of the modified Anderson relationship. Furthermore, the coefficient of instability for this value of K is

$$\phi_i = \beta C_o M_2(N_1 - 1) \tag{2.4}$$

In the case of braiding an explicit relationship for K must be obtained numerically; however, an estimate of this relationship is $K \approx C_o$ or

$$\frac{\lambda}{D_o} \approx 2\pi C_o^{-1} \tag{2.5}$$

The Role of Sediment Transport. It is clear from equation (AII. 11) of Appendix II that instability vanishes as β becomes small. Thus, sediment transport is a necessary condition for the formation of bar instability both in the flow and on the bed. However, the stationary points of this equation are independent of β. It is concluded that if no sediment transport exists, no tendency for meandering or braiding will develop, even in the flow. However, if sediment is transported, the occurrence of meandering or braiding and the longitudinal bar wave length will be independent of the sediment transport rate. It is shown in Appendix III that in sufficiently wide channels, bar instability characteristic of meandering or braiding always exists in channels which carry sediment.

2.5 Stability Analysis with Bank Effects

Wide-channel analysis has been used to distinguish meandering and braiding regimes. However, Chang, et al. (1971), Ackers (1962), and Vincent (1967) have

observed that for sufficiently large values of $\frac{D_o}{B}$, alternate bar patterns do not form. It is shown in Appendix IV that bank effects, which are negligible in wide channels, exert a damping influence on bar instability. It is found that stable channels become possible for values of $\frac{D_o}{B}$ greater than 10^{-1}. This information is used to provide a modified, meander-braid-straight regime diagram, which is illustrated in Fig. 2-12.

The new criterion indicates that initially straight canals may remain straight if the channel is designed so that on the one hand it is wide enough to transport the design discharge without general bank erosion and on the other hand is narrow enough so that bar instability is damped. The fact that straight streams are observed only rarely in the field is perhaps related to the fact that natural bank-full depth-width ratios greater than 10^{-1} are almost non-existent. Thus it appears that natural rivers cannot be trained permanently into a straight course without complete bank protection or continuous maintenance.

2.6 Comparison with Field and Laboratory Data

A comparison of the results of stability analysis with data was attempted. In Table AV-1 of Appendix V, basic data from 167 laboratory experiments carried out by nine groups of researchers is compiled for reference purposes. The data includes channels which maintained a straight alignment and channels in which meandering or braiding developed. The discharges range from 0.31 liters/sec. to 113 liters/sec. The St. Anthony Falls experiments are described in more detail in later section of this report.

The meander-braid-straight diagram of Fig. 2-12 is tested in Fig. 2-13 using laboratory data from Table AV-1. Field data have been similarly plotted in Fig. 2-13. The field data includes 22 stable, straight canals from Simons (1957) and the 53 reaches of natural rivers tabulated in Table AV-2 of Appendix V. As the stability theory predicts the boundaries between the several regimes only to an order of magnitude, their actual exact position has been adjusted on the basis of the observed data. According to the graph, Fig. 2-13, braiding occurs when

$$\frac{D_o}{B} < \frac{1}{2}\frac{S}{F}$$

and the meander-braid transition falls in the region

$$\frac{1}{2}\frac{S}{F} < \frac{D_o}{B} < \frac{S}{F}$$

and meandering develops when

$$\frac{S}{F} < \frac{D_o}{B} < 6 \times 10^{-2}$$

so the transition to straight falls in the region

$$6 \times 10^{-2} < \frac{D_o}{B} < 2 \times 10^{-1}$$

and channels remain straight when

$$2 \times 10^{-1} < \frac{D_o}{B}$$

The plot shows that good agreement with theoretical results is obtained over a wide range of channel sizes from that of laboratory experiments to that of the Mississippi River.

Where possible, field data estimated for bank full flow were used; however, in some cases the lack of such data required the inclusion of data from rivers based upon mean or other flow conditions. The discrepancies thus introduced do not appear to be critical; for example, point 3 ($D/B = 1.4 \times 10^{-2}$, $S/F = 6 \times 10^{-4}$) on Fig. 2-13 is for a reach of the Mississippi River flowing at mean discharge, while point 4 ($D/B = 1.9 \times 10^{-2}$, $S/F = 1 \times 10^{-3}$) represents bank full flow. Other sources of inaccuracy include the fact that some of the data had to be estimated from information in the literature. However it is felt that all the data used were extracted in a reliable fashion and are appropriate for the analysis.

Where possible, field data estimated for bank full flow were used; however, in some cases the lack of such data required the inclusion of data from rivers based upon mean or other flow conditions. The discrepancies thus introduced do not appear to be critical; for example, point 3 on Fig. 2-13 is for a reach of the Mississippi River flowing at mean discharge, while point 4 represents bank full flow. Other sources of inaccuracy include the fact that some of the data had to be estimated from information in the literature. However it is felt that all the data used were extracted in a reliable fashion and are appropriate for the analysis.

Figure 2-13 applies only to cases in which sediment transport occurred since, as equation (A2.11) shows, instability disappears when sediment transport is zero. The limit for straight natural rivers can then be estimated from a consideration of the conditions for zero transport. For values of τ^* that are below the critical shear stress, τ_c^*, given in Fig. 1-5, or for

$$\frac{S}{F} < \frac{r\tau^*_c}{RF} \equiv \varphi^*$$

no sediment transport occurs and a channel can be expected to remain straight. Figure 2-12 has been modified in Fig. 2-14 to include this new straight region corresponding to $\varphi^* = .0005$, as an example.

The data from Table AV-1 were also used to test various theoretical relationships for meander length, including the relationships given by equations (2.2) and (2.3) which predict (respectively) the meander length scales. The relations

$$\lambda \sim 2\sqrt{\pi}\sqrt{B D_o}\ C_o^{-1/2}\ F^{1/2} \qquad (2.2)$$

$$\lambda \sim 2\sqrt{\pi}\sqrt{B D_o}\ C_o^{-1/2} \qquad (2.3)$$

as well as the Hansen (1967) relationship,

$$\lambda \sim 7\ D_o C_o^{-1}$$

the Werner (1951) relationship,

$$\lambda \sim 2\,BF$$

and the original Anderson (1967) relationship,

$$\lambda \sim 72\sqrt{B D_o}\ F^{1/2}$$

were compared with data.

These comparisons are shown in Figs. 2-15a through 2-15e. Since none of these equations can be expected to be exact, and at best can provide estimates of appropriate scales, the method of plotting has been chosen to provide a test of this feature. The figures represent a dimensional plot of observed values of λ against the theoretical estimate of meander length, λ_{A1}, calculated for the first form of the modified Anderson relationship (Fig. 2-15a); λ_{A2}, calculated from the second form of the modified Anderson relationship (Fig. 2-15b); and λ_A, λ_H, and λ_W from the original Anderson relationship and the Hansen and Werner relationships (Figs. 2-15c, d, and e). The units are meters, so the dimensioned graph will indicate the range of the data.

The requirements for a good scale relationship $\lambda \sim \lambda_T$, where λ_T is some meander length scale, is that (1) λ_T should estimate the order of magnitude of λ, and (2) when λ is plotted against λ_T on log-log graph paper over two decades or more, a general linear trend between the two should be visible. In short, λ_T should estimate and be loosely linearly correlated with λ.

Using these criteria it is apparent from Fig. 2-15 that the first modified Anderson, Hansen, and Werner relationships are poor, whereas moderately good estimates are provided by the original and the second modified Anderson relation. Evaluating by eye the constant Φ_1 in equation (2.14), it is found that meander length can be roughly estimated by either of the formulas

$$\lambda = 1.25\ \lambda_{A2}$$

$$\lambda = \lambda_A$$

where $\lambda_{A2} = 2\sqrt{\pi}\ C_o^{-1}\sqrt{D_o B}$ and $\lambda_A = 72\sqrt{D_o B}\ F^{1/2}$.

Note that no data from natural rivers have been included. The developed tortuosity of many natural rivers indicates circumstances which cannot be directly compared to the relatively small sinuosity of the laboratory, and thus the above two equations cannot be expected to apply. However they should provide estimates of the wave length of the meander pattern that first develops after straightening through channelization.

Zeller (1967) has provided an empirical relationship for meander length as a function of width, which closely approximates

$$\frac{\lambda}{B} = 10$$

This relationship was tested for the data of Table AV-1a in Fig. 2-16 which plots λ versus B. It is seen that although λ correlates well with B the relationship is not linear. This indicates that the dimensionless parameter $\frac{\lambda}{B}$ is not a constant but a function of other dimensionless parameters. It appears that relationships of the form $\frac{\lambda}{B}$ = constant are poor approximations and do not apply to meandering as it is observed in the laboratory.

2.7 The St. Anthony Falls Hydraulic Laboratory Experiments

Some of the data included in Table AV-1 were collected at the St. Anthony Falls Hydraulic Laboratory during the course of this investigation of river channel stability. A series of six experiments were performed in a multi-purpose channel and eight were performed in a tilting flume.

The portion of the multi-purpose channel used for these studies was 36 meters long, 2.74 meters wide, and 1.8 meters deep (Fig. 2-17). It was filled with sand to a depth of 20 40 cm. Wooden rails along each side of the channel were set at a longitudinal slope of .0049. Initial straight channels of various geometries were screeded by moving a template with the appropriate geometry along the rails.

The top of the channel was equipped with steel rails that supported a movable carriage. The carriage was fitted to serve as an observation platform as well as a mount for an automatic point gauge (Fig. 2-18) designed to track either the bed or the water surface. All three coordinates could be read by the probe and stored on magnetic tape for computer processing. This data-acquisition system permitted the collection of a comparatively large quantity of data with an accuracy of $\pm$ .1 cm.

Both water and sediment transported through the model channel were discharged into a large circular (radius 1.5 m, depth .5 m) basin. This basin had a hole in the bottom center which was connected to pumps so that the water-sediment mixture could be recirculated. A large rotating paddle prevented undue deposition of sediment in the basin. The speed and position of the paddle regulated the amount of sediment in suspension and thus controlled the rate at which the sediment was recirculated. Neither temperature nor sediment load was measured during the course of the multi-purpose channel experiments.

Two pumps controlled by timers were used to develop an artificial hydrograph. Hourly repeating hydrographs consisting of at most three component discharges (two pumps singly, both together) could be imposed. Discharge could be varied from .3 liters/sec. to 30 liters/sec.

The sand used was of moderately irregular shape with a mean diameter D_{50} = 0.22 mm, and a standard deviation, σ, of 1.44 mm. The sand contained a small but noticeable quantity of silt and clay.

Photographic apparatus included equipment for time-lapse movies.

The tilting flume is 12 meters long, .9 meter wide, and 0.3 meters deep (Fig. 2-19). It was filled with sand to a depth of approximately 10 cm. The slope of the flume could be adjusted mechanically from 0.0 to 0.02. Both the screeding template and the observation carriage ride on the channel walls.

A manual point gauge was used for data acquisition.

Both sediment-feed and sediment recirculating systems were available, but only the recirculating system was used. A constant head was maintained in the outlet tank to facilitate recirculation. Discharge range was .2 liters/sec. to 1.2 liters/sec. The sediment load was measured by determining the sediment concentration of samples extracted from the return pipe. The sand in the tilting flume had a mean diameter D_{50} = 0.62 mm and a standard deviation, σ = 1.39 mm; it was moderate-to well-rounded and the content of fines was negligible.

Photographic apparatus again included equipment for time-lapse photography.

2.8 Experimental Results

Preliminary experiments in the multi-purpose channel set at a slope of 0.007 resulted in exclusively braided channels. Subsequently the slope was lowered to 0.0049 in an attempt to generate both meandering and braided channels by varying discharge and initial channel size and shape. Six experiments were conducted under these conditions.

Basic data obtained from these experiments is tabulated in Table 2-1. The experiments were allowed to run from 264 to 524 hours. They were characterized by relatively low Froude numbers (F = .21 to .31, extremely high resistance coefficients ($C \approx 0.06$ or Darcy-Weisbach $f \approx 0.5$), and the general final development of a pattern that exhibited neither intense meandering nor intense braiding. The pattern rather was transitional. Another feature, apparently due to the small size of the bed material, was a characteristically rippled bed. There was a tendency for deposition of fines on the bars. Some of these aspects are illustrated in Fig. 2-20 a, which illustrates Run M-1-3, classified as meandering, and in Fig. 2-20 b, which illustrates Run M-1-4, which was classified as transitional meandering-braiding but appears closer to braiding. Both photographs were taken at lowered discharges with the addition of red dye to improve the visibility of the bed patterns.

In both photographs bed patterns of markedly different length scales, ripples, and bars are visible. In some cases the fine rippling tends to obscure the location and shape of the bars. The bar patterns, while visible at low discharges, were usually completely submerged at the high discharges

which formed them (Fig. 2-21). Sediment transport was in the mode of bed load except for the fines, which were carried in suspension.

The initial width for Run M-1-1 was much narrower than for the other runs. Initially meandering was observed, but as time passed the channel widened considerably due to the erosive power of the stream. The extra sediment supplied to the bed due to bank erosion was so great that it could not be transported, and since the apparatus was a recirculating system, sediment could not be extracted. In this extreme case aggradation occurred in the channel, particularly at the inlet of the flume. Here the channel width increased to the entire three meters of width of the channel, and a classically braided (5 to 10 branch) pattern was observed. Data from cross-sections in this region formed the basis for the St. Anthony Falls braided channel data listed in Table AV-1. This localized region of extreme braiding, where the excess sediment was deposited, was followed by a more or less uniform, constant-width channel extending from a section about 10 meters downstream of the inlet, to the outlet. Figure 2-22 shows typical water surface heights and width as a function of downstream distance. An alternate-bar pattern characteristic of meandering could be perceived by eye after 36 hours of operation. (In general, at least a day was required.) As time progressed the channel became wider, the depth was reduced, and meander wave length increased while average slope remained relatively constant (except near the inlet). This is shown in Fig. 2-23. After about 350 hours the increase in channel width caused a lateral distension of the bars to the point that they were cut off, and a transition to braiding occurred. After 490 hours, when the run was terminated, Fig. 2-23 shows that width increase and depth decrease had essentially ceased, and thus a stable braided channel (2 to 3 braids) had developed in all regions of the flume except the inlet region. The width of this channel was over twice that of the original channel.

It was hypothesized that for the given flow conditions the initial cross-section was unrealistically narrow. The ensuing bank erosion resulted in the movement of bank material to the bed in such a quantity that it could not be transported. In an attempt to adjust for this, Run M-1-2 was conducted at the same slope and the same discharge, but with a considerably wider initial channel. The result was that although bank erosion took place, it did not

strain the model river beyond its capacity, and a stable meandering channel without significant aggradation and with a final width smaller than that of Run M-1-1 was developed.

The two experiments make clear that initial channel size is an important variable for recirculating systems. In this case it meant the difference between meandering and braiding. The localized extreme braiding at the inlet of Run M-1-1 was apprently due to an overload of sediment, but the moderately braided channel occurring outside this region, and the meandering channel of Run M-1-2, were apparently close to equilibrium at the time of termination.

In Run M-1-3 a simple hourly repeating hydrograph consisting of a high discharge of 2.83 liters/sec. continuing for seven minutes and a low discharge of 1.27 liters/sec. for the remaining 53 minutes was applied to the system. This implies an average discharge of 1.45 liters/sec., nearly equal to that of Run M-1-2. Experience indicated that the initial channel must be such that the river system is not unduly strained by bank erosion even at the highest discharge if a spatially uniform channel is to be eventually formed. For this reason it was decided to make the initial channel wider than in the previous run. It was found that with such a wide channel very little sediment was transported at the low discharges, so that the channel was morphologically active only during the high discharge for the seven minutes of each hour. Thus the 524 hours of actual run time is equivalent to only 61 hours of equivalent run time at the high discharge. For this reason channel development appeared to be very slow. It was assumed that a meandering channel in equilibrium had been reached at the time of termination (Fig. 2-20), but this proved to be erroneous in light of the results of Run M-1-4.

Run M-1-4 was a constant-discharge run with the same initial channel shape, size and slope as Run M-1-3 and with the high discharge of the latter. Upon termination the channel was wider than the previous run and was in transition between meandering and braiding, although closer to braiding (Figs. 2-20b and 2-21). These experiments suggest that the higher discharge ranges are dominant in regard to the formation of channel morphology.

Run M-1-5 was another hydrograph run with the same initial channel and high discharge as Run M-1-3, but with a high discharge duration of 10 minutes and a low discharge of .42 liters/sec. for the remainder of the hourly cycle.

Thus the average discharge was .84 cfs. It was hypothesized that the great difference between the high and the low discharges might encourage deposition on the bars and scour in the channel thalweg, leading to a much more definite pattern. This was not found to be the case. Channel development was completely dominated by the high discharge, and thus closely paralleled that of Run M-1-3. The channel was meandering at the termination of the run, but most likely would have gone into a transition stage, as did Run M-1-4, if it had been continued.

Run M-1-6 was a constant-discharge run with an initial channel size and a discharge that were much smaller than any of the previous runs. Unfortunately detailed data were not taken subsequent to the commencement of the run. However, a time-lapse movie showed that very little bank erosion took place and the tendency toward alternate bar formation, although perceptible, was slight. For this reason the channel has been classified as straight. After one week of operation, an initial bend was artificially shaped near the inlet to determine if such an artifice could trigger meandering. It was apparent, however, that the bend had no effect. It was at first assumed that the lack of tendency toward bar formation was due to small transport rates, but the time-lapse movie showed clearly that the bed ripples migrated downstream. However, it was observed that the depth-width ratio was much smaller than the other runs which, in light of the discussion of section 2-5, may account for the weak tendency for bar formation.

The inability to vary initial channel slope, the long times required for the formation of bar patterns, and the occurrence of ripples which tended to obscure the bar pattern were drawbacks of the multi-purpose channel as a testing facility. These were remedied by the use of the tilting flume. A total of 27 runs were completed, of which the first 16, Runs 101 to 116, were exploratory and involved no data acquisition. Runs 120, 122 and 123 were rendered useless by mechanical failures, but the remaining eight are reported in Table 2-2. Experiments were completed within two to twelve hours, and the development of bar patterns was very rapid compared to that in the multi-purpose channel. Figure 2-6 shows the development of Run 118 with respect to time. It can also be seen that the meander pattern is much more clearly defined and of greater sinuosity than in the multi-purpose channel. Braided channels could also be attained, as Fig. 2-24 illustrates. However, it is believed that none of the channels represent equilibrium conditions because of the short operating times. In the case of meandering, the coherency of the pattern is eventually altered or destroyed when the apex of the bends reached the flume walls or when the bends

migrate a complete wave length downstream widening the channel and eventually creating flow conditions less favorable to meandering and more favorable to braiding. High slopes and high Froude numbers (.57 to 1.2) were required for sediment transport (which was exclusively bed load) because of the coarseness of the sediment. On the other hand, the lack of bed forms other than the bars themselves dictated resistance coefficients that were low compared to those measured in the large channel. It was furthermore found that in the tilting flume no channel remained straight if even the slightest amount of sediment was in transport. Another feature noted was a tendency for areal sorting, which is illustrated photographically and schematically in Fig. 2-25.

2.9 Discussion: The Laboratory River as a Model of Nature

In all of the experiments, the sinuosity of the channels developed was quite small compared to that commonly observed in nature. Schumm and Khan (1972) have succeeded in increasing sinuosity somewhat by inducing clay deposition on, and consequent emergence of, the bars, but the discrepancy is still large. The relatively low degree of sinuosity has been interpreted to mean that laboratory models of meandering do not simulate conditions in nature. However, the relevance of laboratory experiments to field conditions has not been determined.

The discrepancy in sinuosity appears to be illusory to a large degree. The well-defined sinuous or anastomosing planview of natural rivers is only visible at low flow conditions, which because of their comparatively long duration are most commonly observed. During such flows the river channel carries discharges that are only a small fraction of its capacity, and sediment transport is small; the river is inactive in a geomorphologic sense. Rivers are geomorphologically active only during flood periods when the bars characteristic of meandering or braiding are partially or totally inundated. With the exception of bank-caving, a process conducive to bar building, erosion or migration can take place only when there is water above the bars to transport the sediment. Such flood discharges by definition exceed bank full, and when they are imposed the river itself appears straighter due to the inundation of the point bars. In general, the higher the flood discharge the straighter the river appears (see, for example, Figs. 2 and 3 of Neill, 1965). It may be inferred that for meandering rivers at geomorphologically active discharges, the sinuosity of rivers (as manifested by the water surface pattern) is small.

This principle provides a tool for interpreting laboratory experiments. In a constant-discharge experiment, the water surface width essentially defines the model river valley walls, and the imposed discharge represents a flood that fills the entire valley. The results of this flood can only be seen by either stopping the flow of water entirely or reducing the discharge to a small remnant of the formative value. The sinuosity of the water-filled laboratory channel under these conditions is on the one hand nearly equal to thalweg sinuosity, and on the other hand comparable to channel sinuosity observed in nature, as can be seen by comparing Figs. 2-6 and 2-1.

The analogy between these two photographs suggests that the laboratory can provide a good model of a specific type of natural morphology. Rivers have been loosely classified according to age. "Young" rivers usually lie at the bottom of steep V-shaped valleys, and valley walls coincide with river banks. "Mature" rivers have developed small river-valley flood plains, in which they meander or braid in a belt as wide as the valley itself. In the case of meandering, the meanders are said to be "confined" by the valley walls. Valley widening is accomplished when the river impinges on either side of the valley. "Old" rivers lie in extremely large flood plains, much wider than their wandering belts. In such valleys the river pattern is said to be "unconfined." The Klaralven (Fig. 2-1) is an example of a mature river, and it is this river valley morphology which is best modelled in the laboratory. Another example of a mature river, Fig. 2-26, illustrates the active erosion of valley walls that is evident in the laboratory river of Fig. 2-6.

Although the qualitative similarity of the model provided by laboratory rivers appears to be better than previously assumed, important drawbacks do exist. Laboratory models generally fail to form well-defined low-flow channels within the flood plain that have cohesive banks and are capable of carrying all discharges up to bank full without significant channel modification. This is related to the fact that in most humid regions certain natural phenomena invariably tend to reduce the bank full width in the flood plain to its smallest value, and in doing so build coherent banks for the flow. The two most important processes involved are silt and clay deposition and vegetation (see Schumm, 1960). During a flood, sediment, including fines, is deposited on the bars; with the adequate supply of water typical of humid regions, conditions are conducive of vegetative growth, which then provides a matrix for the collection of more fines during the next flood. Thus, the height of the flood plain is built up above the

low-flow channel. Vegetation generally grows up to the water's edge and, in the form of anchored aquatic plants, on shallow submerged bars. This and the observed fact that fines are often deposited on the part of bars adjacent to the low-flow channel itself (natural levees) implies that banks composed of matted roots in cohesive sediment are comparatively erosion-resistant and constantly tend to encroach on the low-flow channel. There is evidence (Northrup, 1963) that periodic extreme floods do tend to flush out thick vegetation and thus place a limit on the channel-narrowing process.

It was shown earlier (see Fig. 2-13) that large values of $\frac{D}{B}$ favor meandering over braiding. The channel-narrowing effect tends to convert braided channels into a small number of coherent anastomosing channels and, thence, to a single meandering channel. The relative rarity of braided streams in humid regions is perhaps explained in this fashion. The channel-narrowing effect also acts to preserve channel coherency as meandering rivers migrate laterally and longitudinally, and although the exact mechanism is unclear, it is related to the ability of many natural rivers to develop loops of such an extent that natural cutoffs become common.

Thus many of the processes which account for fluvial morphology are not present in laboratory models. It is interesting to note that natural rivers in noncohesive alluvium which is void of vegetation often have ill-defined low-flow channels. The meandering and braiding in such channels have many similarities with that of laboratory models.

2.10 Conclusion - Implications for Channelization

The goal of channelization is the alteration of the alignment of a graded stream in such a way that a new state that transports flood discharges more efficiently is attained. Since the rate at which a given reach of river must transport sediment to maintain grade is determined upstream of the reach and not at the reach itself, modifications in channel alignment cannot circumvent the fact that all alluvial rivers transport sediment to a greater or lesser degree. Analysis has indicated that in all but the narrowest of rivers meandering or braiding instability is in direct proportion to the rate of sediment transport. The depth-width ratio required for stable straight channels is generally much higher than that which can be maintained in nature. It must be concluded that alluvial streams with erodible banks which have been channelized in a straight alignment will almost invariably return to a

migrate a complete wave length downstream widening the channel and eventually creating flow conditions less favorable to meandering and more favorable to braiding. High slopes and high Froude numbers (.57 to 1.2) were required for sediment transport (which was exclusively bed load) because of the coarseness of the sediment. On the other hand, the lack of bed forms other than the bars themselves dictated resistance coefficients that were low compared to those measured in the large channel. It was furthermore found that in the tilting flume no channel remained straight if even the slightest amount of sediment was in transport. Another feature noted was a tendency for areal sorting, which is illustrated photographically and schematically in Fig. 2-25.

2.9 Discussion: The Laboratory River as a Model of Nature

In all of the experiments, the sinuosity of the channels developed was quite small compared to that commonly observed in nature. Schumm and Khan (1972) have succeeded in increasing sinuosity somewhat by inducing clay deposition on, and consequent emergence of, the bars, but the discrepancy is still large. The relatively low degree of sinuosity has been interpreted to mean that laboratory models of meandering do not simulate conditions in nature. However, the relevance of laboratory experiments to field conditions has not been determined.

The discrepancy in sinuosity appears to be illusory to a large degree. The well-defined sinuous or anastomosing planview of natural rivers is only visible at low flow conditions, which because of their comparatively long duration are most commonly observed. During such flows the river channel carries discharges that are only a small fraction of its capacity, and sediment transport is small; the river is inactive in a geomorphologic sense. Rivers are geomorphologically active only during flood periods when the bars characteristic of meandering or braiding are partially or totally inundated. With the exception of bank-caving, a process conducive to bar building, erosion or migration can take place only when there is water above the bars to transport the sediment. Such flood discharges by definition exceed bank full, and when they are imposed the river itself appears straighter due to the inundation of the point bars. In general, the higher the flood discharge the straighter the river appears (see, for example, Figs. 2 and 3 of Neill, 1965). It may be inferred that for meandering rivers at geomorphologically active discharges, the sinuosity of rivers (as manifested by the water surface pattern) is small.

Table 2-1. Results of Meander Experiments in Multi-Purpose Channel

Run Number	M-1-1	M-1-2	M-1-3	M-1-4	M-1-5
Discharge (ℓ/s) (Q)	1.41	1.41	2.83	2.83	2.83
Time of Initial Data (hrs.)	60	20	72	24	24
Initial Width (cm) (B_I)	59.8	81.7	118	118	114
Initial Depth (cm) (D_I)	1.89	1.51	1.34	2.06	1.65
Initial Slope (cm) (S_I)	.00443	.00478	.00599	.00487	.00467
Initial Froude No. (F_I)	.288	.295	.484	.257	.372
Initial Resistance Coefficient (C_I)	.0532	.0546	.0254	.0735	.0337
Time of Final Data (hrs.)	490	463	524	264	332
Final Width (cm) (B)	120	107	136	157	123
Final Depth (cm) (D)	1.17	1.50	1.77	1.96	1.75
Final Slope (S)	.00526	.00505	.00446	.00562	.00476
Final Froude No. (F)	.295	.227	.280	.208	.314
Final Resistance Coefficient (C)	.0601	.0974	.0569	.130	.0481
Pattern	B	M	M	T	M
Wandering Belt (m) (B_W)	-	1.34	1.67	1.68	1.27
Meander Wave Length (m) (λ)	-	4.91	4.59	3.89	6.07
λ_A	-	4.34	5.91	5.76	5.92
λ_{A1}	-	.69	1.22	.79	1.33
λ_{A2}	-	1.44	2.31	1.72	2.37

Table 2-2. Basic Data of the Tilting-Flume Experiments

Run Number	117	118	119	121	124	125	126	127
Discharge (ℓps) (Q)	0.7	0.8	0.9	0.5	0.7	0.7	0.7	0.7
Initial Width (cm) (B_I)	29.97	30.5	30.6	29.53	29.87	30.17	29.6	32.13
Initial Depth (cm) (D_I)	.85	.848	.891	.669	.786	.923	.87	.708
Initial Slope (S_I)	.00655	.00655	.0063	.00664	.00688	.00582	.00505	.00902
Initial Froude No. (F_I)	.951	1.072	1.116	.988	1.074	.835	.93	1.168
Initial Resis. Coeff. (C_I)	.00724	.00569	.00505	.0068	.00596	.00834	.00583	.00661
Sediment Discharge (gm/sec) (Q_s)	1.40	2.50	1.441	0.833	0.806	1.257	0.574	2.133
Final Width (cm) (B)	44.35	42.75	49.17	40.30	49.02	37.60	41.70	39.45
Final Depth (cm) (D)	.773	.789	.809	.603	.672	.879	.957	.803
Final Slope (S)	.00805	.00743	.0071	.00628	.00609	.00572	.00595	.008675
Final Froude No. (F)	.741	.852	.803	.846	.828	.713	.572	.787
Final Resis. Coeff. (C)	.0147	.01023	.01101	.00877	.00888	.01125	.01818	.0140
Pattern	M	M	M	M	B	M	M	T
Wandering Belt (m) (B_W)	.712	.699	.701	.593	-	-	.658	-
Meandering Wave Length (m) (λ)	2.8	3.0	3.0	3.3	-	-	3.9	-
Temperature ^oC	9°C	8°C	6°C	7°C	8°C	6°C	10°C	5°C
Rate of Migration (m/hr.)	.23	.22	.35	.09	-	-	-	-
Run Time (hrs.)	3.5	3.0	3.0	6.0	6.0	4.0	12.0	20

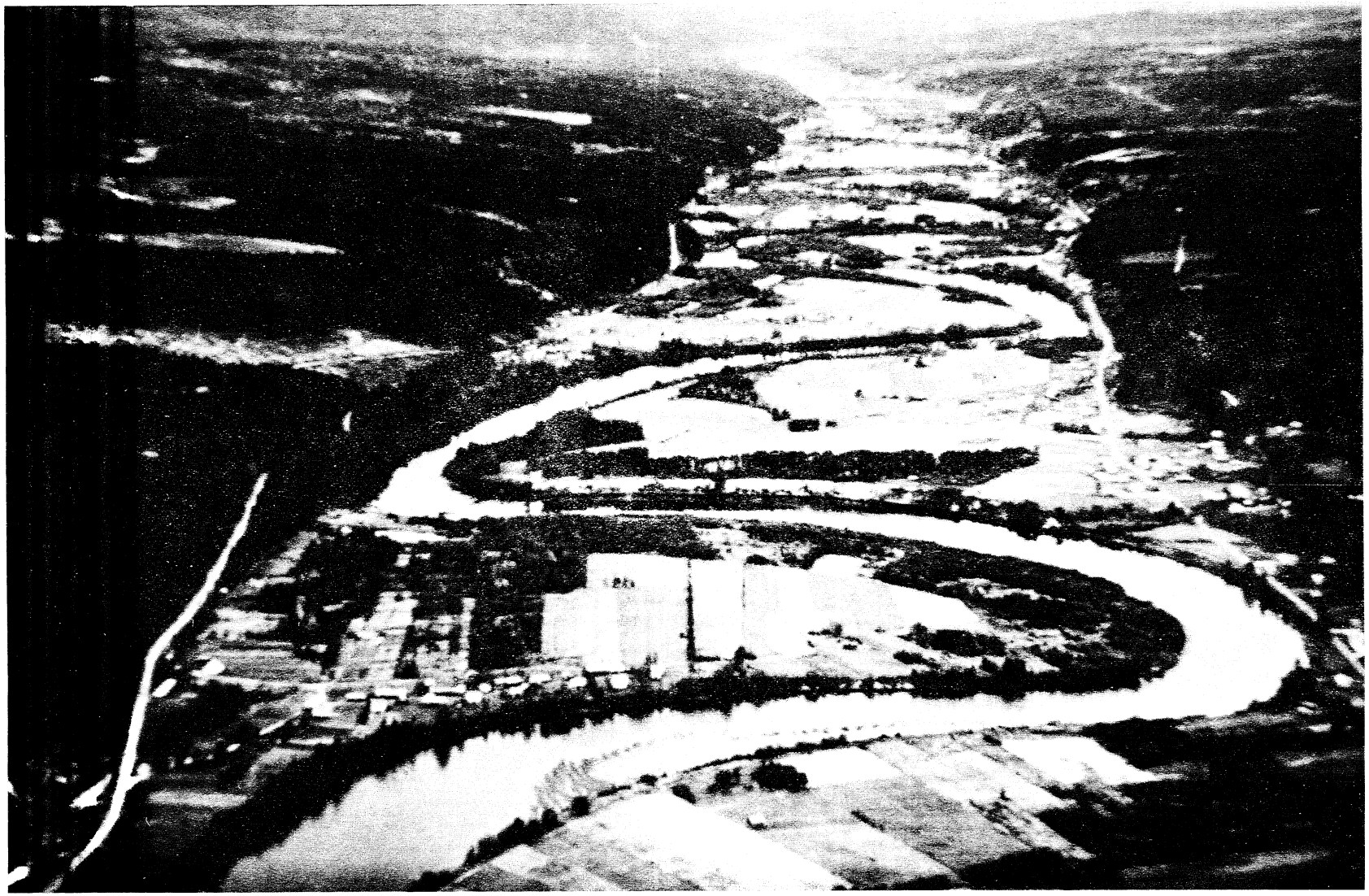

Fig. 2-1. The Klaralven River of Sweden, a typical mature river with developed, confined meanders. (Photo courtesy A. Sundborg)

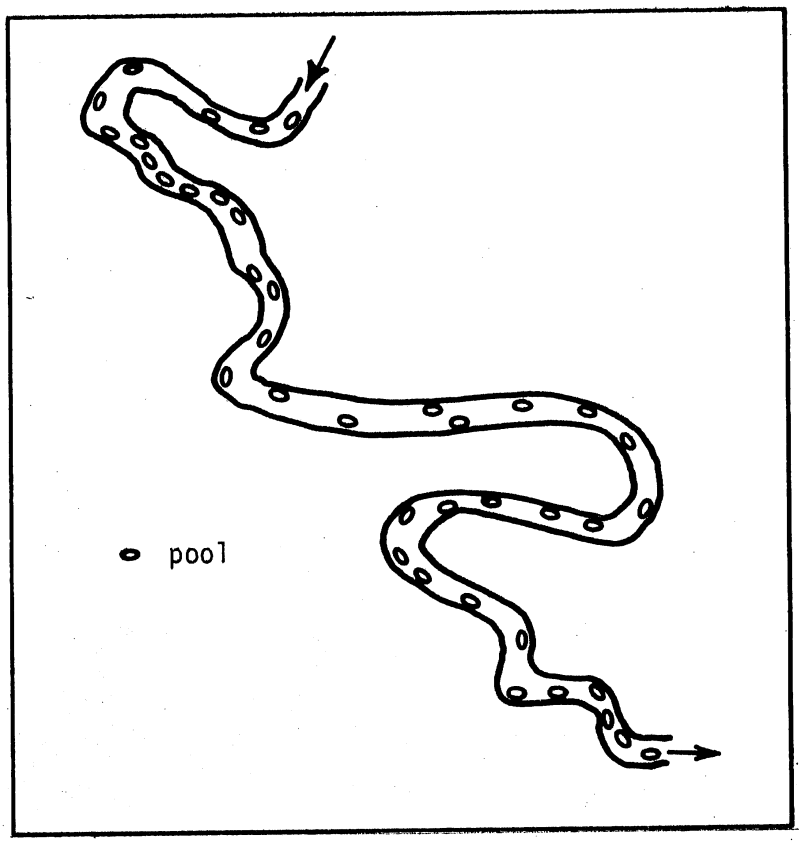

Fig. 2-2. Features of Meandering

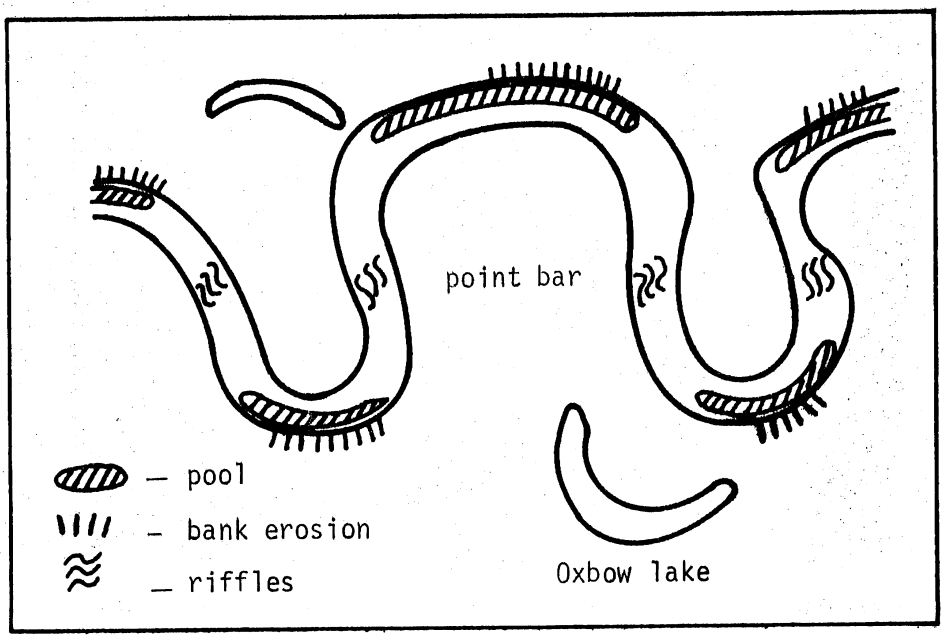

Fig. 2-3. The pool pattern of Dry Creek near Winters, California (after Keller, 1972).

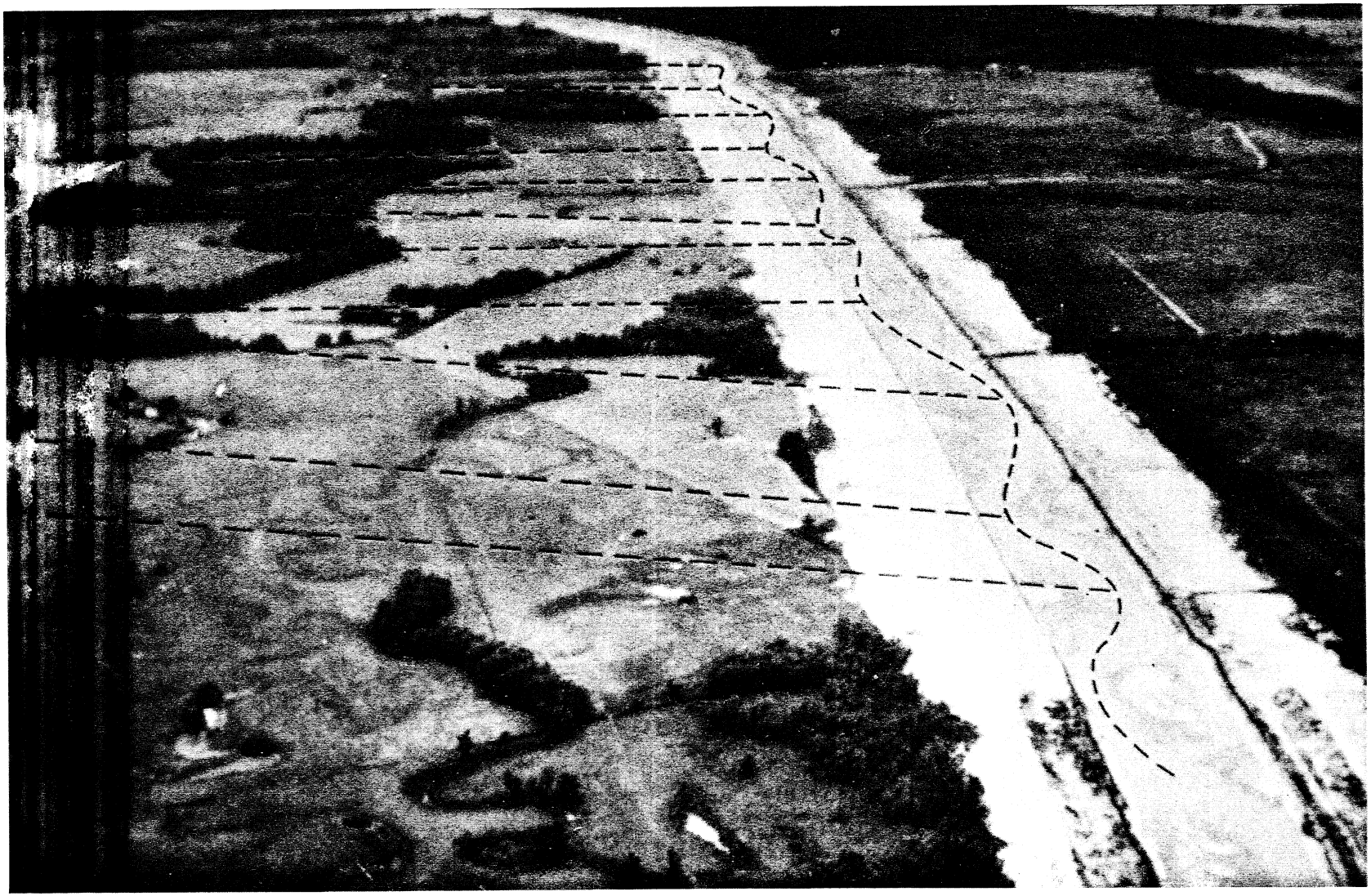

Fig. 2-4. Channel pattern of the Skuna River before and after channelization. (Photo from Yang and Stall, 1973)

Fig. 2-5. A drainage ditch in Georgia showing the alternate bars characteristic of incipient meandering (after Anderson, 1967).

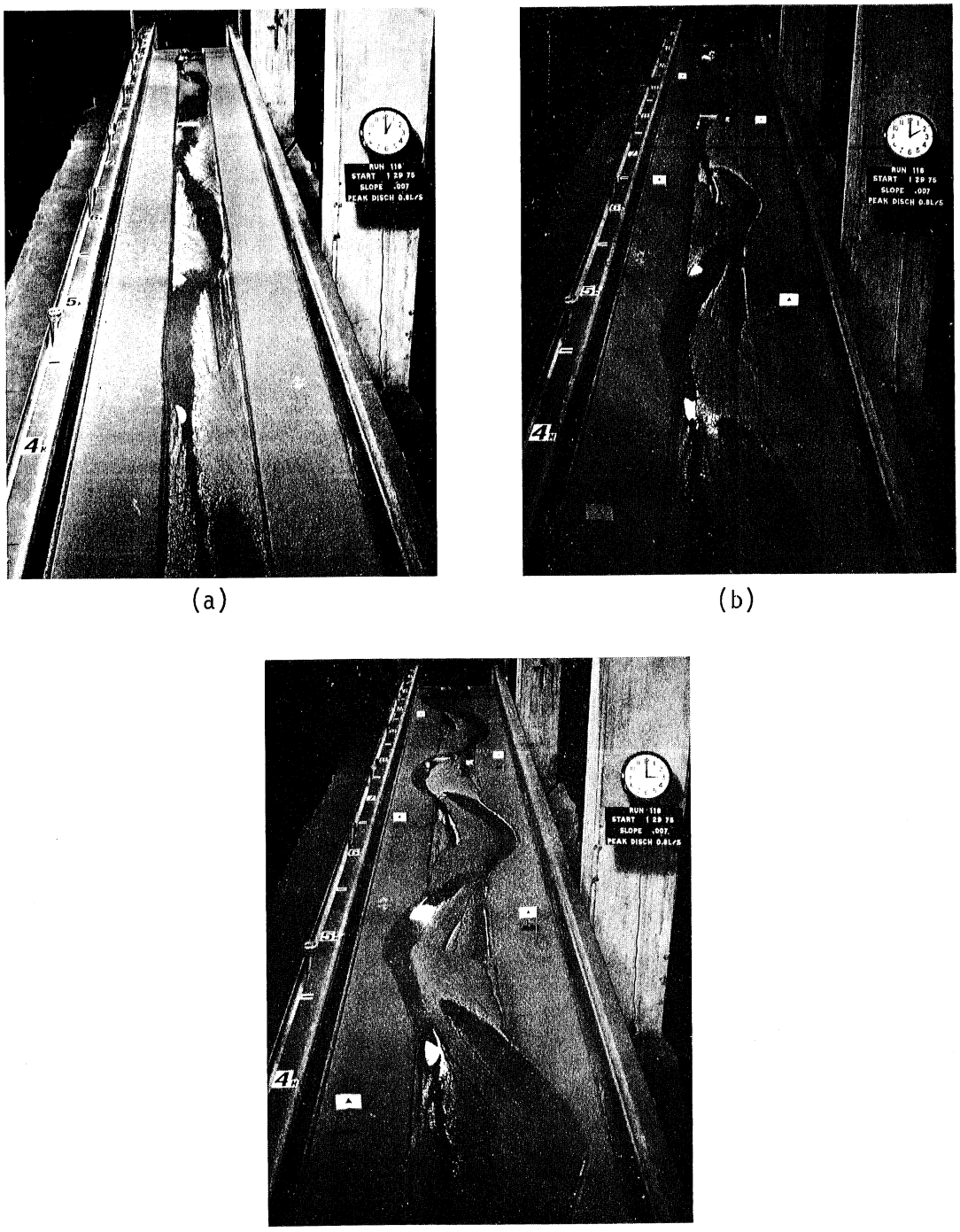

Fig. 2-6. Development of meandering in the laboratory during run 118. Discharge has been lowered to clarify the bar patterns:
(a) after one hour of flow an alternate bar pattern has formed in the channel, which remains essentially straight;
(b) after two hours, the bar pattern has induced local bank erosion;
(c) after three hours, a developed meander pattern is observed.

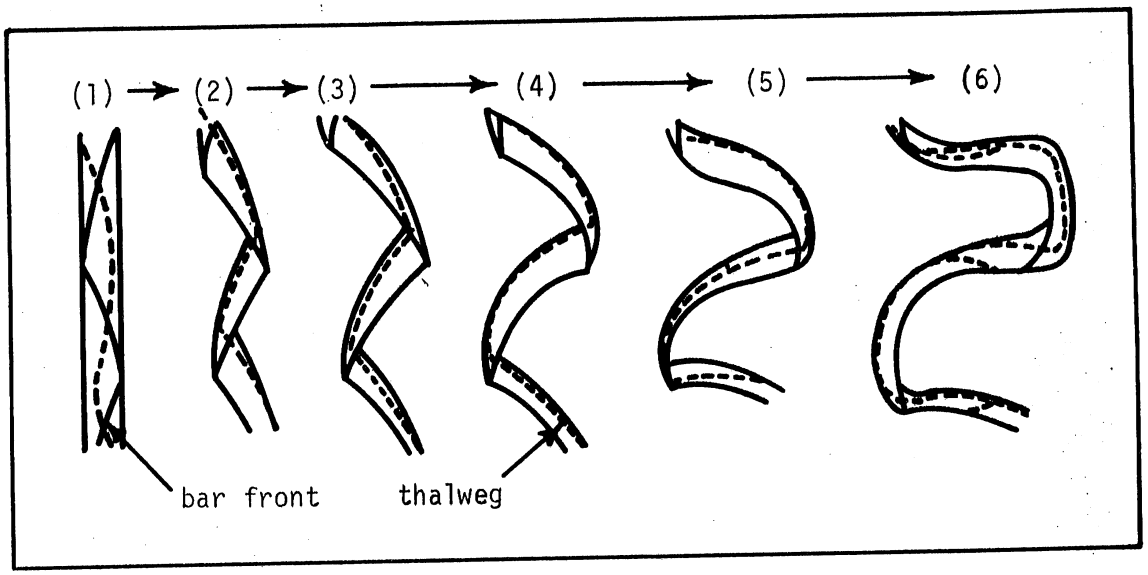

Fig. 2-7(a)

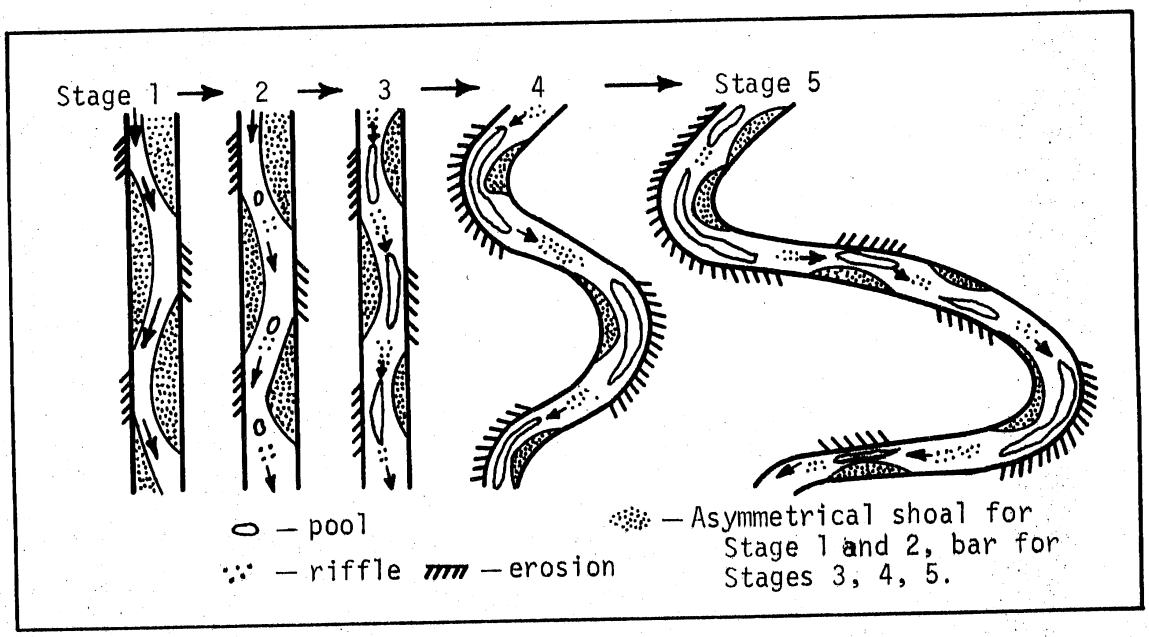

Fig. 2-7(b)

Fig. 2-7. Models of meander development; (a) Kinoshita's model, (b) Keller's model.

Fig. 2-8. Canal in Oklahoma showing meandering and secondary bank erosion. (Photo courtesy Dr. Don DeCoursey, ARS)

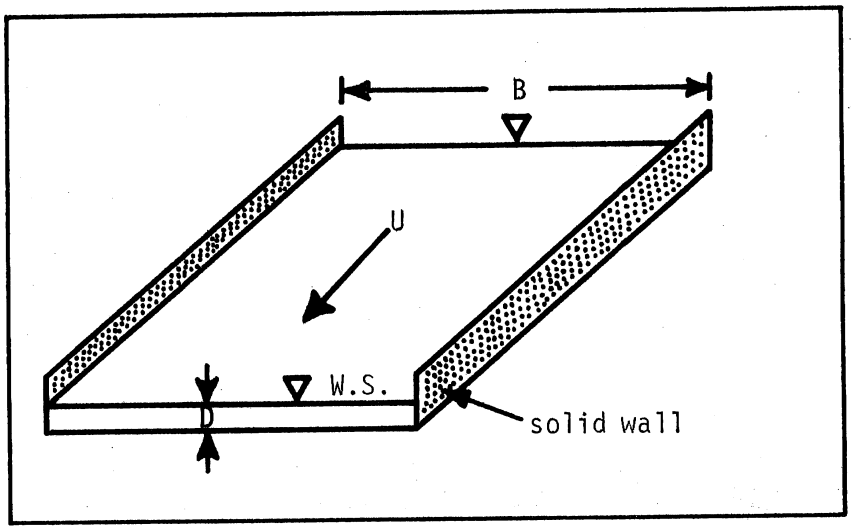

Fig. 2-9. The model alluvial river; B is width, D is depth, and U is velocity.

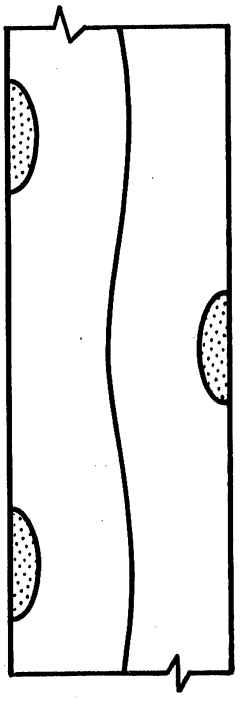

m = 1

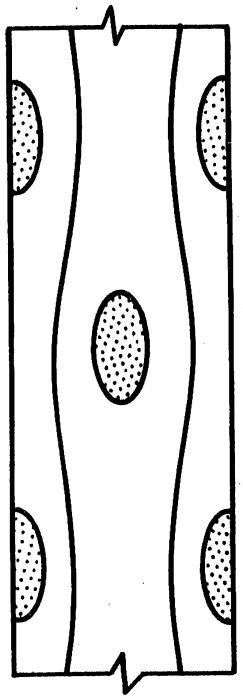

m = 2

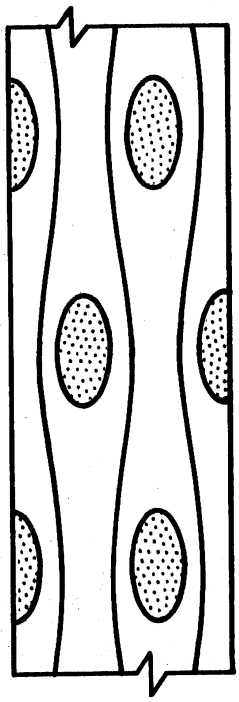

m = 3

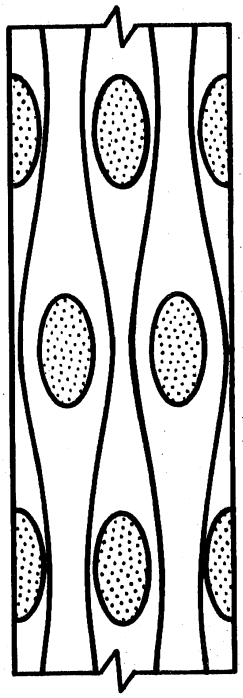

m = 4

Fig. 2-10. Bar-like perturbations in the model alluvial river, exposed at low flow. The number of braids is given by m. Note that for meandering m = 1.

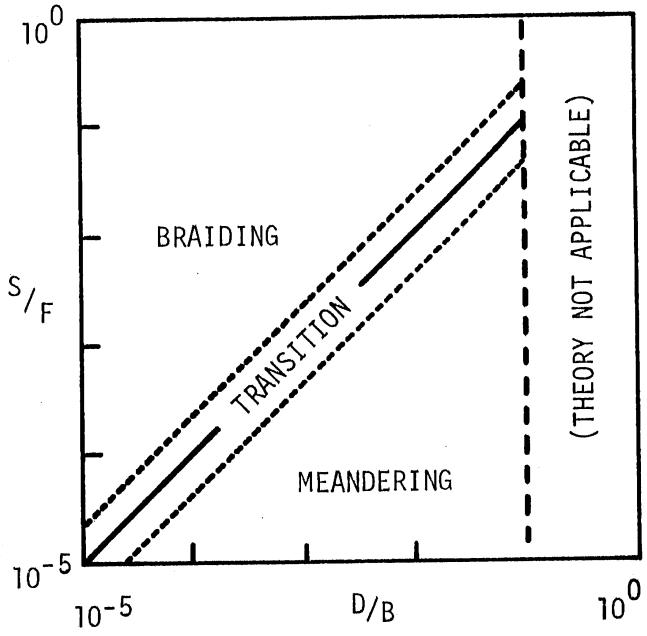

Fig. 2-11. Proposed meander-braid regime diagram.

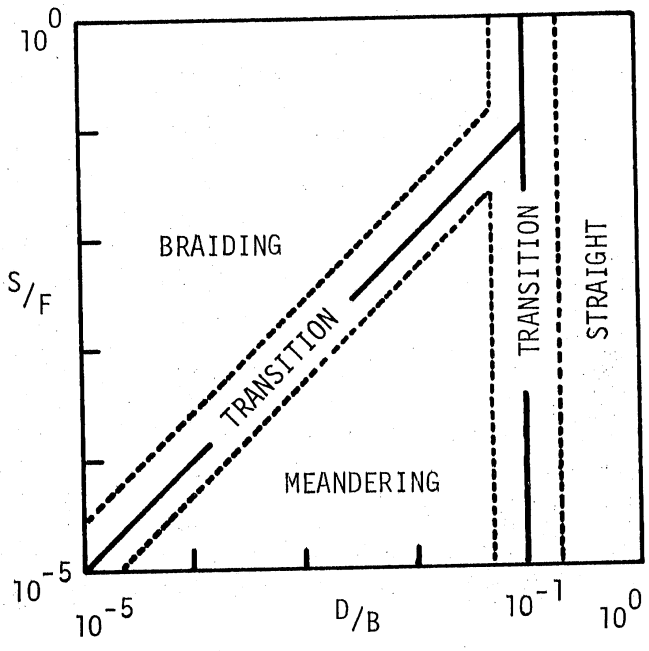

Fig. 2-12. Revised meander-braid-straight regime diagram.

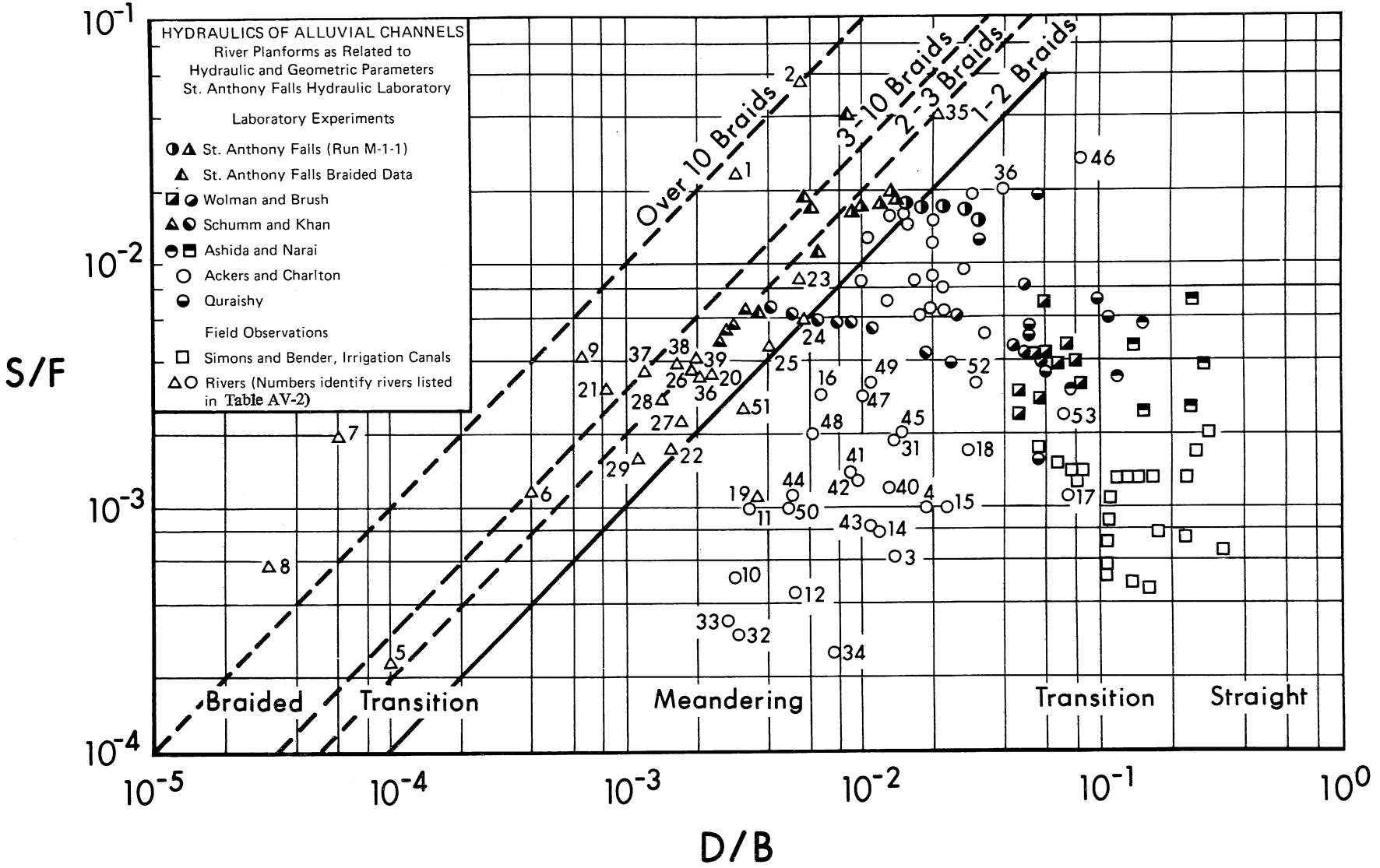

Fig. 2-13. Comparison of the theoretical meander-braid-straight diagram with data. Circles denote meandering, triangles denote braiding and squares denote straight reaches of rivers.

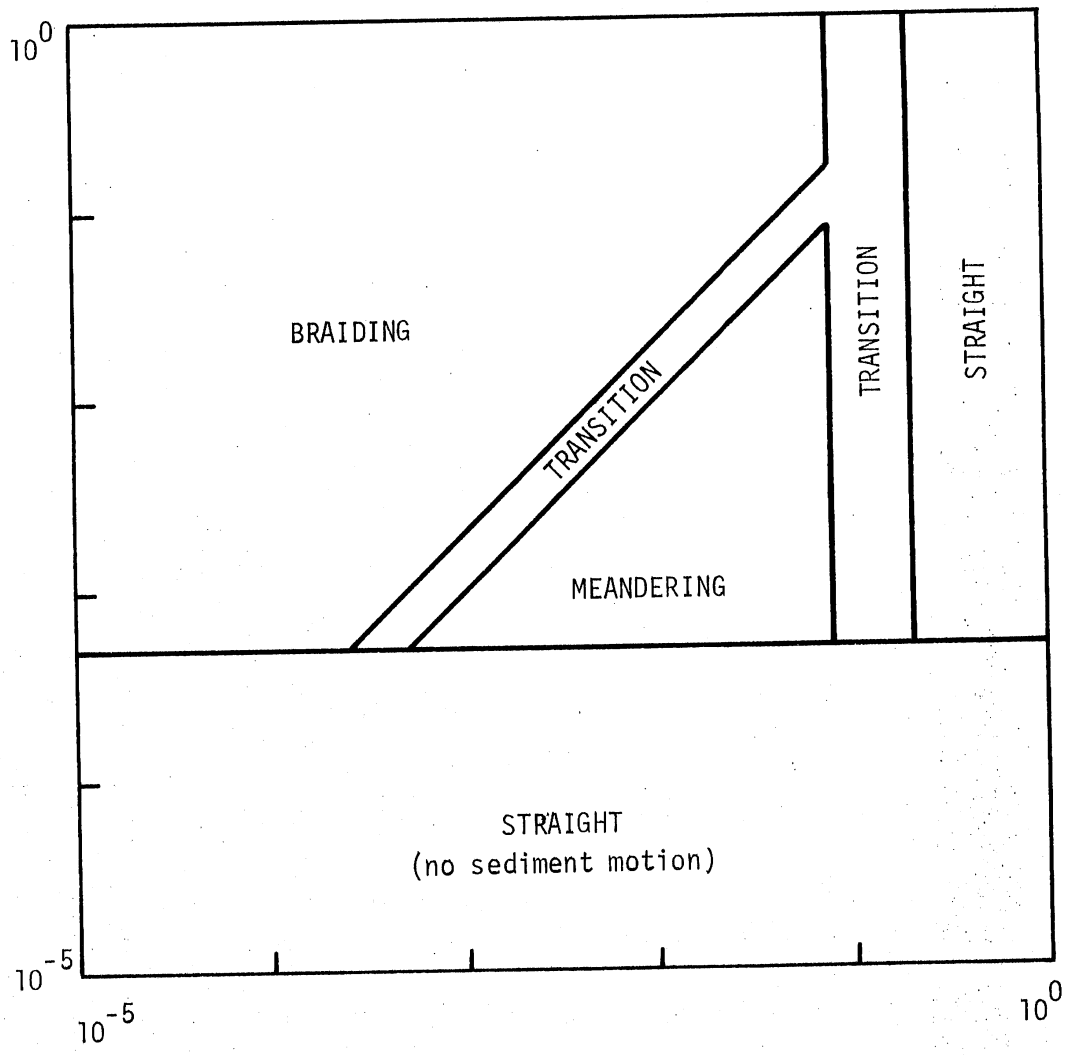

Fig. 2-14. Meander-braid-straight regime diagram for a value of φ^* of .0005.

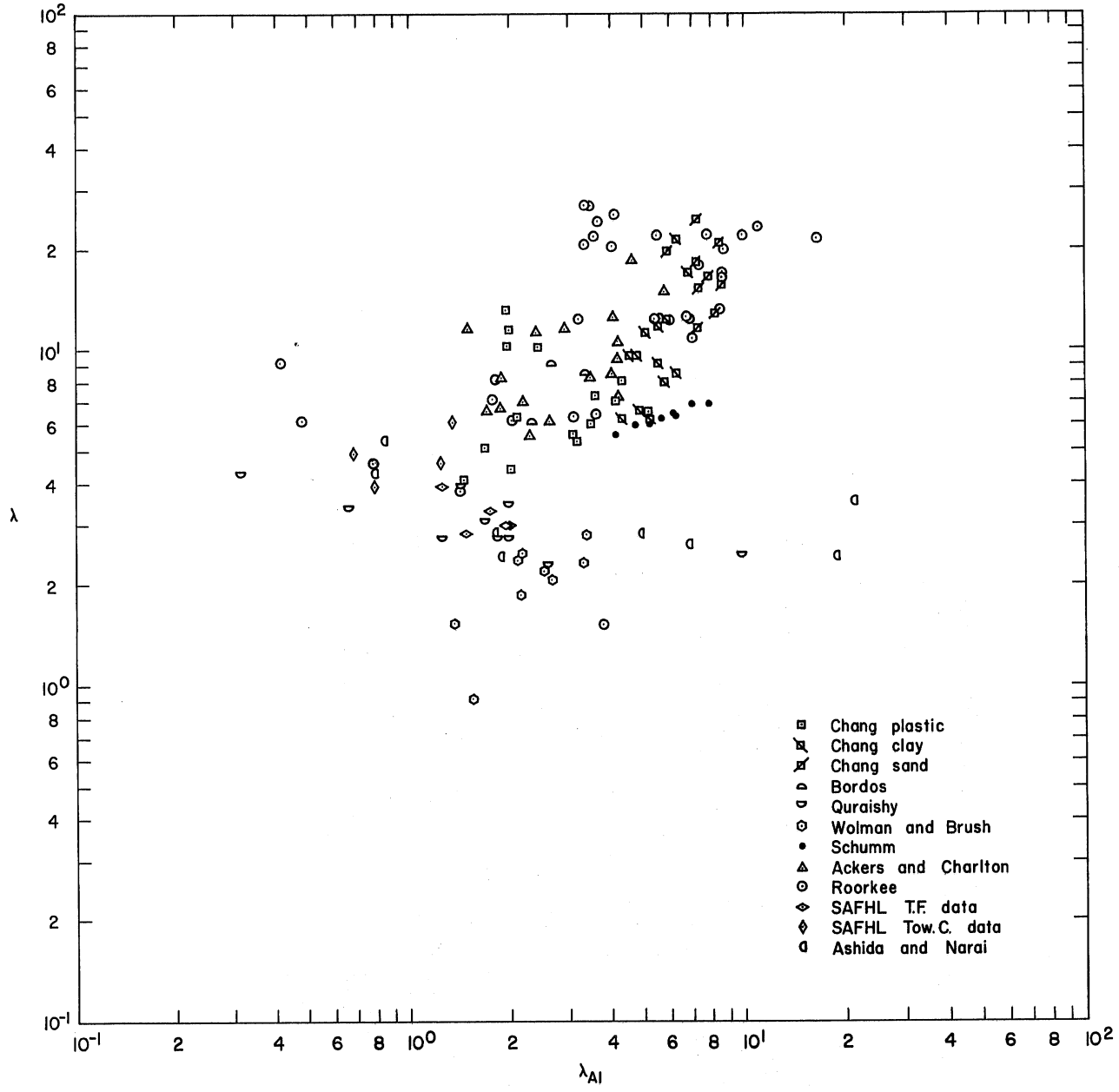

Fig. 2-15a. Actual wave length λ plotted against wave length estimate λ_{Al} provided by the first form of the modified Anderson equation. The units are meters.

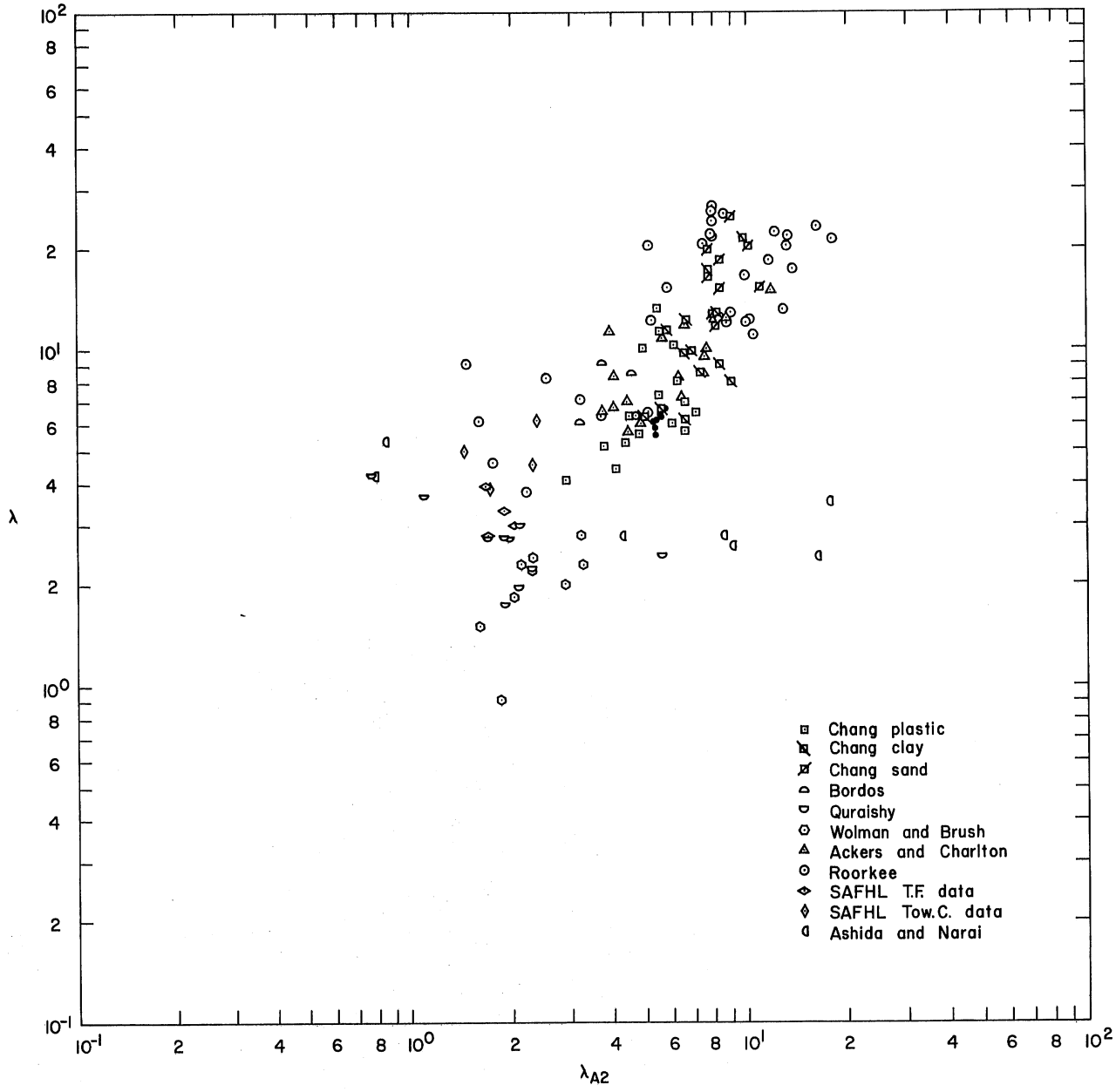

Fig. 2-15b. Actual wave length λ plotted against wave length estimate λ_{A2} provided by the second form of the modified Anderson equation. The units are meters.

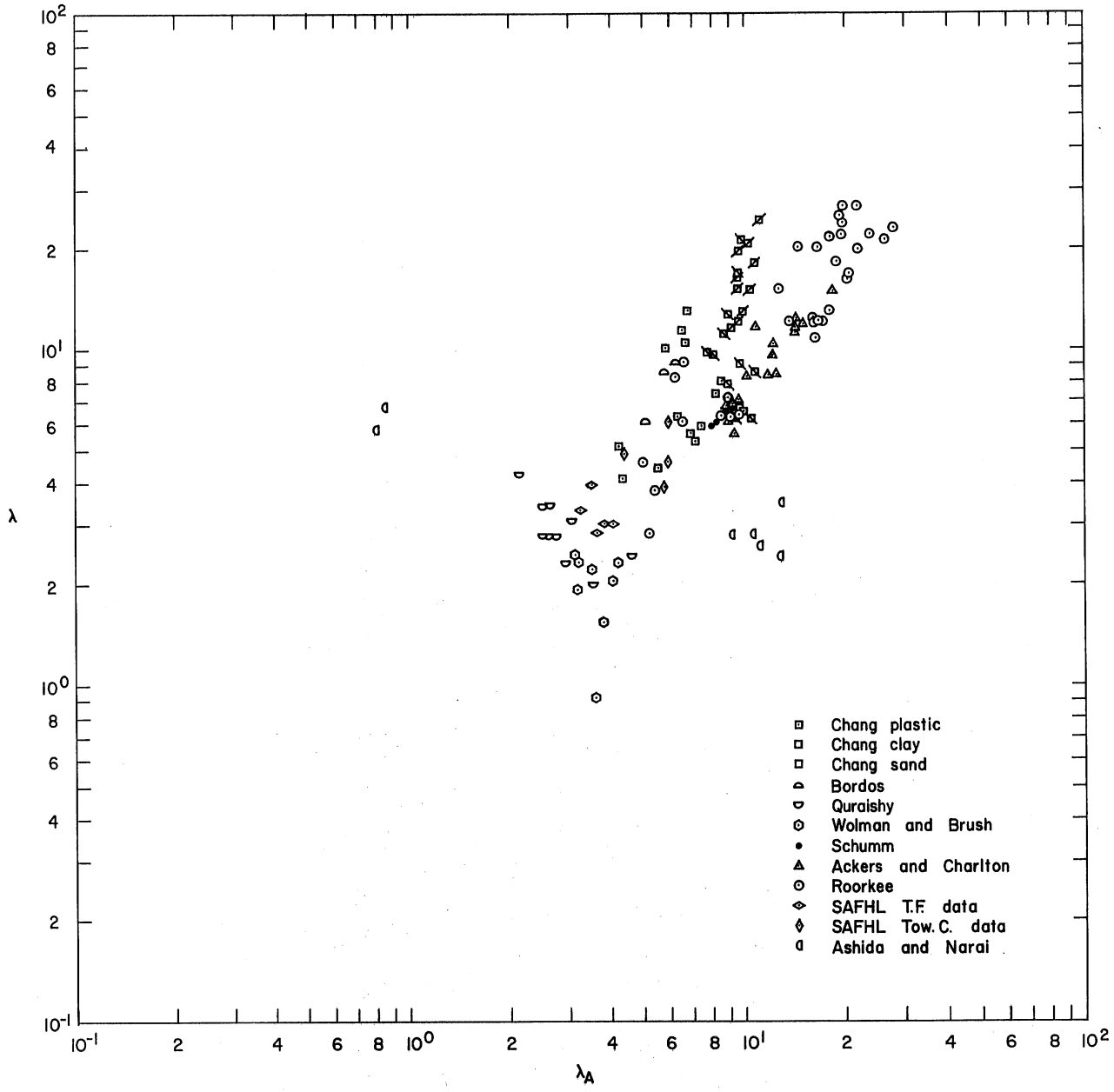

Fig. 2-15c. Actual wave length λ plotted against wave length estimate λ_A provided by the Anderson (1967) equation. The units are meters.

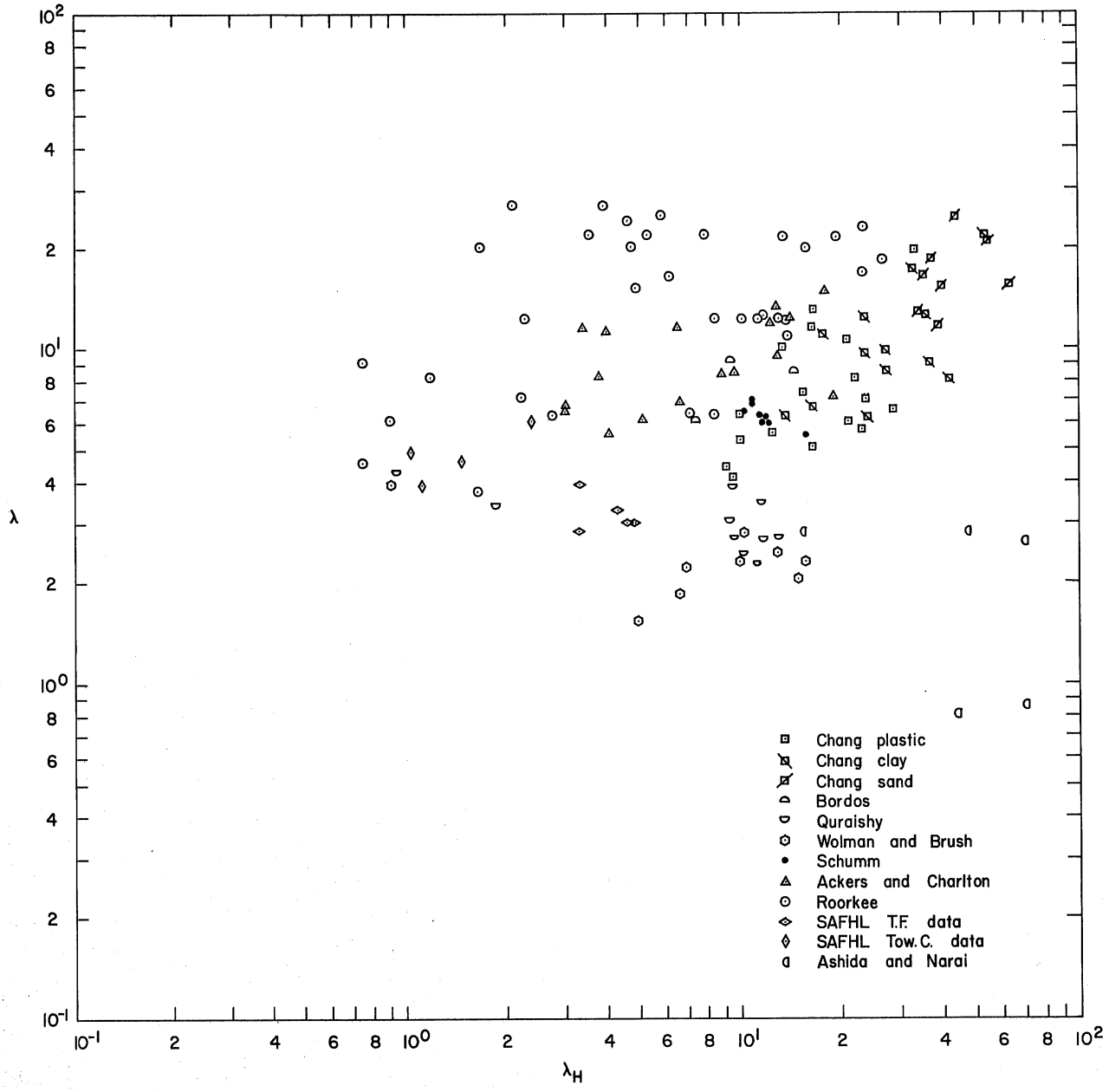

Fig. 2-15d. Actual wave length λ plotted against wave length estimate λ_H provided by the Hansen (1967) equation. The units are meters.

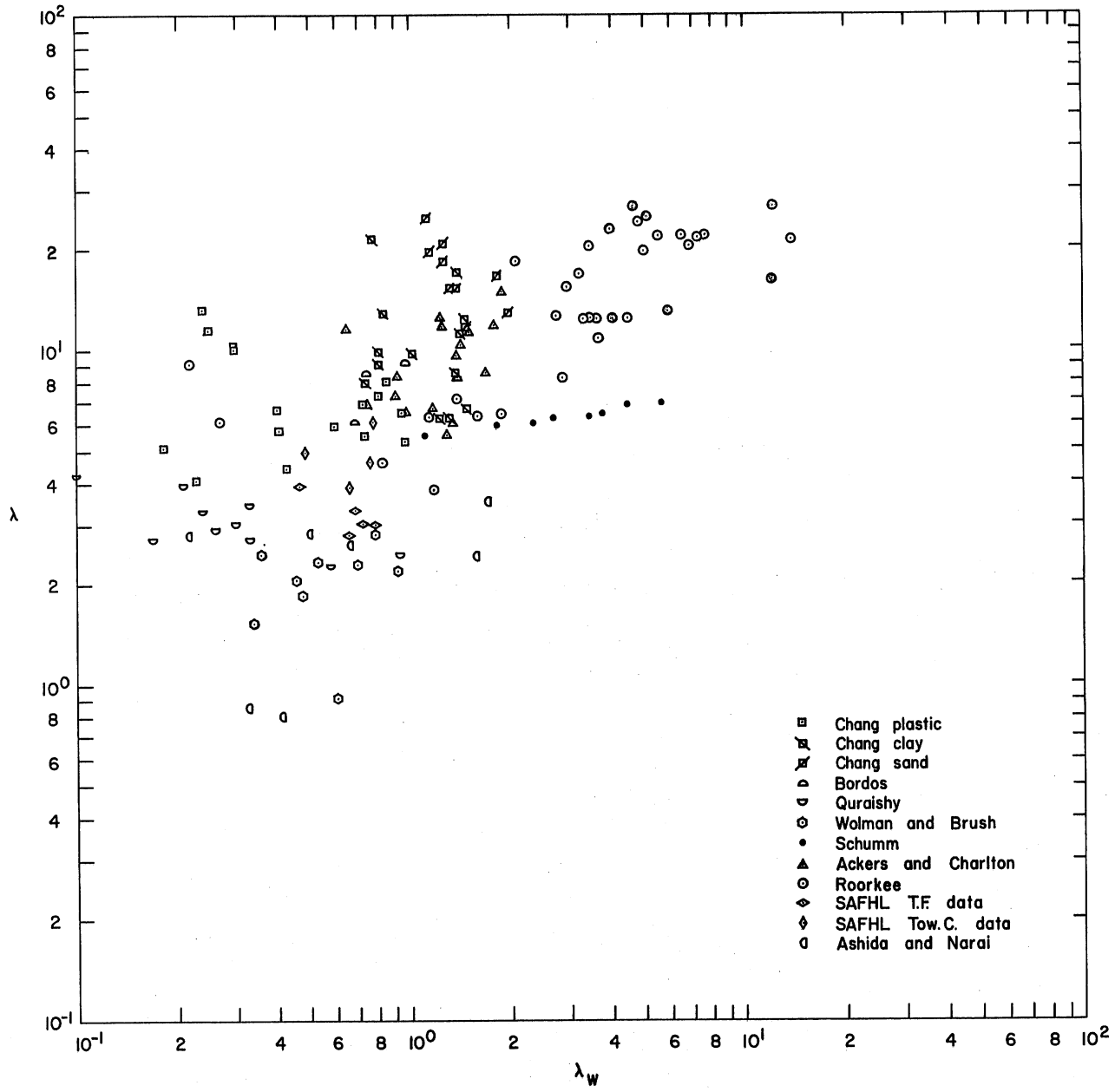

Fig. 2-15e. Actual wave length λ plotted against wave length estimate λ_W provided by the Werner (1951) equation. The units are meters.

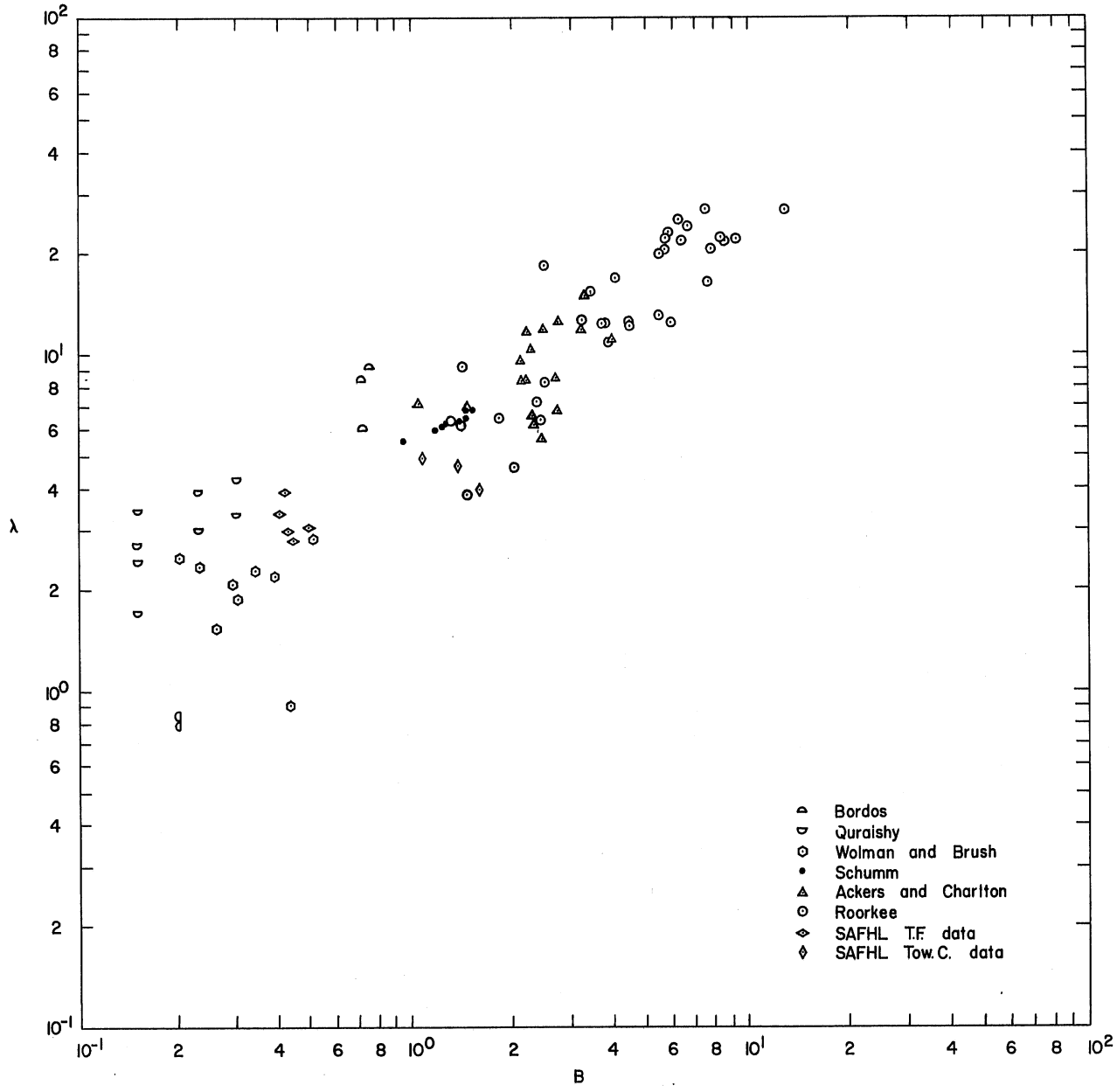

Fig. 2-16. Meander length λ plotted against B. Only data from model rivers which were free to erode their banks have been included. The units are meters.

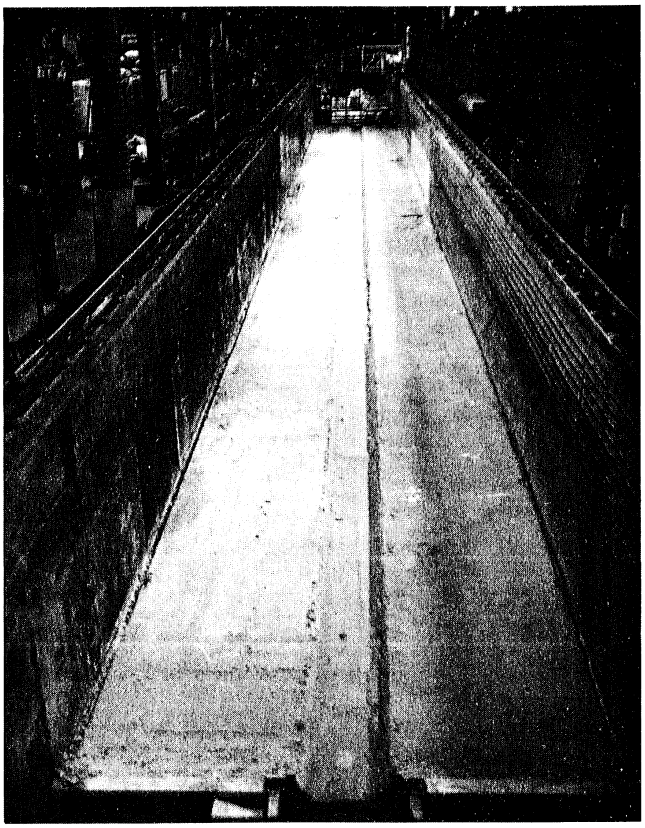

Fig. 2-17. The towing channel model river multi-purpose facility.

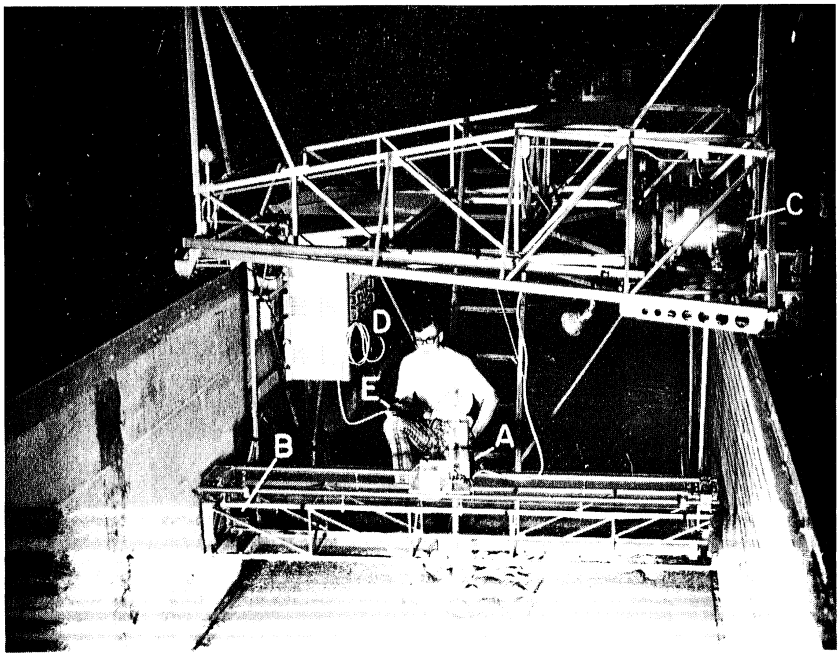

Fig. 2-18. The automatic point gauge.

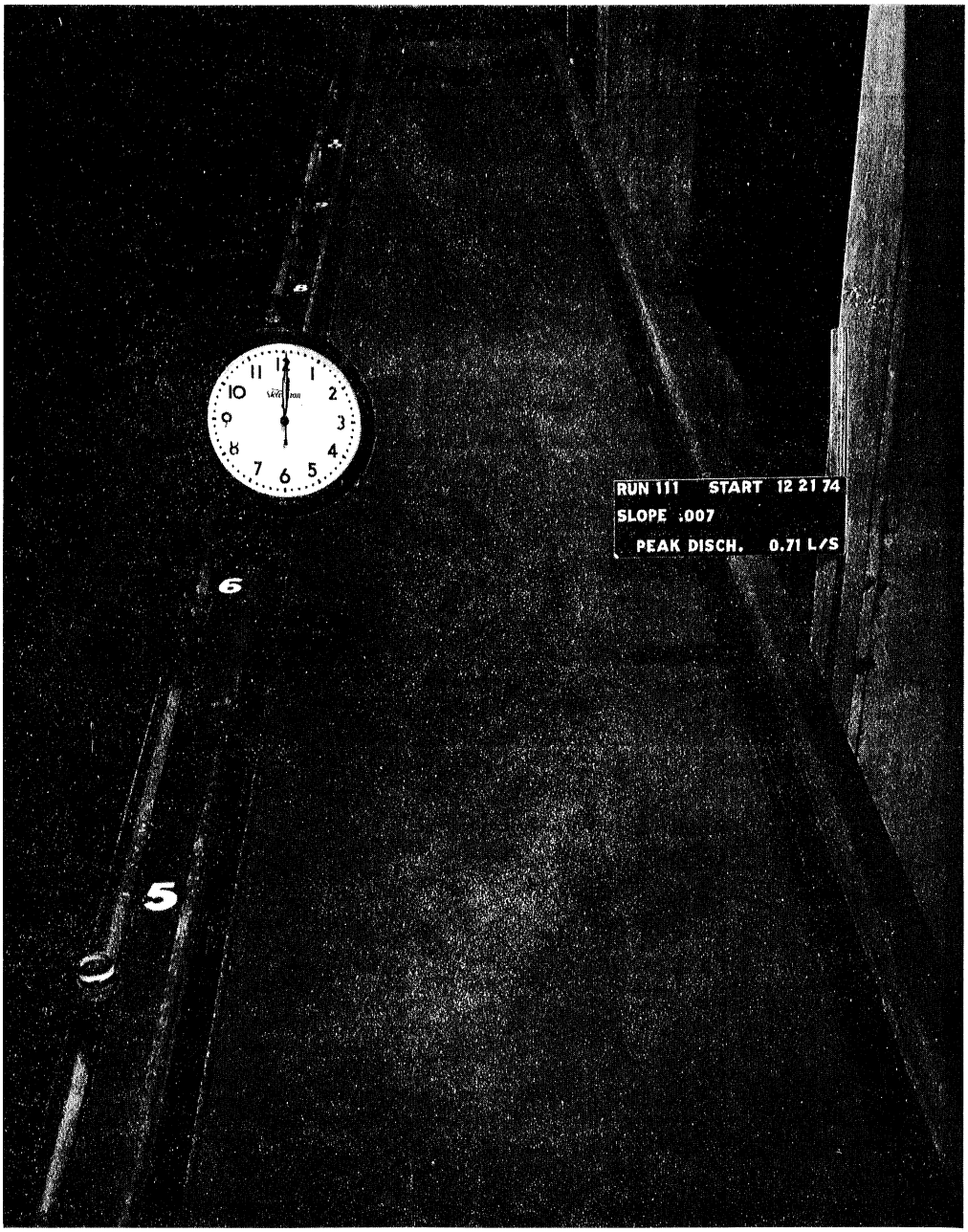

Fig. 2-19. The tilting flume model river facility.

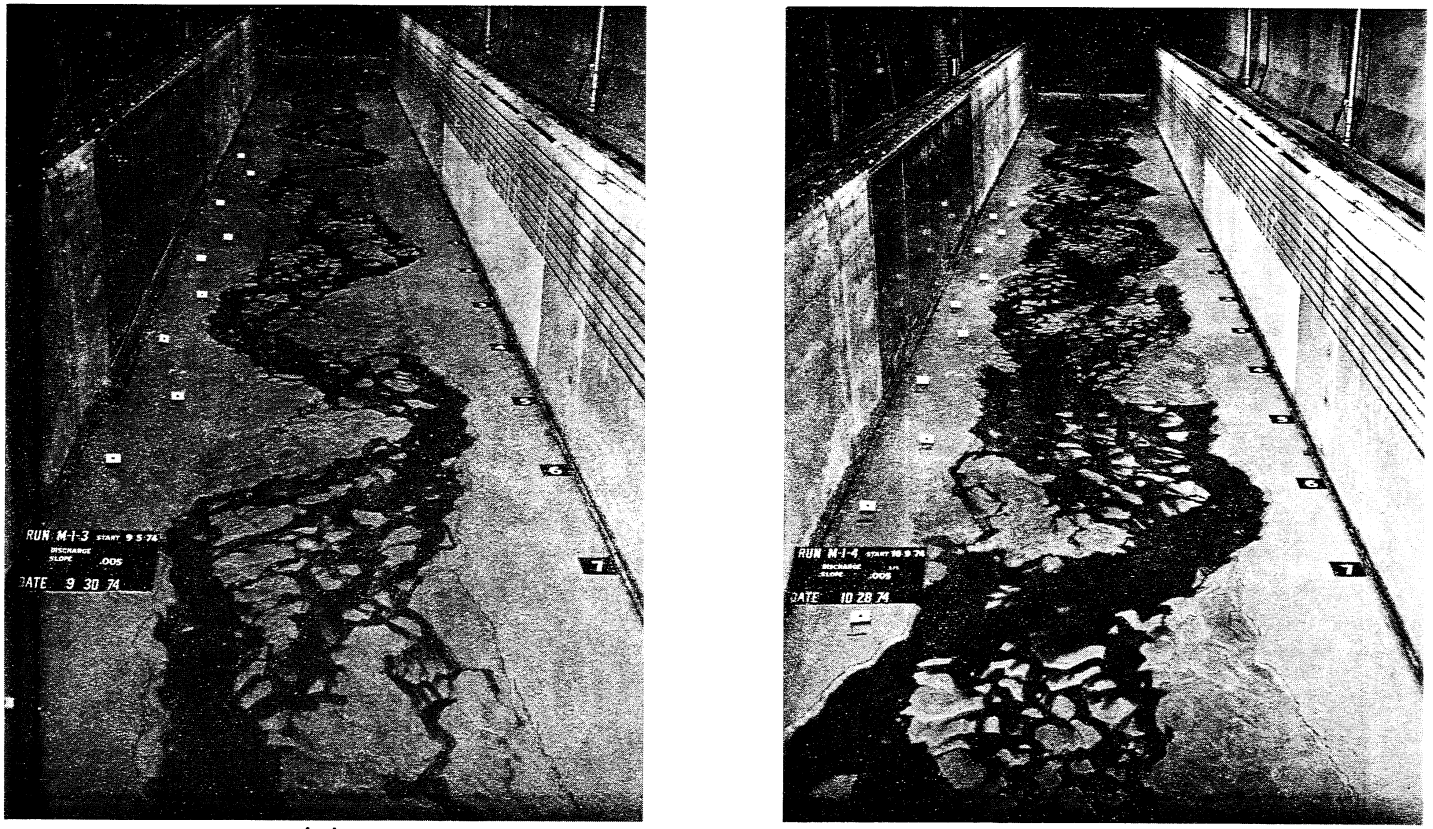

(a) (b)

Fig. 2-20. (a) Run M-1-3 at completion. The discharge has been lowered and dye introduced to make the pattern more apparent. The channel is transitional but tends more toward meandering than braiding.

(b) Run M-1-4 at completion. Again the flow has been lowered and dye added. The channel is transitional-braided.

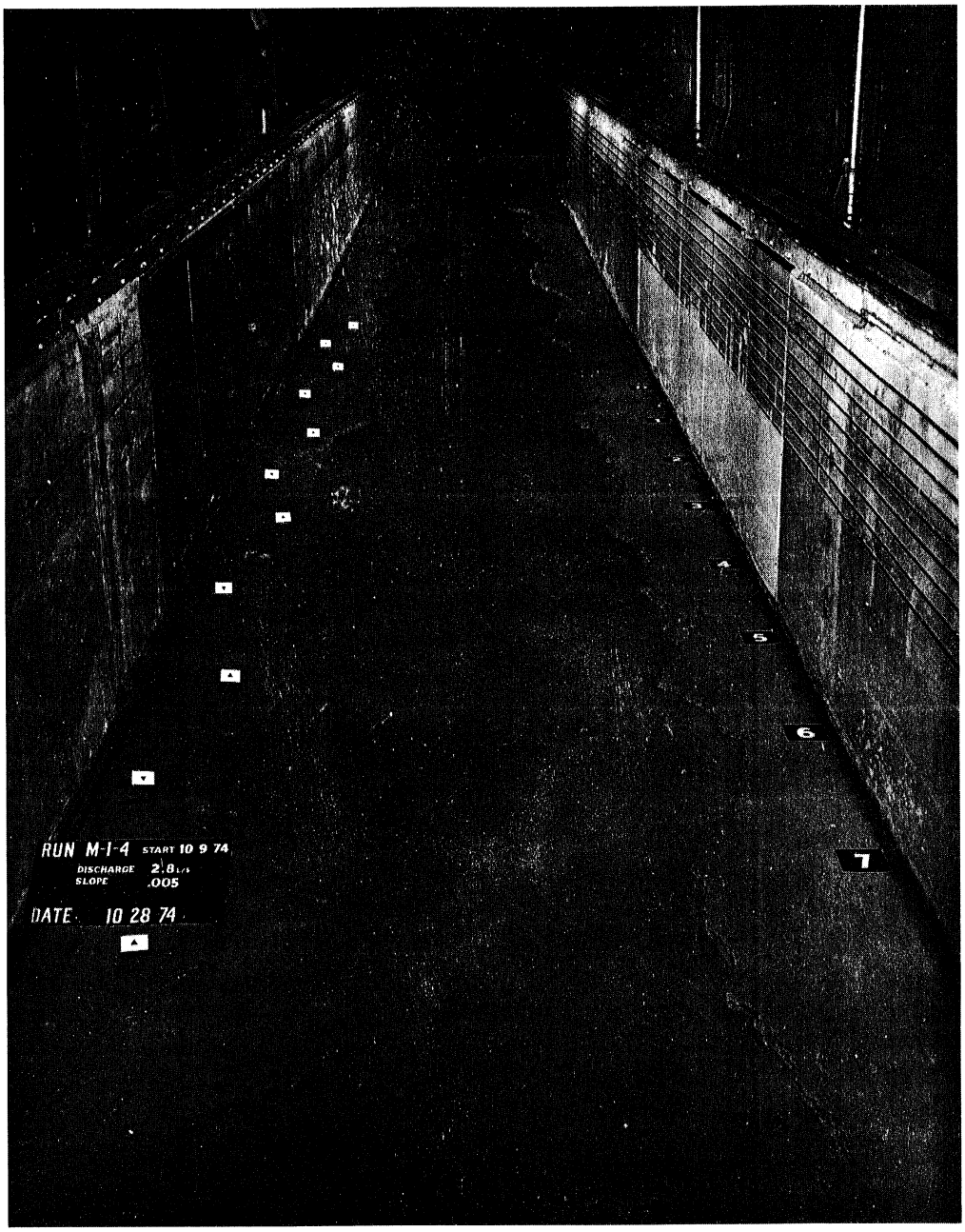

Fig. 2-21. Run M-1-4 at completion. The flow conditions are that of the high flow of the hydrograph.

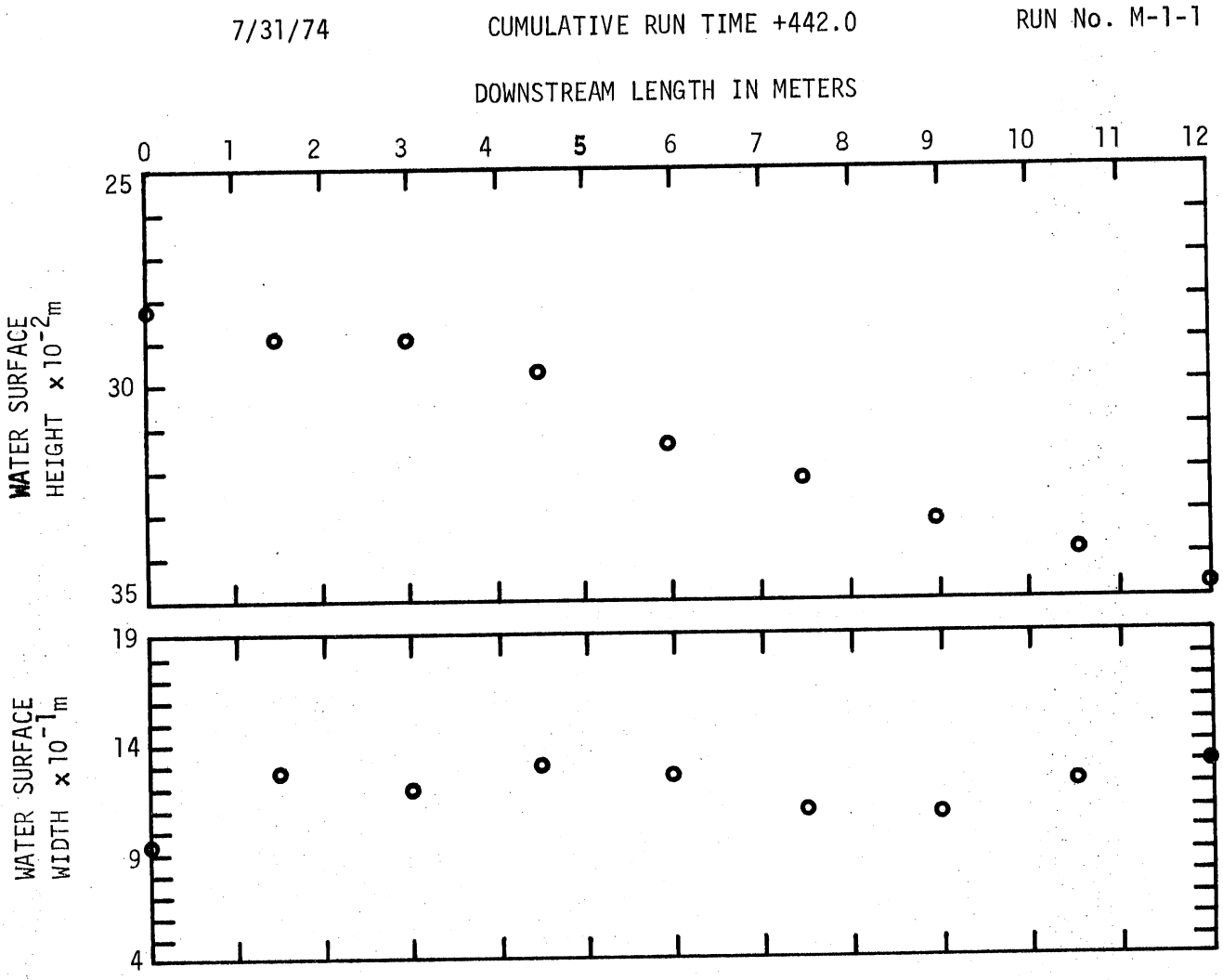

Fig. 2-22. Typical water-surface height and width profiles down the channel for Run M-1-1.

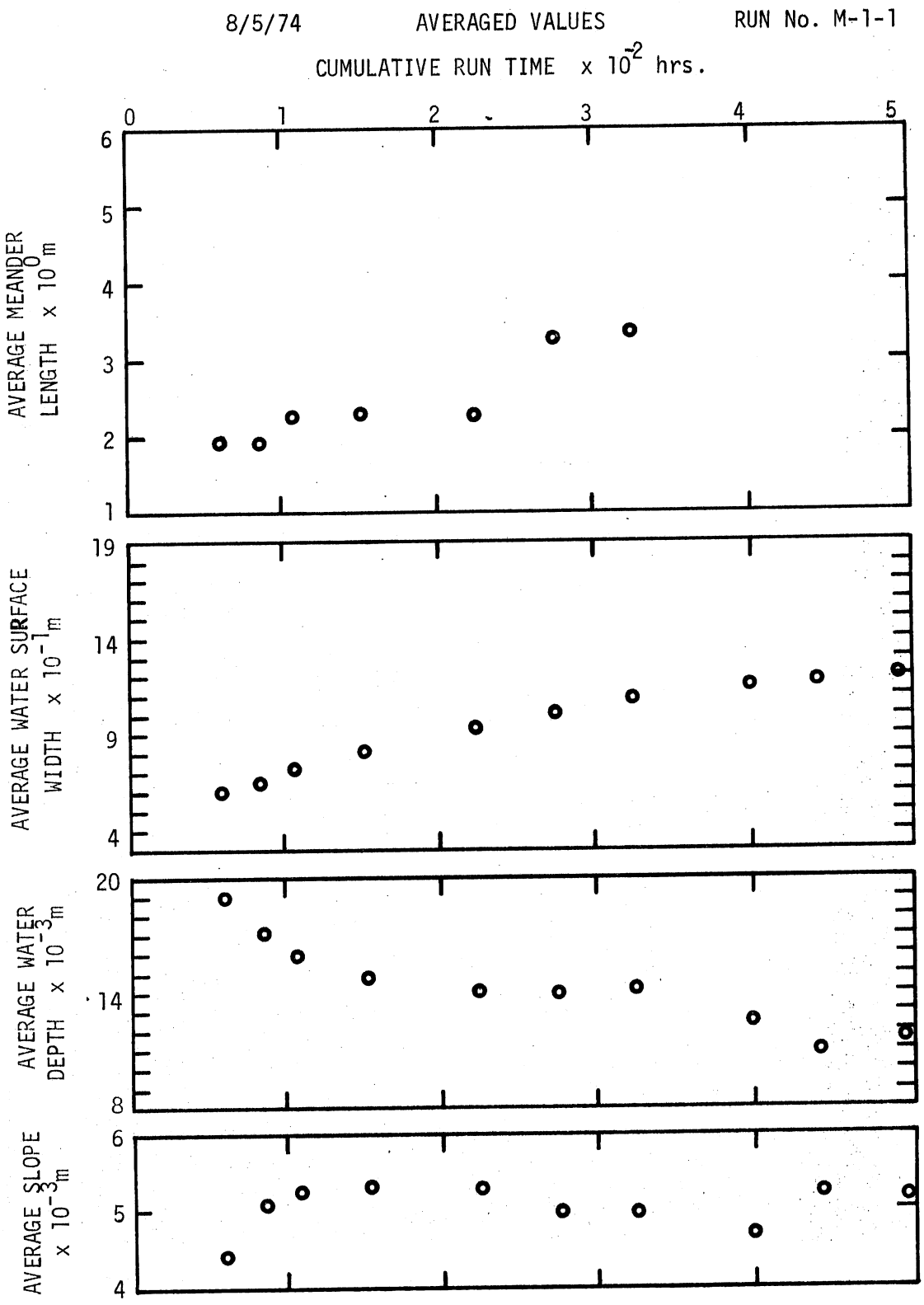

Fig. 2-23. Time development of channel-averaged water surface width, slope, depth, and meander length for Run M-1-1.

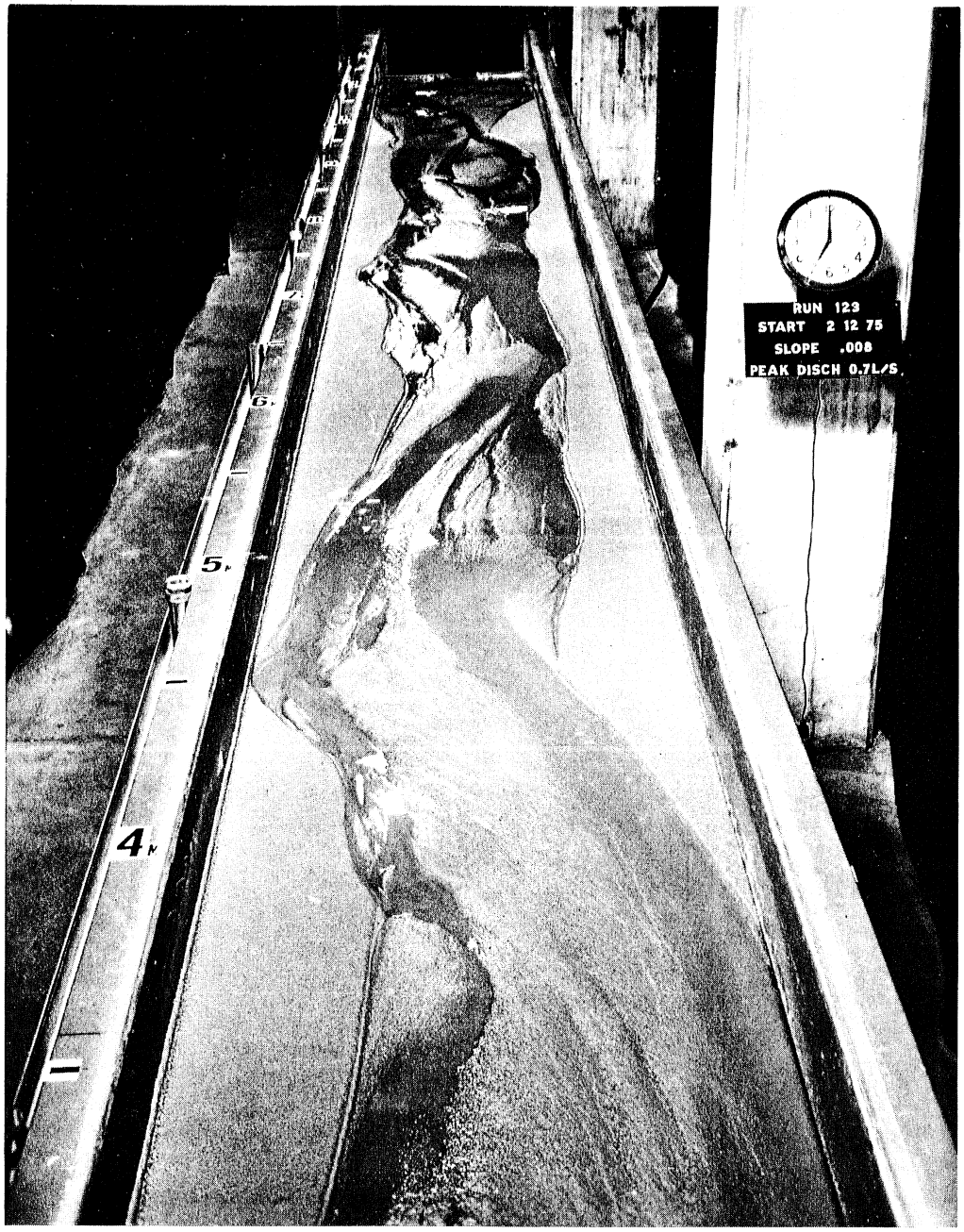

Fig. 2-24. An example of a braided channel achieved in the tilting flume.

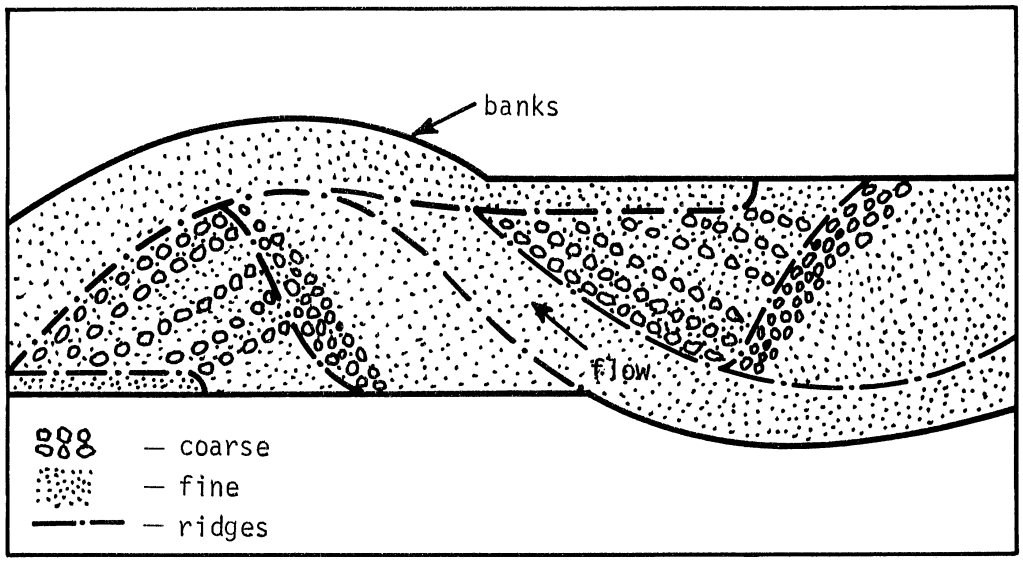

(a) Illustrated schematically.

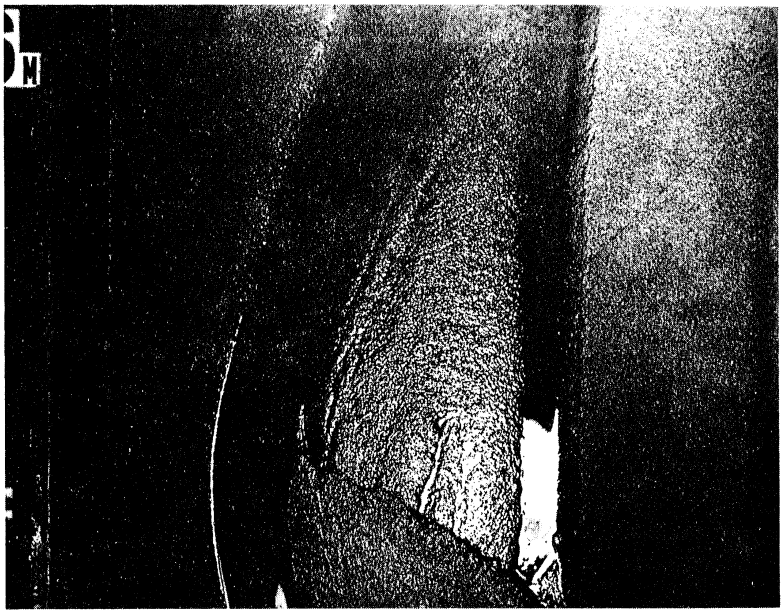

(b) Illustrated photographically.

Fig. 2-25. Patterns of areal sorting and bed topography in the tilting flume.

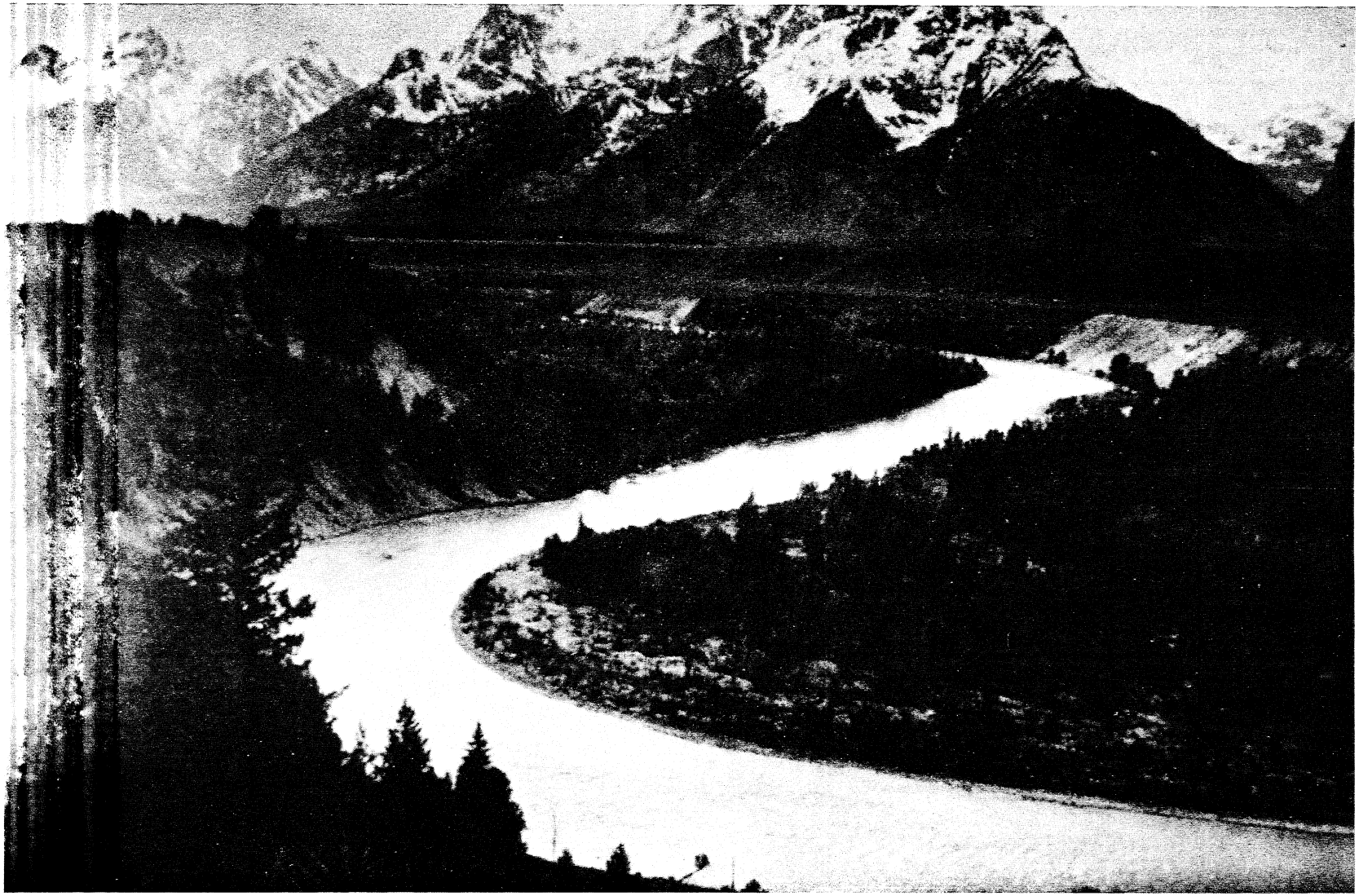

Fig. 2-26. A mature river illustrating active encroachment on valley walls similar to that of the laboratory experiment shown in Fig. 2-6.

References for Chapter 2

Ackers, P. Experiments on Small Streams in Alluvium, Rpt. No. INT. 28, Hydraulics Research Station, Wallingford, England, 1962.

Anderson, A.G. "On the Development of Stream Meanders," Proc., 12th Congress Intl. Association for Hydraulic Research, Fort Collins, Colorado, Vol. I, Paper No. A46, 1967, pp. 370-378.

Anderson, A.G. Tentative Design Procedure for Riprap-Lined Channels, Project Report No. 96, St. Anthony Falls Hydraulic Laboratory, 1970, 75 pp.

Anderson, A.G. Tentative Design Procedure for Riprap-Lined Channels - Field Evaluation, Project Rpt. No. 146, St. Anthony Falls Hydraulic Laboratory, 1973, 53 pp.

Chang, H.Y., D.B. Simons, and D.A. Woolhiser. "Flume Experiments on Alternate Bar Formation," Proc., Journal of Waterways, Harbors and Coastal Engineering Div., American Society of Civil Engineers, Vol. 97, No. WW1, 1971, pp. 155-165.

Dury, G.H. "Relation of Morphometry to Runoff Frequency," In Introduction to Fluvial Processes (R. Chorley, ed.), Methuen, London, 1969.

Fahnestock, R.K. and W.C. Bradley. "Knik and Matanuska Rivers, Alaska: A Contrast in Braiding," In Fluvial Geomorphology. (Proc., 4th Annual Geomorphology Symposium, Binghamton, New York, M. Mousawa, ed.), 1973.

Fahnestock, R.K. and T. Maddock, Jr. Preliminary Report on Bed Forms and Flow Phenomena in the Rio Grande near El Paso, Texas, U.S. Geological Survey, Prof. Paper 501-B, 1964.

Gildea, A.P. Design Practice for Levee Revetment on West Coast Intermittent Streams, Paper No. 57, Proc., Federal Interagency Sedimentation Conference, Misc. Pub. No. 970, Agricultural Research Service, 1963, pp. 492-507.

Hansen, E. The Formation of Meanders as a Stability Problem, Basic Research Progress Rpt. No. 13, Hydraulic Library, Tech. Univ. of Denmark, 1967.

Henderson, C.M. Report on the 1960 Improvement Scheme, Waimakariri River, Report to the North Canterbury Catchment Board, North Canterbury, New Zealand, 1960.

Johnson, J.W. "The Importance of Considering Sidewall Friction in Bed Load Investigations," Civil Engineering, March, 1942, pp. 329 ff.

Keller, E.A. "Development of Alluvial Channels: A Five Stage Model," Geological Society of America Bulletin, Vol. 83, No. 5, 1972.

Kinoshita, R. "Formation of Dunes on River Bed - An Observation on the Condition of River Meandering," Proc., Japan Society of Civil Engineers, No. 42, 1957.

Neill, C.R. "Measurements of Bridge Scour and Bed Changes in a Flooding Sand-Bed River," Proc., Institute of Civil Engineers, Vol. 30, February 1965.

Ning, Chien. "The Braided Stream of the Yellow River," Scientia Sinica, Vol. X, No. 6, 1961.

Northrup, W.L. Republican River Channel Deterioration, U.S. Dept. Agriculture Misc. Pub. No. 970, 1963, pp. 409-424.

Parker, G. "On the Cause and Characteristic Scales of Meandering and Braiding in Rivers," Journal of Fluid Mechanics, in press.

Schumm, S.A. The Shape of Alluvial Rivers in Relation to Sediment Type, U.S. Geological Survey Prof. Paper 454-H, 1960.

Schumm, S.A. and H.R. Khan. "Experimental Study of Channel Patterns," Bulletin of Geological Society of America, Vol. 88, pp. 1755-1770, 1972.

Schumm, S.A. and R.W. Lichty. Channel Widening and Floodplain Construction Along the Cimarron River in Southwestern Kansas, U.S. Geological Survey Prof. Paper 352-D, 1963, 88 pp.

Simons, D.B. Theory and Design of Stable Channels in Alluvial Material, Ph.D. thesis, Colorado State University, May, 1957, 394 pp.

Vincent, J. "Effect of Bed Load Movement on the Roughness Coefficient Value," Proc., 12th Congress Intl. Association for Hydraulic Research, Fort Collins, Colorado, Vol. I, Paper No. A20, 1967, pp. 162-171.

Werner, P.W. "On the Origin of River Meanders," Transactions, American Geophysical Union, Vol. 32, No. 6, 1951, pp. 898-902.

Yang, C.T. and J.B. Stall. "Unit Stream Power in Dynamic Stream Systems," In Fluvial Morphology, (Proc., 4th Annual Geomorphology Symposium, Binghamton, New York, M. Mousawa, ed.), 1973.

Zeller, J. "Meandering Channels in Switzerland," International Association of Hydr. Sci. Symposium on River Morphology, Bern, Switzerland, 1967.

CHAPTER 3

RIVER BED STRESS AND PRIMARY BANK EROSION

3.1 Introduction

The ability of rivers to transport water and sediment in the absence of primary bank erosion is intimately related to the distribution of shear stress at the water-sediment interface. The concept of "hydraulic radius" allows for the simplest treatment; the interface stress τ is assumed to be constant across the cross-section and given by the relationship

$$\tau = \rho g R S \qquad (3\text{-}1)$$

where ρ is the density of water, g is the acceleration of gravity, S is the energy slope, and R, the hydraulic radius, is given by $R = \frac{A}{P}$ where A is channel cross-sectional area and P is the length of the wetted perimeter. In channels that are sufficiently wide and shallow, P may be closely approximated by width B and equation (3-1) reduces to

$$\tau = \rho g \bar{D} S$$

where $\bar{D}$ is the cross-sectionally averaged depth.

However, interface shear stress is clearly not constant in the cross-stream direction y. A rough approximation in the case of variable depth is given by

$$\tau(y) = \rho g D(y) S \qquad (3\text{-}2)$$

where $D(y)$ is the lateral depth distribution (Fig. 3-1). However, neither this model nor a similar one due to Bretting (1958)* account for the observed lateral transfer of downstream shear stress from the center of the channel, where the bed is flat, to the bank regions of the channel, where the bed is curved.

Keulegan (1938) introduced the assumption that the velocity distribution along normals to the channel bottom is logarithmic (Fig. 3-2). Lundgren and Jonsson (1964) used a generalized form of the assumption to derive a differential equation for the cross-stream stress distribution in shallow channels of moderate lateral bank curvature. The treatment accounts for the alteration of stress distribution and the transfer of momentum across normals to the bottom caused by channel curvature. Lundgren and Jonsson presented a numerical method for the solution of their stress relation. Herein singular perturbation techniques

*For Chapter 3 references see page 94.

are used to obtain an analytical solution. The fact that this solution includes the effect of lateral transfer of momentum allows for a resolution of a paradox concerning the ability of rivers to transport bed sediment without primary bank erosion, and provides a tool for the future development of stable channel theory.

The "stable channel paradox" results from a direct extension of Glover and Florey's (1951) theory of noncohesive stable channel geometry. They calculated the geometry of least excavation of a channel in which shear stress is slightly below critical value at every point along the channel bottom. Bed stress was calculated from equation (3-2) and equated everywhere with critical bed stress; the analysis indicates that the channel geometry must be

$$D(y) = D_o \cos\left(\pi \frac{Y}{B}\right)$$

where D_o is maximum channel depth and $\frac{B\mu}{D_o} = \pi$, $\tan^{-1}\mu$ being the submerged static angle of repose of the bed material. This channel geometry is depicted in Fig. 3-3.

In that rivers are by their nature required to serve as conduits for the transport of both water and earth down potential energy gradients, the result of Glover and Florey is inadequate to explain natural river geometry. It is desirable to extend their result to the case where stable banks and sediment transport coexist. To this end a straight, laterally symmetrical channel composed of uniform noncohesive sediment and subjected to bank full discharge is contemplated. The bottom is divided into a bed region of width $B-B_s$, where depth D has the constant value D_o, and two bank regions. Each bank region has width $\frac{1}{2}B_s$. On the bank regions depth $D(y)$ varies smoothly and monotonically from D_o at the junction point A of the bed and bank regions, where $y = \pm\frac{1}{2}(B-B_s)$, to 0 at the water's edge, where $y = \pm\frac{1}{2}B$ (Fig. 3-4). According to equation (3-2), stress depth $\delta = \frac{\tau}{\rho g S}$ is equal to the actual depth D. In order for sediment to be transported on the bed region, the depth must exceed the critical value for sediment motion. Since D is a continuous function, the stress depth must also exceed the critical depth, and thus sediment transport must occur somewhere on the bank region $\frac{1}{2}(B-B_s) < y < \frac{1}{2}B$. Any particle put in motion on the bank region will be subject to a component of gravitational force which will pull the particle down and toward the bed region. Thus bank erosion is accomplished and a stable channel cannot be maintained. Likewise, it can be shown that a stable bank full geometry is incompatible with sediment transport. A channel transporting bed material should continue to widen until either sediment transport vanishes or the channel itself eventually disappears.

The paradox is resolved easily for a large class of rivers which have beds composed of loose alluvium and banks composed primarily of cohesive materials such as clay and silt, often matted with vegetative roots. The banks are so much tougher than the bed that they are not eroded at bank full discharge even when sediment motion occurs on the bed. However, for another large class of rivers in which both the bed and banks are composed of non-cohesive material, as exemplified by the reaches of the Elbow River described by Hollingshead (1971), and which can be reproduced in the laboratory (Wolman and Brush, 1961), the paradox is not easily resolved. It may be argued that secondary currents concentrated in the bank region provide an extra lateral bed shear stress that counteracts gravity, thus stabilizing the banks. However, secondary currents in equilibrium flow in wide, straight channels of small lateral curvature are so small that they do not provide an adequate stabilizing mechanism. A more likely stabilizing mechanism is the lateral transfer of shear stress induced by the curved bottom. Due to curved bottom the stress depth δ should be somewhat lower than D on the bed region and part of the bank region adjacent to the bed region but be higher than D elsewhere (Fig. 3-5). If it is now assumed that (1) the configuration of the bank region is such that critical stress occurs everywhere, including the junction point, and (2) that stress depth δ is a smooth, monotonically decreasing function of y, then δ is greater than critical on the bed region, thus resolving the paradox. The existence of a stress distribution with just these properties can be illustrated by a solution of Lundgren and Jonsson's stress depth equation.

3.2 Solution of Lundgren and Jonsson's Equation

The channel described in Fig. 3-4 is assumed to be composed of noncohesive alluvium of uniform size. The velocity distribution along normals to the bed is assumed to be

$$\frac{U(Z)}{U_*} = 2.5 \ln \left(J \frac{Z}{K}\right)$$

where $U_* = \sqrt{\tau/\rho}$, Z is normal distance from the channel bottom, K is bed roughness, assumed to be constant across the channel, and J is a constant which Lundgren and Jonsson evaluate as 30. Lundgren and Jonsson's equation for

stress depth is then

$$\delta = (1 - \tfrac{1}{2} j) D + \xi \frac{d}{dy} \left[\psi(j, \tfrac{D}{K}) \, D^2 \, \xi \frac{d\delta}{dy} \right] \qquad (3\text{-}3)$$

where

$$j = -D D_{yy} / \left[1 + (D_y)^2 \right]^{3/2} , \quad \xi = \left[1 + (D_y)^2 \right]^{-1/2}$$

and

$$\psi(j, \tfrac{D}{K}) = \left[\frac{4 + j}{24(2 - j)} \ell n \left(J \tfrac{D}{K} \right) - \frac{5}{36(2 - j)} \right] \left[1 + \frac{1}{2 \ell n (J \frac{D}{K}) - \frac{17}{3}} \right]$$

On the bed region the equation reduces to

$$\frac{\delta}{D_o} = 1 + \bar{C} \cosh \left(\alpha \frac{y}{D_o} \right) \qquad (3\text{-}5)$$

where $R = \frac{D_o}{K}$. Since the stress profile is to be symmetric in y, the boundary condition

$$\left. \frac{d\delta}{dy} \right|_{y = 0} = 0$$

must be obeyed. A solution to equation (3-4) subject to this boundary condition is

$$\delta = D_o + \psi(0, R) \, D_o^2 \, \frac{d^2 \delta}{dy^2} \qquad (3\text{-}4)$$

where $\alpha = \psi(0, R)^{-1/2}$. The constant $\bar{C}$ must be determined by matching this bed solution to a bank solution under the conditions that δ and $\frac{d\delta}{dy}$ be continuous at the junction point.

Before attempts at solving for bank solutions can be made, it is necessary to specify the depth profile. As y varies from $\frac{1}{2}(B - B_s)$ to $\frac{1}{2} B$, D must vary smoothly from D_o to 0. Thus at the junction point the conditions

$$\left. D \right|_{y = \frac{1}{2}(B - B_s)} = D_o , \qquad \left. \frac{dD}{dy} \right|_{y = \frac{1}{2}(B - B_s)} = 0$$

must be satisfied, and at the water's edge the condition

$$D_{y = \frac{1}{2} B} = 0$$

must hold. Furthermore, if no bank erosion is to occur, $\frac{dD}{dy}$ must be greater

than $-\mu$, the coefficient of friction of wet bank material, at the water's edge. In a self-formed channel, bank erosion must barely not occur at bank full discharge, so the condition

$$\left.\frac{dD}{dy}\right|_{y = \frac{1}{2}B} = -\mu$$

must also hold. Furthermore, in order to satisfy lateral symmetry the function $D(y)$ must be even.

Other than these general conditions, the depth profile is left arbitrary at this point. In non-dimensional form, the profile is expressed as

$$s = f(\eta)$$

where $s = \frac{D}{D_o}$,

$$\eta = \frac{y}{2B_s} - (1 - \epsilon_1)\frac{1}{\epsilon_1}$$

and $\epsilon_1 = \frac{B_s}{B}$. The parameter η varies from 0 to 1, and s varies from 1 to 0 as the bank region is traversed. The conditions on f are

$$f(0) = 1, \quad f'(0) = 0, \quad f(1) = 0, \quad f'(1) = -\mu\epsilon_2^{-1/2}, \quad f(-\eta) = f(\eta)$$

where the prime denotes differentiation with respect to η and $\epsilon_2 = \left(\frac{2D_o}{B_s}\right)^2$ is a parameter that estimates the curvature of the bank region.

Examples of profiles that satisfy these conditions are

$$s = 1 - \eta^{2N}, \quad N = \frac{1}{2}\mu\epsilon_2^{-1/2} = 1, 2, 3, \ldots$$

and the Glover-Florey profile,

$$s = \cos\frac{\pi}{2}\eta, \quad \frac{\pi}{2} = \mu\epsilon_2^{-1/2}$$

Equation (3-3) is now solved on the bank region, in terms of an asymptotic expansion in the parameter ϵ_2, which is assumed to be small. Physically this implies that the lateral curvature of the bank region is small. If equation (3-3) is written in terms of s, η, and dimensionless stress depth $\sigma = \frac{\delta}{D_o}$, it is found that

$$\sigma = s\left(1 + \frac{1}{2}\epsilon_2 s_{\eta\eta} s\right) + \epsilon_2 \frac{d}{d\eta}\left[\psi(0, Rs)\, s^2 \sigma_\eta\right] + O(\epsilon_2^2) \qquad (3\text{-}6)$$

An asymptotic expansion of the form

$$\sigma = \tilde{\sigma}_0 + \epsilon_2 \tilde{\sigma}_1 + \epsilon_2 \tilde{\sigma}_2 + \cdots \tag{3-7}$$

is assumed; replacing in equation (3-6), it is found that

$$\tilde{\sigma}_0 = s \tag{3-8a}$$

$$\tilde{\sigma}_1 = \frac{1}{2} s^2 s_{\eta\eta} + \frac{d}{d\eta}\left[\psi(0, Rs)\, s^2 s_\eta\right] \tag{3-8b}$$

The bank solution must satisfy the boundary conditions that σ and σ_η match smoothly with the bed solution at the junction point. It is seen from equations (3-5) and (3-8) that the only free constant is $\bar{C}$, and that both conditions cannot be satisfied simultaneously. The reason for this is the existence of a boundary layer on the bank region near $\eta = 0$, where the expansion (3-7) fails to be accurate due to the dropping of derivative terms containing σ_η and $\sigma_{\eta\eta}$ in the equations for $\tilde{\sigma}_0$, $\tilde{\sigma}_1$, etc. Thus expansion (3-7) is an outer bank expansion and η is an outer variable.

In order to satisfy the boundary conditions at $\eta = 0$ an inner bank expansion

$$\sigma = \sigma_0 + \epsilon_2 \sigma_1 + \epsilon_2^2 \sigma_2 + \cdots \tag{3-9}$$

with the inner variable

$$\rho = \eta / \sqrt{\epsilon_2}$$

is considered. Thus s is an even function of ρ;

$$s = f(\epsilon_2^{1/2} \rho) = 1 + \frac{1}{2} \epsilon_2 f_{\eta\eta}(0) \rho^2 + O(\epsilon_2^2)$$

and the equation for stress depth (3-3) becomes

$$\sigma = 1 - \epsilon_2 \gamma(1 + \rho^2) + \left\{A - \epsilon_2 \gamma\left[2B + (2A + C)\rho^2\right]\right\} \frac{d^2\sigma}{d\rho^2} - 2\epsilon_2 \gamma(2A + C) \frac{d\sigma}{d\rho} + O(\epsilon_2^2) \tag{3-10}$$

where $\gamma = -\frac{1}{2} f_{\eta\eta}(0)$, (the minus sign makes γ positive for the physically applicable case of an upward-curving bank region), and

$$A = \psi(0, R) = 1/a^2$$

$$B = -\frac{\partial \psi}{\partial a}(0, R)$$

$$C = R\frac{\partial \psi}{\partial b}(0, R)$$

$$a = -ss_{\rho\rho}\left[1+(s_\rho)^2\right]^{-3/2} = j$$

$$b = Rs = \frac{D}{K}$$

Note that ψ has been expanded about the state of zero curvature and depth equal to D_0.

Between equations (3-9) and (3-10), it is found that

$$\sigma_0 = 1 + A\frac{d^2\sigma_0}{d\rho^2} \qquad (3\text{-}11a)$$

$$\sigma_1 = -\gamma\left\{1+2B\frac{d^2\sigma_0}{d\rho^2}+2(2A+C)\rho\frac{d\sigma_0}{d\rho}+\left[1+(2A+C)\frac{d^2\sigma_0}{d\rho^2}\right]\rho^2\right\}+A\frac{d^2\sigma_1}{d\rho^2}$$

The solution to equation (3-11a) is (3-11b)

$$\sigma_0 = C_1\epsilon^{a\rho} + C_2\epsilon^{-a\rho} + 1$$

The inner bank solution must match with both the bed solution ("left matching") and the outer bank solution ("right matching"). In order to facilitate left matching, the constant $\bar{C}$ in equation (3-5) is expanded asymptotically in ϵ_2;

$$\bar{C} = \bar{C}_0 + \epsilon_2\bar{C}_1 + \epsilon_2^2\bar{C}_2 + \cdots$$

Left matching (σ and σ_ρ must be continuous) imposed to lowest order requires that $\bar{C}_0 = C_2 = 0$. Right matching (the outer expansion of the inner expansion must equal the inner expansion of the outer expansion) imposed to the lowest order requires that $C_1 = 0$, in which case

$$\sigma_0 = 1 \qquad (3\text{-}12)$$

Progressing to the next highest order, the general solution to equation (3-11b) is

$$\sigma_1 = \tilde{C}_1 e^{\alpha\rho} + \tilde{C}_2 e^{-\alpha\rho} - \gamma(1 + 2A + \rho^2)$$

Again, right matching with equation (3-8b) is satisfied if $\tilde{C}_1 = 0$. The results of left matching are

$$\tilde{C}_2 = \frac{\gamma(1 + 2A)}{1 + \coth\theta}$$

$$\bar{C}_1 = -\frac{\gamma(1 + 2A)}{\sinh\theta\,(1 + \coth\theta)}$$

where

$$\theta = \frac{1}{\sqrt{A}}(1 - \epsilon_1)\frac{1}{\epsilon_1\sqrt{\epsilon_2}}$$

Thus the solution of equation (3-3) is complete to the first order in ϵ_2 on all regions of the bed.

The bed stress on the bed region is given by

$$\frac{\delta}{D_o} = 1 - \epsilon_2 \frac{\gamma(1 + 2A)}{\sinh\theta + \cosh\theta} \cosh\left(\frac{1}{\sqrt{A}}\frac{y}{D_o}\right) \qquad (3\text{-}13)$$

Since θ, γ, and A are positive for physically realistic cases, this equation indicates a stress deficiency on the bed region of order ϵ_2, which becomes progressively more severe as the bank region is approached. As was noted previously, this is exactly the situation that has been postulated to allow for the coexistence of bed sediment transport and stable banks in non-cohesive channels composed of uniform sediment.

3.3 The Form of the Bank Region

In the previous section the depth profile of the bank region was taken to be arbitrary within certain general restrictions. Herein a specific form for the profile is derived.

According to equations (3-8a) and (3-12), on the bank region

$$\sigma = s + O(\epsilon_2) \qquad (3\text{-}14)$$

It is assumed that critical conditions for sediment movement exist everywhere on

the bank region. At the junction of the bank and bed regions, it is required, then, that

$$\sigma_{CB} = 1 + O(\epsilon_2)$$

where σ_{CB} is the critical dimensionless stress depth on the bed. According to Lane (1953), critical stress on bank slopes σ_C is related to critical bed stress by the relation

$$\frac{\sigma_C}{\sigma_{CB}} = \left[1 - \frac{1}{2}\,\epsilon_2 s_\eta^2\right]\left[1 - \left(\frac{\epsilon_2 s_\eta}{\mu}\right)^2\right]^{1/2}$$

Expanding in ϵ_2,

$$\sigma_C = \left[1 - \left(\frac{s_\eta}{s_\eta(1)}\right)^2\right]^{1/2} + O(\epsilon_2)$$

Since bed stress on the bank region is actually given by equation (3-14), σ must be equal to σ_C; thus to lowest order in ϵ_2,

$$S = \left[1 - \left(\frac{s_\eta}{s_\eta(1)}\right)^2\right]^{1/2}$$

This differential equation has the solution

$$S = \cos\left[s_\eta(1)\,\eta\right]$$

which satisfies the boundary conditions $s(0) = 1$, $s_\eta(0) = 0$, and $s(1) = 0$ if $s_\eta(1) = \frac{\pi}{2}$. The boundary condition $s_\eta(1) = -\mu\epsilon_2^{-1/2}$ is satisfied by the constraint $\frac{\pi}{2} = \mu\epsilon_2^{-1/2}$.

This is the Glover-Florey solution discussed previously. The parameter $\gamma = -\frac{1}{2}\,s_{\eta\eta}(0)$ is then equal to $\frac{1}{2}\left(\frac{\pi}{2}\right)^2$. The physical meaning of this result is that in a straight, noncohesive river with bed and banks composed of uniform sediment and with negligible secondary currents and meandering or braiding tendencies, a channel of the following nature is formed by bank full discharges: lateral cross-sections consist of a relatively flat bed region above which sediment is transported, adjacent to two stable bank regions which are approximated by cosine curves.

3.4 Discussion

The equation for stress depth (equation 3-13) can be combined with sediment transport and bed resistance relationships to provide width, depth, and sediment transport relationships for noncohesive channels in uniform sediment at bank-full discharge, for which primary bank erosion does not occur. These relationships can be summarized in the dimensionless forms

$$S = f_1 (\tilde{Q}_B, R_B; R_P, r, P_i)$$

$$C_{sB} = f_2 (\tilde{Q}_B, R_B; R_P, r, P_i)$$

$$\Omega_B = f_3 (\tilde{Q}_B, R_B; R_P, r, P_i)$$

where $\tilde{Q}_B = \frac{Q_B}{\sqrt{rgD_s}\, D_s^2}$, $R_B = \frac{\bar{D}_B}{D_s}$, $R_P = \frac{\sqrt{rgD_s}\, D_s}{\nu}$, $r = (\frac{\rho_s}{\rho} - 1)$, and $\Omega = \frac{\bar{D}_B}{B}$;

Q_B is bank full discharge, $\bar{D}_B$ is average bank full depth, D_s is a typical sediment grain diameter, ρ_s and ρ are sediment and water densities, C_{sB} is total concentration of sediment in motion (bed and suspended load) at bank-full discharge, and P_i, i = 1, 2, 3, ... are dimensionless sediment size distribution, shape, porosity, friction, and other factors. Thus analytical equivalents of the empirical equations of regime theory can be derived in principle.

This has not been done herein because the theory does not apply to sediment mixtures and lateral variation of sediment size. It is clear from equation (3-13) that for uniform noncohesive channels depth cannot exceed the critical depth by much before the banks become unstable. However, observation indicates a rather wide range of depths for which stable channel geometry and sediment transport coexist. Hollingshead (1971) has noted a range of depths at which sediment is transported from less than .34 meter to more than 1.16 meters, all below bank-full in a reach of the Elbow River, an essentially noncohesive stream. Such behavior may be attributable to the extremely wide range of sediment sizes on the river bed, such that the average bed sediment size is 2.5 cm whereas the average size of sediment transported as bed load is only 1.5 cm. The mobility of bed material is roughly scaled by the Shields stress $\tau^* = \frac{\tau}{\rho(\frac{\rho_s}{\rho} - 1)gD_s}$; greater values of τ^* imply greater mobility. The Shields stress is larger for smaller particles. Thus, as river stage increases, smaller particles are first put into motion, and subsequently larger particles begin to move. As a consequence

sediment discharge will be considerably higher than that predicted from the uniform theory using average diameter, and a wide range of depths at which sediment transport exists will be observed.

Appropriate modification of the theory to account for variation in sediment size, perhaps along the lines of Egiazaroff (1965) and Michiue (1972), should eventually allow for the analytical derivation of river regime equations for the noncohesive case.

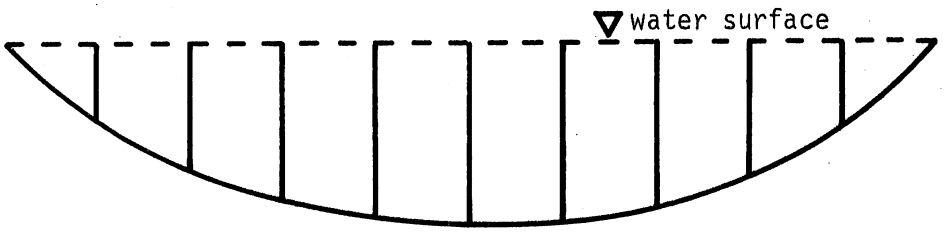

Figure 3-1

A rough approximation to the lateral stress distribution can be obtained by assuming that the velocity distribution along verticals from the bed is logarithmic, and that bed stress τ is related to depth D by the equation $\tau = \rho gDS$.

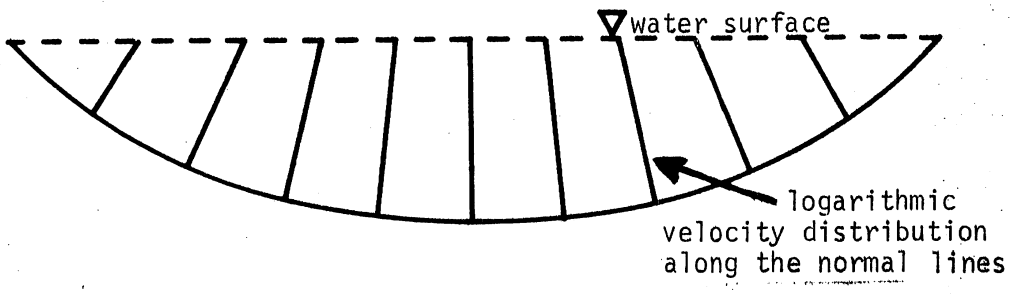

Figure 3-2

The velocity distribution along normals to the bed is assumed to be logarithmic for channels of small lateral curvature.

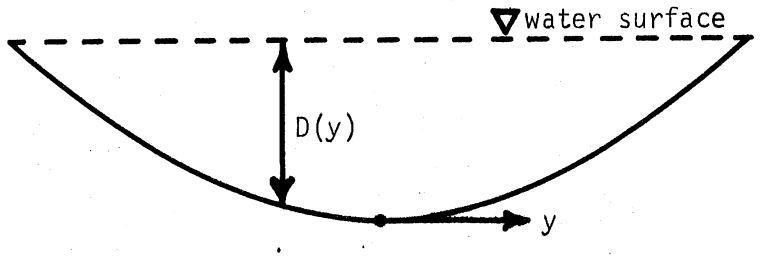

Figure 3-3

Glover and Florey's (1951) cosine lateral depth profile.

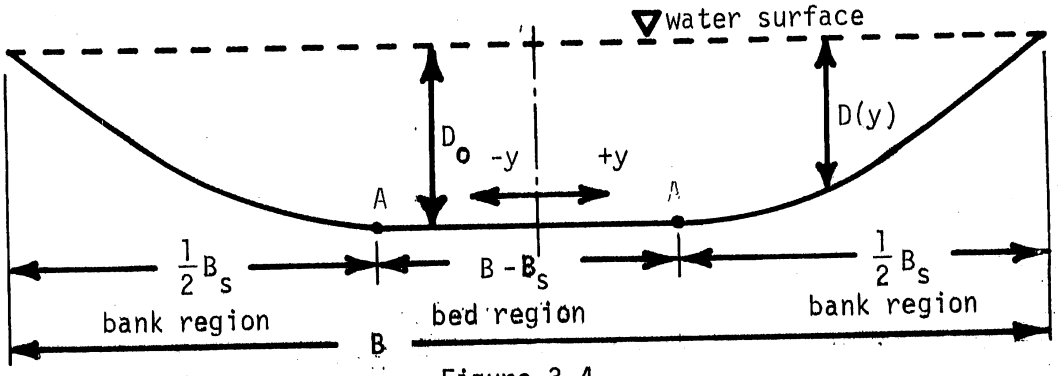

Figure 3-4

The lateral channel profile is divided up into a bed region, where depth has the constant value D_o, and two symmetrical bank regions where depth varies from D_o at the junction point A to 0 at the water's edge.

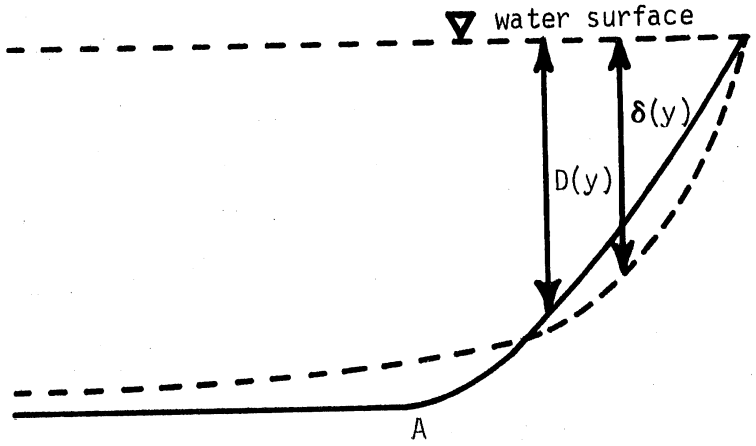

Figure 3-5

Channel curvature induces a lateral transfer of stress, so that on the bed region and part of the bank regions, stress depth δ is less than the actual depth D, and on the rest of the bank regions δ exceeds D.

References for Chapter 3

Bretting, A.E. "Stable Channels," Acta Polytechnica Scandinavica, No. 245, New Series, Ci. 1, 116 pp.

Egiazaroff, I.V. "Calculation of Nonuniform Sediment Concentrations," Proc., American Society of Civil Engineers, Journal of the Hydraulics Division, Vol. 91, No. HY 4, 1965, pp. 225-247.

Glover, R.E. and Q.L. Florey. Stable Channel Profiles, U.S. Bureau of Reclamation, Hydr. 325, 1951.

Hollingshead, A.B. "Sediment Transport Measurements in Gravel River," Proc., American Society of Civil Engineers, Journal of the Hydraulic Division, Vol. 97, No. HY 11, 1971.

Keulegan, G.H. "Laws of Turbulent Flow in Open Channels," Research Paper RP 1151, National Bureau of Standards, U.S. Dept. of Commerce, Washington, D.C., Vol. 21, 1938, pp. 707-741.

Lane, E.W. "Progress Report on Studies on the Design of Stable Channels of the Bureau of Reclamation, Proc., American Society of Civil Engineers, Journal of the Hydraulics Division, Vol. 79, Separate No. 280, 1953.

Lundgren, H. and I.G. Jonsson. "Shear and Velocity Distribution in Shallow Channels," Proc., American Society of Civil Engineers, Journal of the Hydraulics Division, Vol. 90, No. HY 1, 1964, pp. 1-21.

Michiue, M. Basic Research Concerning Sediment Transport and Bed Movement (in Japanese), Ph.D. thesis, Kyoto University, 1972.

Wolman, M.G. and L.M. Brush. Factors Controlling the Size and Shape of Stream Channels in Coarse Noncohesive Sands, U.S. Geological Survey Prof. Paper 282-G, 1961, pp. 183-210.

APPENDIX I

Derivation of a Constraint for Recirculating Model Rivers with Erodible Banks

Consider a flume filled with sand that has length L_f and width B_f. In the flume a channel of width B_I and depth D_{fI} is molded in the sand. This uniformly molded initial channel continues downstream to a constant-elevation weir of height Z_o above some datum. If e is the porosity of the sand and S_I the slope of the initial channel, the total mass of sediment initially in the flume M_I is

$$M_I = \rho_s(1-e)\left\{B_f L_f (Z_o + \tfrac{1}{2} S_I L_f) + (B_f - B_I) D_{fI} L_f\right\}$$

Furthermore, it is subsequently assumed that the flume, after having been operated for a time, reaches a final equilibrium, uniform state that is different from the initial state. Flow is assumed to be confined to the channel, so the longitudinal slope of the benches on either side remains S_I. At final equilibrium the total mass M of bed material in the flume is

$$M = \rho_s(1-e)\left\{B_f L_f (Z_o + \tfrac{1}{2} S L_f) + (B_f - B) \int_0^{L_f} (D_{fI} + (S_I - S)x\, dx\right\}$$

where S is the equilibrium slope.

If there are no sources or sinks of sediment and storage in the pipes and pumps is negligible, $M_I = M$, yielding

$$B = B_I / \left[1 + (S_I - S)(L_f / 2 D_{fI})\right]$$

APPENDIX II

Stability Analysis - The Wide Channel

The model alluvial channel provides a framework appropriate to the analysis of bar instability. Channels that are wide enough so that bank effects are negligible are considered. In fact nearly all natural rivers and most laboratory streams have channels for which the depth-width ratio $\frac{D}{B}$ is less than 0.1 and the above assumption can be justified.

The details of the analysis can be found in Parker (1975) (see Chapter 2); the highlights and results of the theory, together with some extended analysis, are presented in brief form in this section. The two-dimensional equations for momentum and mass balance, in which velocities are vertically averaged and pressure is taken to be hydrostatic, are

$$\left.\begin{aligned}
&\frac{\partial u_1}{\partial t} + u_1 \frac{\partial u_1}{\partial x_1} + u_2 \frac{\partial u_1}{\partial x_2} = -g \frac{\partial H}{\partial x_1} - \frac{\tau_1}{\rho D} \\
&\frac{\partial u_2}{\partial t} + u_1 \frac{\partial u_2}{\partial x_1} + u_2 \frac{\partial u_2}{\partial x_2} = -g \frac{\partial H}{\partial x_2} - \frac{\tau_2}{\rho D} \\
&\frac{\partial}{\partial x_1}(u_1 D) + \frac{\partial}{\partial x_2}(u_2 D) + \frac{\partial D}{\partial t} = 0 \\
&\frac{\partial}{\partial t}(H - D) + \frac{1}{1-e}\left(\frac{\partial q_1}{\partial x_1} + \frac{\partial q_2}{\partial x_2}\right) = 0
\end{aligned}\right\} \quad \text{(AII.1)}$$

where x_1 is the downstream coordinate, x_2 is the lateral coordinate, and

D is depth of flow,

H is water surface height above an arbitrary datum,

(u_1, u_2) is the stream velocity vector,

(q_1, q_2) is the vector of volumetric sediment transport,

(τ_1, τ_2) is the bed stress vector,

ρ is the density of water, and

e is the bed porosity

If the momentum balance equations are written in tensor notation, they appear as

$$\tau_i = \rho g D \Sigma_i \qquad \text{(AII.2)}$$

where

$$\Sigma_i = -\left(\frac{\partial H}{\partial x_i} + \frac{1}{g}\frac{\partial u_i}{\partial t} + \frac{u_j}{g}\frac{\partial u_i}{\partial x_j}\right) \qquad \text{(AII.3)}$$

is a generalized slope vector.

As before, the problem is not determinate until constitutive relations for q_i and τ_i are introduced. Equations (1-7) and (1-8) are adopted herein. Generalized for two-dimensional slowly-varying flow, they appear as

$$\tau_i = C u u_i \qquad \text{(AII.4a)}$$

$$q_i = (\tau g D_s)^{1/2} D_s q^* \frac{u_i}{u} \qquad \text{(AII.4b)}$$

where

$$C = \phi_1\left(\frac{u}{\sqrt{\tau g D_s}}, \Sigma; R_p, \tau, P_i\right) \qquad \text{(AII.5a)}$$

$$q^* = \phi_2\left(\frac{u}{\sqrt{\tau g D_s}}, \Sigma; R_p, \tau, P_i\right) \qquad \text{(AII.5b)}$$

and $u = \sqrt{u_i u_i}$ and $\Sigma = \sqrt{\Sigma_i \Sigma_i}$.

Unperturbed solutions to equations (AII.1), (AII.4) and (AII.5), corresponding to steady, uniform flow, can be found; if δ_{ij} is the Kronecker delta, $u_i = \delta_{il} U$, $\tau_i = \delta_{il} \tau_o$, $q_i = \delta_{il} q_s$, $\Sigma_i = \delta_{il} S$, where the relationship $\tau_o = \rho g D S$ and the unperturbed forms of relationships (AII.4) and (AII.5) are satisfied.

Slight perturbations about the unperturbed flow are considered,

$$\left.\begin{aligned} u &= U\delta_{1i} + u_i' \\ q_i &= q_s\delta_{1i} + q_i' \\ \tau_i &= \tau_o\delta_{1i} + \tau_i' \\ H &= H_o - Sx_1 + H' \\ D &= D_o + D' \end{aligned}\right\} \qquad \text{(AII.6)}$$

where, for example, u_1' is the perturbed part and $U\delta_{1i}$ is the unperturbed part of u_i. These forms are inserted into equations (A2.1), (A2.4), and (A2.5); since the perturbed parts are assumed to be much smaller than the unperturbed parts, complete linearization of the equations for the perturbed parts can be accomplished by expanding in Taylor series and retaining the linear terms. The equations reduce to the following determinate dimensionless form.

$$\begin{aligned}
&\frac{\partial u_1}{\partial t} + \frac{\partial u_1}{\partial x_1} = -F^{-2}\frac{\partial H}{\partial x_1} - C_o(M_1 u_1 - M_2 D)\\
&\frac{\partial u_2}{\partial t} + \frac{\partial u_2}{\partial x_1} = -F^{-2}\frac{\partial H}{\partial x_2} - C_o u_2\\
&\frac{\partial u_1}{\partial x_1} + \frac{\partial u_2}{x_2} + \frac{\partial D}{\partial t} + \frac{\partial D}{\partial x_1} = 0\\
&\frac{\partial}{\partial t}(H - D) + \beta\left[N_1\frac{\partial u_1}{\partial x_1} - N_2\frac{\partial D}{\partial x_1} + \frac{\partial u_2}{\partial x_2}\right] = 0
\end{aligned} \qquad \text{(AII.7)}$$

In these equations u_1, u_2, H, and D, which are now defined to be perturbed parts, and the parameters x_1, x_2, and t have been made dimensionless with the unperturbed length and velocity scales D_o and U (e.g. $u_1 = \frac{u_1'}{U}$). The constants all refer to the unperturbed flow; C_o is the resistance coefficient, $F = \frac{U}{\sqrt{gD_o}}$ is the Froude number, $\beta = q_s/(1-e)UD_o$ is essentially the ratio of sediment to water transport and is usually small ($<10^{-3}$), and

$$\left.\begin{aligned}
M_1 &= 2\left(1 - \frac{S}{C_o}\frac{C_o}{\partial S}\right)^{-1}\left(1 + \frac{1}{2}\frac{U^*}{C_o}\frac{C_o}{\partial U^*}\right)\\
M_2 &= \left(1 - \frac{S}{C_o}\frac{C_o}{\partial S}\right)^{-1}\\
N_1 &= \frac{U^*}{q_o}\frac{\partial q_o}{\partial U^*} + \frac{S}{q_o}\frac{\partial q_o}{\partial S}M_1\\
N_2 &= \frac{S}{q_o}\frac{\partial q_o}{\partial S}M_2
\end{aligned}\right\} \qquad \text{(AII.8)}$$

where $U^* = \frac{U}{\sqrt{rgD_s}}$ and D_s is grain size.

Both form and specific evaluation indicate that the constants M_1, M_2, N_1, and N_2 are of the order of magnitude of unity.

Generalized dimensionless sinusoidal perturbations are introduced into equations (AII.7).

$$\left.\begin{aligned} u_1 &= \hat{u}_1(x_2)\ \exp\left\{i(Kx_1 - \phi t)\right\} \\ u_2 &= \hat{u}_2(x_2)\ \exp\left\{i(Kx_1 - \phi t)\right\} \\ H &= \hat{H}(x_2)\ \exp\left\{i(Kx_1 - \phi t)\right\} \\ D &= \hat{D}(x_2)\ \exp\left\{i(Kx_1 - \phi t)\right\} \end{aligned}\right\} \quad \text{(AII.9)}$$

Herein K is the dimensionless bar instability wave number, related to dimensional instability wave length by the relation $\frac{\lambda}{D_o} = \frac{2\pi}{K}$, and ϕ is the complex wave celerity, the real part ϕ_r being related to downstream bar migration rate C by $\phi_r = KC$, and the imaginary part ϕ_i being the coefficient of instability. Clearly ϕ_i must be positive for instability. The functions $\hat{u}_1(x_2)$ etc. and the parameters K and ϕ must be obtained from the equations of motion, (AII.7). Let $\eta = H - D$ be the dimensionless perturbed part of the bed height. Then the kinematic boundary condition that u_2 vanishes at the channel banks provides the result that $\hat{\eta}$ takes only the forms

$$\hat{\eta} = \hat{\eta}_o \begin{cases} \sin\left(\frac{m}{2} K_B x_2\right), & m = 1, 3, 5, \ldots \\ \cos\left(\frac{m}{2} K_B x_2\right), & m = 2, 4, 6, \ldots \end{cases} \quad \text{(AII.10)}$$

and that $\hat{u}_1$, $\hat{u}_2$, $\hat{H}$, and $\hat{D}$ must take corresponding forms. Here $K_B = \frac{2\pi D_o}{B}$ is dimensionless channel width wave number. In the above $\hat{\eta}_o$ is the amplitude of the disturbance. It is fortunate that the bed forms implied by disturbance forms (AII.9) and (AII.10) correspond exactly with the alternate bar pattern given in Fig. 2-10, with m being equal to the number of braids.

The equations of motion also lead to a polynomial equation with ϕ as a function of meander or braid wave number K and the parameters of the unperturbed flow $K_1 = \frac{1}{2} m F^{-1} K_B$, F, C_o, β, M_1, M_2, N_1, and N_2. Only one root ϕ of this

equation applies to fluvial bar instability; the imaginary part ϕ_i of this root is given by

$$\phi_i = \beta C_o \frac{(A_{11}K_1^4 + A_{12}C_o^2K_1^2)K^2 + (A_{21}K_1^2 + A_{22}C_o^2)K^4 + A_3K^6}{A_4C_o^2K_1^4 + (A_{51}K_1^4 + A_{52}C_o^2K_1^2 + A_{53}C_o^4)K^2 + (A_{61}K_1^2 + A_{62}C_o^2)K^4 + A_7K^6} \qquad \text{(AII.11a)}$$

where the coefficients A_{ij} are formed from the parameters M_1, M_2, N_1, N_2, and F^{-2}, e.g.

$$\left.\begin{aligned} A_{11} &= M_2(N_1 - 1) \\ A_{12} &= -(M_1 + M_2)(M_1 + M_2 - N_1M_2 + N_2M_1) \\ A_4 &= M_1^2 \\ A_{51} &= 1 \end{aligned}\right\} \qquad \text{(AII.11b)}$$

The assumption that, for a range of values of instability wave number K, $\phi_i > 0$ and instability does exist is verified in Appendix 3. It suffices to note that the observed value of K should be equal to that value at which ϕ_i is a positive maximum. Thus the appropriate value of K is one of the roots of the equation

$$\frac{\partial \phi_i}{\partial K} = 0$$

Analysis of the roots of equation (AII.11a) in conjunction with the assumption that instability does exist provides a number of interesting results. These are outlined in Chapter 2-4.

APPENDIX III

Quantitative Verification of Instability

The results of wide-channel stability analysis are valid if instability occurs. This can be verified only by the calculation of the coefficients M_1, M_2, N_1, and N_2 with respect to a specific pair of constitutive equations. For illustrative purposes the equations due to Engelund presented in Chapter 1 are used. They apply to dune resistance for hydraulically rough, lower-regime flow. (This is the case that occurs predominately in the field.)

After some manipulation it is found that

$$M_2 = (1 - \eta)^{-1}$$

$$M_1 = 2\xi M_2$$

$$N_2 = 1.5\eta M_2$$

$$N_1 = 3\xi + 2 + 1.5\eta M_1$$

where

$$\eta = \frac{5(\psi C_o)^{1/2}}{[1+5(\psi C_o^{1/2}] (1+\frac{\bar{\psi}}{\psi})}$$

$$\xi = \frac{1}{[1+5(\psi C_o^{1/2}] (1+\frac{\bar{\psi}}{\psi})}$$

and

$$\psi = .06\, r^{*-1} + .4\, r^*$$

$$\bar{\psi} = -.06\, r^{*-1} + .4 r^*$$

It can easily be shown that $0 < r, < \frac{5}{6}$ and $\frac{2}{3} < \xi < 2.5$ for $C < 10^{-2}$, a value rarely exceeded in natural rivers. Thus the following bounds can be obtained;

$1 < M_2 < 6$ $\qquad M_1 > M_2$

$\frac{4}{3} < M_1 < 30$ $\qquad N_1 > N_2$

$0 < N_2 < 7.5$

$4 < N_1 < 47$

From this it can be deduced that bar instability will always exist in channels with negligible bank resistance. Expanding equation (AII.11) about $K = 0$ (infinitely long disturbance wave length) it is found that for K sufficiently small

$$\phi_i(K) \cong \beta C_o \frac{(A_{11}K_1^4 + A_{12}K_1^2 C_o^2)}{A_4 C_o^2 K^2} K^2 \qquad \text{(AIII.1)}$$

The parameters C_o and K are positive by definition, and β is either zero (in which case instability vanishes) or positive. It can be seen from equations (A2.11b) that A_4 is also positive. Likewise

$$A_{11} = M_2(N_1 - 1) > 3$$

$$A_{12} = -(M_1 + M_2)\left[(1 - N_1)M_2 + (1 + N_2)M_1\right] = (1 + 2\xi)(1 + \xi)M_2^2 > 0$$

Thus it is clear that a range of wave numbers for which ϕ_i is positive always exists, and it may be concluded that bar instability characteristic of meandering or braiding always exists in channels with negligible bank effects. Thus no such channel can be expected to remain straight.

APPENDIX IV

Stability Analysis with Bank Effects

Chang et al. (1971) and Vincent (1967) (see Chapter 2) have observed that for sufficiently large values of $\frac{D_o}{B}$ alternate bar patterns do not form. This leads to the hypothesis that bank friction (which is significant when $\frac{D_o}{B}$ is large) may damp bar instability. To test this hypothesis friction is divided into wall and bed components according to Johnson's (1942) (see Chapter 2) method. Although such an analysis is approximate, it is expected that the physical situation is represented accurately in a qualitative sense. The total friction coefficient C_T can be formed from C_o, the bed component that satisfied equation (1-7) and a wall component C_w which satisfies the known frictional relationship for smooth walls;

$$C_w = (1/8)((.87 \ln(4\sqrt{8}\, r R_p C_w^{3/2} U^{*3} S^{-1}) - .47)^{-2} = C_w(U^*, S; R_p, r)$$

According to Johnson

$$C_T = (1 + 2\frac{D_o}{B})^{-1} C_o + \frac{2D_o}{B} C_w$$

Thus it can be seen that as $\frac{D_o}{B}$ becomes small C_T approaches C_o.

In a treatment that includes wall effects the momentum equations must be amended to

$$\frac{\partial u_i}{\partial t} + u_j \frac{\partial u_i}{\partial x_j} = -g\frac{\partial H}{\partial x_i} - \frac{\tau_i}{\rho D}(1 + 2\frac{D}{B}) \qquad i = 1, 2$$

where $D/(1 + 2\frac{D}{B})$ is the hydraulic radius.

Reduction shows that the equations AII.7 apply to the stability analysis with wall effects if C_o is replaced by C_E, where

$$C_E = C_o + \frac{2D_o}{B}(1 + \frac{2D_o}{B}) C_w$$

and if

$$M_1 = 2\left(1 - \frac{S}{C_E}\frac{\partial C_E}{\partial S}\right)^{-1}\left(1 + \frac{1}{2}\frac{U^*}{C_E}\frac{\partial C_E}{\partial U^*}\right)$$

$$M_2 = \sigma\left(1 - \frac{S}{C_E}\frac{\partial C_E}{\partial S}\right)^{-1} = \sigma \bar{M}_2$$

$$N_1 = \frac{U^*}{q_o}\frac{\partial q_o}{\partial U^*} + \frac{S}{q_o}\frac{\partial q_o}{\partial S} M_1$$

$$N_2 = \frac{S}{q_o}\frac{\partial q_o}{\partial S} M_2$$

where

$$\sigma = \frac{C_o - 4\left(\frac{D_o}{B}\right)^2 C_w}{C_o + 2\frac{D_o}{B}\left(1 + \frac{D_o}{B}\right) C_w}$$

Numerical evaluation of these parameters is accomplished with Engelund constitutive equations. It is found that

$$M_2 = \sigma(1 - \eta_E)^{-1} \equiv \sigma \bar{M}_2$$

$$M_1 = 2\xi_E (1 - \eta_E)^{-1}$$

$$N_2 = 1.5\eta(1 - \eta)^{-1}$$

$$N_1 = 3\xi + 2 + 3\eta\xi(1 - \eta)^{-1}$$

where η and ξ retain their previous meanings and

$$\eta_E = \frac{C_o\eta + 2\frac{D_o}{B}\left(1 + \frac{2D_o}{B}\right) C_w \eta_w}{C_E}$$

$$\xi_E = \frac{C_o\xi + 2\frac{D_o}{B}\left(1 + 2\frac{D_o}{B}\right) C_w \xi_w}{C_E}$$

and

$$\eta_w = \frac{1}{1.5}\,\frac{7.4\,C_w^{1/2}}{1+7.4\,C_w^{1/2}}$$

$$\xi_w = \frac{1}{1+7.4\,C_w^{1/2}}$$

If the bound $C_B < 1 \times 10^{-2}$ is again satisfied, then it can be shown that

$$1 < \bar{M}_2 < 6 \qquad 0 < \xi_E < 2.5$$

$$0 < M_1 < 30 \qquad 0 < \eta_E < \frac{5}{6}$$

$$0 < N_2 < 7.5$$

$$4 < N_1 < 47$$

$$-1 < \sigma < 1$$

The parameter σ approaches 1 for sufficiently wide channels, but decreases as $\frac{D_o}{B}$ increases, and takes negative values for $\frac{D_o}{B} > \frac{1}{2}\sqrt{\frac{C_o}{C_w}}$. This introduces a stabilizing influence into the equation for ϕ_i. For example,

$$A_{11} = \sigma \bar{M}_2 (N_1 - 1)$$

$$A_{12} = (\sigma + 2\xi_E)\,(\sigma + 3\sigma\xi - 2\xi_E + 3(\sigma\xi - \xi_E)\,\eta\,(1-\eta)^{-1})\,\bar{M}_2^{\,2}$$

from which it can be seen that A_{11} becomes negative for values of $\sigma < 0$, and A_{12} becomes negative for even larger values of σ (smaller values of $\frac{D_o}{B}$); thus, according to equation (AIII.1), instability at small values of K disappears. In the case of meandering a more explicit result can be obtained; maximum instability vanishes for $\frac{D_o}{B} > 2\sqrt{\frac{C}{C_w}}$ according to equation (AIII.1).

Thus it can be concluded that the presence of banks has a stabilizing influence on river channels, tending to damp the formation of bars. The exact value of $\frac{D_o}{B}$ at which instability vanishes varies from river to river. However, the experimental evidence of Chang et al. (1971), Ackers (1962) and Vincent (1967) (see Chapter 2) suggests that stable channels become possible for values of $\frac{D_o}{B} > 10^{-1}$, and that as $\frac{D_o}{B}$ increases the tendency toward stability increases.

It follows that the proposed meander-braid regime diagram of Fig. 2-11 can be revised to provide a meander-braid-straight regime diagram, as is illustrated in Fig. 2-12.

APPENDIX V

Data

Data for 167 laboratory experiments which are useful in delineating the occurrence of meandering, braiding, and straight channels are presented in Table AV-1. A key to the natural rivers referenced in Fig. 2-13 is provided in Table AV-2.

Table AV-1

Source	Specific Gravity	D_s (mm)	Q ltr/sec	S x 10^3	B(m)	D(m) x 10^2	Pattern[2]	λ(m)	Flume Type[3]	Qs gm/sec	Experiment No.
1	2.65	.22	1.41	4.43	1.20	1.17	B	-	R-E	-	1
1	2.65	.22	1.41	4.78	1.07	1.50	M	4.91	R-E	-	2
1	2.65	.22	2.83	5.99	1.36	1.77	M	4.59	R-E	-	3
1	2.65	.22	2.83	4.87	1.57	1.96	M-B	3.89	R-E	-	4
1	2.65	.22	2.83	4.67	1.23	1.75	M	6.07	R-E	-	5
1	2.65	.22	-	-	-	-	S	-	R-E	-	6
2	2.65	.62	0.7	8.05	.44	.77	M	2.8	R-E	-	7
2	2.65	.62	0.8	7.43	.43	.79	M	3.0	R-E	-	8
2	2.65	.62	0.9	7.1	.49	.81	M	3.0	R-E	-	9
2	2.65	.62	0.5	6.28	.40	.60	M	3.3	R-E	-	10
2	2.65	.62	0.7	6.09	.49	.67	M-B	-	R-E	-	11
2	2.65	.62	0.7	5.72	.38	.88	M	-	R-E	-	12
2	2.65	.62	0.7	5.95	.42	.96	M	3.9	R-E	-	13
2	2.65	.62	0.7	8.68	.39	.80	M-B	-	R-E	-	14
3	2.65	.22	1.41	5.90	1.52	.91	B	-	R-E	-	15
3	2.65	.22	1.41	1.05	1.40	1.2	B	-	R-E	-	16
3	2.65	.22	1.41	8.12	1.43	.80	B	-	R-E	-	17
3	2.65	.22	1.41	5.76	1.23	.80	B	-	R-E	-	18
3	2.65	.22	1.41	5.76	1.39	.50	B	-	R-E	-	19
4	1.05	3.2	2.8	1.04	.91	2.6	M	4.4	R-N	-	20
4	1.05	3.2	4.3	3.52	.91	2.0	M	5.3	R-N	-	21
4	1.05	3.2	4.3	2.04	.91	2.4	M	5.5	R-N	-	22
4	1.05	3.2	4.3	1.18	.91	3.6	M	6.3	R-N	-	23
4	1.05	3.2	4.3	.53	.91	4.4	M	10.1	R-N	-	24
4	1.05	3.2	6.7	2.36	.91	3.0	M	7.3	R-N	-	25
4	1.05	3.2	6.7	1.20	.91	3.7	M	5.9	R-N	-	26
4	1.05	3.2	6.7	.68	.91	4.7	M	5.7	R-N	-	27
4	1.05	3.2	6.7	.46	.91	5.9	M	10.4	R-N	-	28
4	1.05	3.2	6.7	.44	.91	6.7	M	11.4	R-N	-	29
4	1.05	3.2	8.0	2.16	.91	3.3	M	8.0	R-N	-	30
4	1.05	3.2	8.0	.69	.91	5.7	M	-	R-N	-	31
4	1.05	3.2	8.0	.49	.91	7.6	M	13.1	R-N	-	32
4	1.05	3.2	9.2	1.70	.91	4.0	M	6.9	R-N	-	33
4	1.05	3.2	12.4	2.54	.91	4.1	M	6.5	R-N	-	34
4	1.05	3.2	2.2	1.36	.46	3.3	M	4.1	R-N	-	35
4	1.05	3.2	2.2	.60	.46	3.9	M	5.1	R-N	-	36
4	1.80	-	6.3	4.32	.91	2.0	M	11.2	R-N	-	37
4	1.80	-	6.3	2.04	.91	2.5	M	9.7	R-N	-	38
4	1.80	-	6.3	1.36	.91	2.9	M	9.8	R-N	-	39
4	1.80	-	8.6	6.38	.91	2.6	M	6.2	R-N	-	40
4	1.80	-	8.6	5.78	.91	2.4	M	6.6	R-N	-	41
4	1.80	-	8.6	4.06	.91	2.4	M	12.2	R-N	-	42
4	1.80	-	8.6	3.04	.91	2.5	M	17.0	R-N	-	43

Table AV-1 (Cont'd) - 2 -

Source	Specific Gravity	D_s (mm)	Q ltr/sec	S x 10^3	B(m)	D(m) x 10^2	Pattern[2]	λ(m)	Flume Type[3]	Qs gm/sec	Experiment No.
4	1.80	-	8.6	1.36	.91	3.5	M	12.7	R-N	-	44
4	1.80	-	8.6	1.02	.91	3.8	M	7.9	R-N	-	45
4	1.80	-	11.3	4.16	.91	3.0	M	8.5	R-N	-	46
4	1.80	-	11.3	2.82	.91	3.3	M	-	R-N	-	47
4	1.80	-	11.3	2.10	.91	3.3	M	-	R-N	-	48
4	1.80	-	11.3	1.50	.91	4.3	M	9.0	R-N	-	49
4	1.80	-	13.6	4.24	.91	3.7	M	6.2	R-N	-	50
4	1.80	-	13.6	2.60	.91	3.7	M	-	R-N	-	51
4	1.80	-	13.6	2.00	.91	3.7	M	-	R-N	-	52
4	1.80	-	13.6	1.04	.91	5.0	M	21.3	R-N	-	53
4	1.80	-	13.6	.80	.91	5.1	M	-	R-N	-	54
4	2.65	.7	8.1	4.00	.91	1.9	M	12.8	R-N	-	55
4	2.65	.7	8.1	3.82	.91	2.0	M	16.5	R-N	-	56
4	2.65	.7	8.1	2.56	.91	2.3	M	11.6	R-N	-	57
4	2.65	.7	9.2	2.52	.91	2.6	M	15.2	R-N	-	58
4	2.65	.7	10.9	2.96	.91	3.1	M	18.3	R-N	-	59
4	2.65	.7	10.9	2.36	.91	3.3	M	19.5	R-N	-	60
4	2.65	.7	10.9	1.76	.91	3.1	M	20.7	R-N	-	61
4	2.65	.7	14.2	2.60	.91	4.0	M	24.4	R-N	-	62
4	2.65	.7	14.2	1.48	.91	3.6	M	15.2	R-N	-	63
5	2.65	.23	28.3	2.7	3.9	2.9	M	10.7	S-E	38	64
5	2.65	.23	28.3	3.0	3.7	3.1	M	12.2	S-E	77	65
5	2.65	.23	28.3	3.5	3.2	3.5	M	12.5	S-E	205	66
5	2.65	.23	28.3	4.0	3.8	2.9	M	12.2	S-E	528	67
5	2.65	.23	56.6	2.2	4.1	5.0	M	16.8	S-E	42	68
5	2.65	.23	56.6	2.7	2.5	6.7	M	18.3	S-E	81	69
5	2.65	.23	56.3	3.0	5.5	3.7	M	19.8	S-E	205	70
5	2.65	.23	84.9	2.7	5.9	5.7	M	22.9	S-E	113	-
5	2.65	.21	28.3	3.0	5.5	2.1	M	13.0	S-E	40	71
5	2.65	.21	28.3	3.3	4.5	2.7	M	12.3	S-E	79	72
5	2.65	.21	28.3	3.6	4.5	3.0	M	12.2	S-E	128	73
5	2.65	.21	56.6	3.6	9.4	2.8	M	21.9	S-E	92	74
5	2.65	.21	56.6	4.0	8.7	1.9	M	21.3	S-E	186	75
5	2.65	.21	56.6	4.3	6.4	2.9	M	21.6	S-E	206	76
5	2.65	.21	84.9	3.2	8.4	4.1	M	21.9	S-E	133	77
5	2.65	.21	84.9	3.3	6.7	5.0	M	23.8	S-E	62	78
5	2.65	.21	84.9	3.0	6.2	4.8	M	25.0	S-E	166	79
5	2.65	.21	84.9	3.4	13.0	2.7	M	26.8	S-E	237	80
5	2.65	.21	113.	3.6	7.6	6.2	M	26.8	S-E	212	81
5	2.65	.50	7.1	3.9	1.3	6.6	M	6.1	S-E	5.3	82
5	2.65	.50	7.1	4.0	1.4	7.5	M	9.1	S-E	5.3	83
										(continued)...	

Table AV-1 (Cont'd.) - 3 -

Source	Specific Gravity	D_s (mm)	Q ltr/sec	S x 10^3	B(m)	D(m) x 10^2	Pattern[2]	λ(m)	Flume Type[3]	Qs gm/sec	Experiment No.
5	2.65	.4	7.1	3.3	1.3	2.5	M	6.3	S-E	-	84
5	2.65	.4	7.1	4.7	2.4	2.0	M	6.3	S-E	2.6	85
5	2.65	.4	7.1	4.0	1.8	1.8	M	6.4	S-E	5.2	86
5	2.65	.4	7.1	5.6	2.3	2.2	M	7.1	S-E	10.5	87
5	2.65	.4	1.7	4.0	2.0	1.2	M	4.6	S-E	-	88
5	2.65	.4	1.7	6.0	1.4	.95	M	3.8	S-E	-	89
5	2.65	.4	28.3	3.7	5.8	3.0	M	20.3	S-E	2.3	90
5	2.65	.4	28.3	6.4	5.7	2.2	M	21.7	S-E	2.3	91
5	2.65	.4	1.7	8.7	2.5	.52	M	8.2	S-E	-	92
5	2.65	.4	14.2	5.0	3.5	2.1	M	15.2	S-E	1.3	93
5	2.65	.4	14.2	6.7	5.9	1.6	M	12.2	S-E	1.3	94
5	2.65	.4	14.2	8.1	7.9	1.2	M	20.3	S-E	1.3	95
5	2.65	.4	28.3	7.7	7.7	1.3	M	16.3	S-E	2.3	96
6	2.65	.45	3.4	3.5	.75	2.0	M	9.0	R-E	-	97
6	2.65	.45	1.7	2.8	.71	1.35	M	6.0	R-E	-	98
6	2.65	.45	2.5	2.0	.71	1.65	M	8.4	R-E	-	99
7	2.65	.7	.36	3.3	.15	.92	M	2.74	S-E	.27	100
7	2.65	.7	.36	5.0	.15	.79	M	2.74	S-E	.27	101
7	2.65	.7	.36	5.0	.15	.79	M	3.48	S-E	.50	102
7	2.65	.7	.59	3.3	.15	1.73	M	2.74	S-E	1.00	103
7	2.65	.7	.59	3.3	.23	1.17	M	3.04	S-E	.72	104
7	2.65	.7	.36	3.3	.30	1.70	M	4.27	S-E	1.50	105
7	2.65	.7	1.13	3.3	.23	2.26	M	3.96	S-E	1.37	106
7	2.65	.7	1.13	5.0	.15	.84	M	2.44	S-E	0.50	107
7	2.65	.7	.38	5.0	.23	.56	M	2.28	S-E	1.50	108
7	2.65	.7	.36	5.0	.30	.98	M	3.35	S-E	1.50	109
8	2.65	.16	10.6	2.2	1.1	3.8	M	7.22	S-E	-	110
8	2.65	.16	9.3	2.4	1.5	4.0	M	6.95	S-E	-	111
8	2.65	.16	8.5	2.9	2.4	2.6	M	5.55	S-E	-	112
8	2.65	.16	18.5	2.0	2.3	4.1	M	10.33	S-E	-	113
8	2.65	.16	17.6	2.8	2.2	6.7	M	11.55	S-E	-	114
8	2.65	.16	17.8	2.1	2.1	4.1	M	9.57	S-E	-	115
8	2.65	.16	32.0	1.4	2.8	6.5	M	12.43	S-E	-	116
8	2.65	.16	54.8	2.1	3.2	7.0	M	14.84	S-E	-	117
8	2.65	.16	30.9	2.4	3.2	6.3	M	11.61	S-E	-	118
8	2.65	.16	28.2	3.0	3.9	5.2	M	11.21	S-E	-	119
8	2.65	.16	30.2	3.3	2.4	4.9	M	11.83	S-E	-	120
8	2.65	.16	12.8	3.4	2.1	4.3	M	8.29	S-E	-	121
8	2.65	.16	16.1	2.6	2.2	3.8	M	8.35	S-E	-	122
8	2.65	.16	10.0	3.2	2.3	3.5	M	6.55	S-E	-	123
8	2.65	.16	6.9	2.5	2.3	2.2	M	6.13	S-E	-	124
											(continued)...

Table AV-1 (Cont'd.) - 4 -

Source	Specific Gravity	D_s (mm)	Q ltr/sec	S x 10^3	B(m)	D(m) x 10^2	Pattern[2]	λ(m)	Flume Type[3]	Qs gm/sec	Experiment No.
8	2.65	.16	17.3	2.2	2.7	3.5	M	8.47	S-E	-	125
8	2.65	.16	8.6	2.8	2.7	2.8	M	6.74	S-E	-	126
9	2.65	.7	4.24	2.6	.94	1.8	M	5.5	S-E	3.2	127
9	2.65	.7	4.24	4.3	1.16	1.3	M	5.9	S-E	4.0	128
9	2.65	.7	4.24	5.9	1.22	1.1	M	6.0	S-E	5.9	129
9	2.65	.7	4.24	6.4	1.25	1.0	M	6.2	S-E	6.5	130
9	2.65	.7	4.24	7.5	1.37	.85	M	6.3	S-E	6.9	131
9	2.65	.7	4.24	8.5	1.43	.80	M	6.4	S-E	7.2	132
9	2.65	.7	4.24	10.0	1.43	.72	M	6.8	S-E	8.5	133
9	2.65	.7	4.24	13.0	1.49	.61	M	6.9	S-E	9.4	134
9	2.65	.7	4.24	15.0	1.55	.53	B	-	S-E	12.3	135
9	2.65	.7	4.24	16.0	1.62	.45	B	-	S-E	13.8	136
9	2.65	.7	4.24	18.0	1.67	.39	B	-	S-E	15.4	137
9	2.65	.7	4.24	20.0	1.72	.34	B	-	S-E	16.7	138
10	2.65	.67	.56	3.9	.20	1.0	M	2.43	S-E	.21	139
10	2.65	.67	1.08	3.9	.29	1.3	M	2.04	S-E	1.05	140
10	2.65	.67	1.10	4.2	.34	1.0	M	2.29	S-E	-	141
10	2.65	.67	.31	6.9	.30	.55	M	1.83	S-E	-	142
10	2.65	.67	.54	6.4	.26	1.0	M	1.52	S-E	2.63	143
10	2.65	.67	1.13	6.8	.51	.94	M	2.80	S-E	3.50	144
10	2.65	.67	.71	6.3	.43	.82	M	.91	S-E	-	145
10	2.65	.67	.54	6.7	.39	.52	M	2.19	S-E	-	146
10	2.65	.67	.68	5.1	.23	.88	M	2.32	S-E	-	147
10	2.65	.67	.31	4.1	.13	.94	S	-	S-E	.062	148
10	2.65	.67	.62	3.5	.20	1.1	S	-	S-E	.14	149
10	2.65	.67	.96	4.2	.27	1.6	S	-	S-E	.44	150
10	2.65	.67	1.16	2.3	.25	2.0	S	-	S-E	.095	151
10	2.65	.67	1.78	2.5	.34	1.6	S	-	S-E	.34	152
10	2.65	.67	.91	2.8	.22	1.5	S	-	S-E	.18	153
10	2.65	.67	.74	1.8	.24	1.3	S	-	S-E	.00045	154
10	2.65	.67	1.39	1.8	.25	2.1	S	-	S-E	.095	155
10	2.65	.67	.62	3.8	.19	1.1	S	-	S-E	.16	156
10	2.65	.67	1.95	1.9	.36	1.7	S	-	S-E	.20	157
11	2.65	.71	20.	2.0	.6	7.1	M	2.6	N-N	-	158
11	2.65	.71	20.	2.0	.6	8.6	M	2.8	N-N	-	159
11	2.65	.71	20.	2.0	.6	4.0	M	2.4	N-N	-	160
11	2.65	.71	20.	2.0	.6	3.8	M	3.5	N-N	-	161
11	2.65	.71	20.	2.0	.6	15.1	M	2.8	N-N	-	162
11	2.65	.71	20.	2.0	.6	2.65	S	-	N-N	-	163
11	2.65	.71	3.0	5.0	.2	3.09	M	.8	R-N	-	164
11	2.65	.71	4.6	2.0	.2	4.72	S	-	R-N	-	165
11	2.65	.71	6.4	3.3	.2	5.33	M	.85	R-N	-	166
11	2.65	.71	2.6	2.0	.2	3.02	S	-	R-N	-	167

FOOTNOTES FOR TABLE AV-1

1) Source of data:

1. St. Anthony Falls Multi-Purpose Channel Data

2. St. Anthony Falls Tilting Flume Data

3. St. Anthony Falls Braiding Data

4. Chang, H.Y., D.B. Simons, and D.A. Woolhiser. Flume Experiments on Alternate Bar Formation, American Society of Civil Engineers, Journal of the Waterways, Harbors and Coastal Engineering, Vol. 97, WW 1, February, 1971, pp. 155-165.

5. Sharma, H.D. Extract of the Work Done at U.P. Irrigation Research Institute, Roerkee, on Meandering, Braiding, and Avulsion of Rivers and Their Prevention, U.P.I.R.I. Report, Roorkee, Uttar Pradesh, India, 1973.

6. Bordas, M. Contribution a L'Etude des Relations Entre le Debit Generateur et les Meandres d'une Riviere. Grafica da Universidade do Rio Grande do Sul, Porto Alegre, Brasil, 1963.

7. Quraishy, M.S. "The Meandering of Alluvial Rivers," Sind University Research Journal, (Science Series) VII (1), 1973, pp. 95-152.

8. Ackers, P. and F.G. Charlton, Meandering of Small Streams in Alluvium, Report No. INT 77, Hydraulics Research Station, Wallingford, Berkshire, England, 1970.

9. Schumm, S.A. and H.R. Khan. "Experimental Study of Channel Patterns," Bulletin of Geological Society of America, Vol. 88, 1972, pp. 1755-1770.

10. Wolman, M.G. and L.M. Brush. Factors Controlling the Size and Shape of Stream Channels in Coarse Noncohesive Sands, U.S. Geological Survey Prof. Paper 282-G, 1961, pp. 183-210.

11. Ashida, K. and S. Narai, "The Structure of Movable Bed Configuration," Bulletin of the Disaster Prevention Research Institute, Kyoto University, Kyoto, Japan, Vol. 19, Part 1, 1969, pp. 15-30.

2) Pattern: B = braiding; M = meandering; S = straight.

3) Flume type: Feed--S = new sediment supplied; R = sediment recirculated; N = no sediment supplied.

Banks--E = erodible; N = non-erodible.

TABLE AV-2

Key to Natural River Data Plotted in Figure 2-13

No.	River	Discharge Conditions	Location	Source
1	White River	instantaneous	Mt. Ranier,USA	Fahnestock (1963)
2	White River	instantaneous	Mt. Ranier,USA	Fahnestock (1963)
3	Mississippi River	mean	Vicksburg,USA	Winkley (1973)
4	Mississippi River	bank full	Vicksburg,USA	Winkley (1973)
5	Yellow River	near bank full	Mengtsing, China	Chien Ning (1961)
6	Glomma River	bank full	Koppangsogene,Norway	Nordseth (1973)
7	Matanuska River	normal summer high	Anchorage,USA	Fahnestock and Bradley (1973)
8	Knik River	normal summer high	Anchorage,USA	Fahnestock and Bradley (1973)
9	Knik River	catastrophic flood	Anchorage,USA	Fahnestock and Bradley (1973)
10	Missouri	high	Pierre,S. Dak.,USA	Einstein and Barbarossa (1952)
11	Missouri	low	Pierre,S. Dak.,USA	Einstein and Barbarossa (1952)
12	Missouri	high	Ft. Randall,USA	Einstein and Barbarossa (1952)
13	Missouri	low	Ft. Randall,USA	Einstein and Barbarossa (1952)
14	Missouri	-	Omaha,Nebr.,USA	Einstein and Barbarossa (1952)
15	Elkhorn	high	Waterloo,USA	Einstein and Barbarossa (1952)
16	Elkhorn	low	Waterloo,USA	Einstein and Barbarossa (1952)
17	Big Sioux	high	Akron,USA	Einstein and Barbarossa (1952)
18	Big Sioux	low	Akron,USA	Einstein and Barbarossa (1952)
19	Platte	high	Ashland,USA	Einstein and Barbarossa (1952)
20	Platte	low	Ashland,USA	Einstein and Barbarossa (1952)
21	Niobrara	-	Butte,USA	Einstein and Barbarossa (1952)
22	Salinas	high	San Lucas,USA	Einstein and Barbarossa (1952)

[continued]

TABLE AV-2 [continued]

No.	River	Discharge Conditions	Locations	Source
23	Salinas	low	San Lucas,USA	Einstein and Barbarossa (1952)
24	Salinas	high	Paso Roblis,USA	Einstein and Barbarossa (1952)
25	Salinas	low	Paso Roblis,USA	Einstein and Barbarossa (1952)
26	Middle Loup	instantaneous	Dunning,USA	Hubbell and Matejka (1959)
27	Middle Loup	instantaneous	Dunning,USA	Hubbell and Matejka (1959)
28	Middle Loup	instantaneous	Dunning,USA	Hubbell and Matejka (1959)
29	Middle Loup	instantaneous	Dunning,USA	Hubbell and Matejka (1959)
30	Middle Loup	instantaneous	Dunning,USA	Hubbell and Matejka (1959)
31	Ganga	bank full	Kankhal, India	Gupta et. al. (1969)
32	Great Gandak	bank full	Chitauni, India	Gupta et. al. (1969)
33	Sarda	bank full	Sarda Sagar, India	Gupta et. al. (1969)
34	Ganga	bank full	Raighat Narora,India	Gupta et. al. (1969)
35	Beaver Creek	mean	Daniel, Wyo.,USA	Leopold and Wolman (1957)
36	Watts Branch	mean	Rockville, Md.,USA	Leopold and Wolman (1957)
37	Platte	mean	Grand Island,Nebr.,USA	Leopold and Wolman (1957)
38	Platte	mean	Odessa, Nebr.,USA	Leopold and Wolman (1957)
39	Platte	mean	Overton, Nebr.,USA	Leopold and Wolman (1957)
40	Missouri	mean	St. Joseph, Mo.,USA	Leopold and Wolman (1957)
41	Missouri	mean	Hermann, Mo.,USA	Leopold and Wolman (1957)
42	Missouri	mean	Pierre, S. Dak.,USA	Leopold and Wolman (1957)
43	Missouri	mean	Kansas City, Mo.,USA	Leopold and Wolman (1957)
44	Missouri	mean	Bismarck, N. Dak.,USA	Leopold and Wolman (1957)
45	Tennessee	mean	Knoxville, Tenn.,USA	Leopold and Wolman (1957)
46	Buttahatchee	mean	Caledonia, Miss.,USA	Leopold and Wolman (1957)

[continued]

TABLE AV-2 [continued]

No.	River	Discharge Conditions	Locations	Source
47	Kansas	mean	Bonner Springs, Kan.,USA	Leopold and Wolman (1957)
48	Kansas	mean	Lecompton, Kan.,USA	Leopold and Wolman (1957)
49	Kansas	mean	Ogden, Kan.,USA	Leopold and Wolman (1957)
50	Maumee	mean	Defiance, Ohio,USA	Leopold and Wolman (1957)
51	Maumee	mean	Waterville, Ohio,USA	Leopold and Wolman (1957)
52	Smoky Hill	mean	Lindsborg, Kan.,USA	Leopold and Wolman (1957)
53	Smoky Hill	mean	Enterprise, Kan.,USA	Leopold and Wolman (1957)

TABLE AV-2

Sources

Fahnestock, R.K. Morphology and Hydrology of a Glacial Stream - White River, Mt. Ranier, Washington, U.S. Geological Survey Prof. Paper 422-A, 1963.

Winkley, B.R. Metamorphosis of a River, Water Resources Research Institute, Mississippi State University, 39762, 1973.

Chien, Ning. "The Braided Stream of the Lower Yellow River," Scientia Sinica, Vol. X, No. 6, 1961.

Nordseth, K. Fluvial Processes and Adjustments on a Braided River. The Islands of Koppangsoyene on the River Glomma, Norsk Geografesk Tidsskrift, Bunde 27, Hefte 2, 1973.

Fahnestock, R.K. and W.C. Bradley. "Knik and Matanuska Rivers, Alaska: A Contrast in Braiding." In Fluvial Geomorphology (M. Mousawa, ed.), Publications in Geomorphology, State University of New York, 1973.

Leopold, L.B. and M.G. Wolman. River Channel Patterns: Braided, Meandering, and Straight, U.S. Geological Survey Prof. Paper 282-B, 1957, 84 pp.

Einstein, H.A. and N.L. Barbarossa. "River Channel Roughness," Trans., American Society of Civil Engineers, Vol. 117, 1952, pp. 1121-1146.

Hubbell, D. and Matejka, D. Investigation of Sediment Transportation Middle Loup River at Dunning, Nebraska, U.S. Geological Survey Water Supply Paper 1476, 1959, 123 pp.

Gupta, S.N. and J.P. Sharma, S.R. Jindal, Satish Chandra, "Alluvial River Behavior - A Few Aspects of its Simulation in a Model," Proc., 13th Congress Intl. Assoc. Hydraulic Research, Kyoto, Japan, Vol. I, Paper No. A-30, 1969, pp. 267-276.